

**A THEORETICAL AND EXPERIMENTAL MODEL TO PREDICT
BIAXIAL FAILURE OF TISSUE ENGINEERED BLOOD VESSELS**

A Dissertation
Presented to
The Academic Faculty

by

Julia Raykin

In Partial Fulfillment
of the Requirements for the Degree
Doctor of Philosophy in the
Wallace H. Coulter Department of Biomedical Engineering at Georgia Tech and Emory
University

Georgia Institute of Technology
December 2013

Copyright © 2013 by Julia Raykin

**A THEORETICAL AND EXPERIMENTAL MODEL TO PREDICT
BIAXIAL FAILURE OF TISSUE ENGINEERED BLOOD VESSELS**

Approved by:

Dr. Rudolph L. Gleason, Jr., Advisor
School of Mechanical Engineering
Georgia Institute of Technology

Dr. Manu Platt
School of Biomedical Engineering
Georgia Institute of Technology

Dr. Luke Brewster
School of Medicine
Emory University

Dr. Alexander Rachev
School of Mechanical Engineering
Georgia Institute of Technology

Dr. Robert M. Nerem
School of Mechanical Engineering
Georgia Institute of Technology

Date Approved: [May 14, 2013]

ACKNOWLEDGEMENTS

My time at Georgia Tech has been an amazing and rewarding experience. Graduate school has been a much more enjoyable and formative than I ever imagined it would be. I owe a debt of gratitude to a large number of people that have supported me through the years and made the completion of this dissertation possible.

Firstly, I would like to thank my advisor, Dr. Rudy Gleason, for his continuous support and encouragement throughout my entire graduate career. His hands-off approach, albeit very frustrating at the time, has really helped me grow and succeed as a scientist. His remarkable understanding of my work and experiments made every discussion with him extremely productive and helpful for my progress. In addition, knowing that he was always on my side helped me to never lose motivation and made the entire process easier and more enjoyable.

I am very grateful to Dr. Robert Nerem for opening up his lab to me. Working in his lab was an invaluable experience throughout my graduate career. I learned laboratory techniques that would have taken a very long time for our lab to figure out on our own. Trying to startup a tissue engineering project in a new lab with no cell or tissue culture experience seemed to be an unattainable task, but Dr. Nerem made it possible. He also gave me invaluable insight and motivation during lab meetings that really helped shape the direction of my project. Most importantly, I would like to thank Dr. Nerem for his

support. His care and genuine interest in my progress really helped motivate me to finish my dissertation.

It is hard to overstate the importance of Dr. Alexander Rachev's assistance for my work. I started working with Dr. Rachev when my project was still in its infancy. He has taught me a lot about experimental design and mechanics. His door was always open whenever I had questions and he would never let me leave without handing me a piece of chewing gum. He has helped shape my project and always challenged me to look at things from a different point of view.

I would also like to thank Dr. Manu Platt. We started collaborating towards the last few years of my graduate experience. His enthusiasm and knowledge helped me to get excited about science again when I was at a very low point and my project seemed to be going nowhere.

I greatly appreciate Dr. Luke Brewster's insight into the clinical side of research. It helped me to better understand the practical applications of research and continues to motivate my current research.

Many members of the Nerem lab have helped me throughout the years. In particular, Stacey Schutte and Taby Ahsan really helped get my project going in the beginning. Stacey helped get me acquainted with the Nerem lab and helped me figure out how to do pretty much everything in lab. She took a lot of time out of her schedule to show me the

ropes and helped get my project off the ground. Even though she has long graduated, she has still taken a lot of time to help edit my thesis and give me valuable input. When I was still trying to develop a project, Taby met with me every week to discuss my ideas. She helped by shooting down my ridiculous ideas and prevented me from wasting a lot of time. She taught me how to approach scientific problems critically and always had a unique perspective on the topic. We were very fortunate to have Steve Woodard around. He was always quick to help with any lab or equipment crisis. Discussions with him were always informative: his scientific knowledge and understanding of experimental design continuously amazed me. And he is also the only person who I worked with that shared my passion for the Falcons. Drs. Casey Ankeny, Randy Ankeny, and Lisa McGinley's persistent concern about me finishing and final pushes helped get me through the last few hurdles. I do not think I could have made it through without them or their motivating concern. Lisa also helped me by encouraging me to get out of the lab for coffee breaks, which were always fun and insightful. We spent a lot of time analyzing science and life. Her sense of humor made the lab a pleasant place to be these last few years. In addition, when Lisa first came to the lab and was waiting for all of her reagents to arrive she helped me a lot with my cell culture and made handling 30 tissue culture flasks at a time a bearable task. Dr. Barbara Nsiah has become a really good friend to me. She was always available to hang out, whenever I asked, no matter how busy she was. I will always cherish our after work dinners together, our discussions on life, and most of all the many laughs. I am also thankful to the rest of the Nerem lab for their scientific input and making the lab a great place to work: Dr. Adele Doyle, Dr. Zannatul Ferdous, Sarah

Griffiths, Rachel Meltzer, Dylan Nass, John Ewing, Kent Wurtz, Minsung Hong, Hansu Jo, Jungbo Shim, and Hyeongseok Kim.

I would also like to thank all of the members of the Gleason lab, who always went of their way to help me and for our insightful discussions. I am very fortunate to have had everyone in the lab with me. In particular, I would like to thank Dr. Roy Wang. His presence in the lab has been formative for me as a researcher. His persistent enthusiasm for everything that we were working on has helped inspire me many times when I needed it the most. He also significantly helped me to design my numerous devices and helped me to understand the nuances of designing mechanical systems. In addition, Roy has been a great friend and roommate for a short time and has been very supportive throughout my experience as a graduate student at Georgia Tech. Dr. Laura Hansen always made herself available to talk about experiments and has become a great friend. Dr. Mike Zaucha, Dr. William Wan, Daniel Howell, and Prem Midha were always available to lend their expertise when I had no idea what I was doing. Alex Caulk took care of everything in the lab, was always eager to help everyone out, and was always fun to talk to. Kelly Straub really made the lab a fun place to be. It seems like when she was around we were always laughing. The members of both labs have made my experience in lab never feel like work at all.

There were also some other members of wings 1D and 2A that have made my life as a graduate student a lot more enjoyable. Dr. Choon Hwai Yap was always really helpful. We started out at the same time and went through all the initial hurdles together. His

intuitive grasp of mechanics and insightful suggestions continuously amazed me. Julia Henkels helped me figure out my PIV analysis. Andrea Para helped me get organized towards the end and finish up everything that I needed to. In addition, Andrea and Julia were always available to talk and help out, despite being busy themselves. Nathan Hotaling would always entertain my questions and crazy new ideas. His knowledge of immunology has been a tremendous asset for me in the projects that I have worked on. He was always a lot of fun to have around outside of lab. It was always very entertaining when he would come out. He also kindly organized my birthday parties. Phil Keegan was very helpful; Phil always seemed to enjoy talking about science and helped me troubleshoot some of the assays that I had to run.

I would have never been able to accomplish this much without the help of some great undergrads along the way. Unfortunately, they got a look at the bad side of research right away, due to the constant lack of success in our endeavors. I know the constant failures must have been frustrating, but the experiments taught us invaluable lessons that will help with this work in the future, and hopefully taught them to be more patient and persevere despite initial failure. Danielle Shaver has been one of the best undergrads I have ever known. She always knew exactly what I wanted without me having to really explain it and always being eager to do it. I am also thankful to Alex Levental for his never-ending desire to help. After my ACL surgery, I could not have been able to continue doing all of the work that I needed to without him. He was always available to bring me materials and get stuff done when I wasn't able to. He was also an incredible editor and helped edit any documents that I needed when I did not have much time. Will Reschly and Chris

Jackman helped me a lot with all of the mechanical testing and I could never have done so many tests without them. Alyssa Shapiro has been a great asset for me while processing my data. In addition, I would like to thank Saira Ahmed, Alison Skala, Christa Caesar, Yue Geng, Rafeed Chaudhury, Sarah Skelton, Abdullah Saif, and Sergey Klimov for allowing me to mentor them. They really taught me how to be a mentor and made it an enjoyable experience.

I also owe a huge debt of gratitude to Briana Morrison, for teaching me how to program. This project was so much easier than it could have been, due to my knowledge of programming and ability to think like a programmer. She also helped me figure out the nuances of Matlab and helped me come up with ways to make my code more efficient, which saved me a lot of sitting around and waiting for my code to run time.

I would also like to thank all of the friends that I have made during graduate career at Georgia Tech. It would be impossible to list all of them but a few require special mention. Dr. Mela Johnson and Priyanka Karan were the first friends I made at Georgia Tech. I really appreciate their open-mindedness and genuineness; they always accepted me and taught me that it was ok to be myself. Ivana Parker and Catera Wilder have been incredibly supportive; they always had this remarkable ability to know something was wrong, even when I refused to tell them. Peng Meng Kou put up with me as a roommate for over four years and was a very good friend to me. We always had enjoyable conversations and she was the best roommate I've ever had. The 'Singaporean' group, which Yap so kindly allowed me join, has been very supportive and always made sure

there was something entertaining to do every weekend. Vivek Kumar, Ji Won Han, Asha Shekaran, and Gopi Jayaprakash were great friends to have around.

Finally, I would like to thank my family, without them none of this would have been possible. They have always given me the motivation and support in all of my endeavors. I thank everyone in my immediate and extended family for being awesome and teaching me the importance of family, kindness, and the pursuit of knowledge. I thank my parents for passing on to me their drive and work ethic, teaching me that I could accomplish anything that I set my mind to, and their constant faith in me. I would particularly like to thank my grandparents for introducing me to science, always encouraging me to try to figure out how things work, teaching me to think critically, and their love and encouragement throughout my life. I thank my sister for her persistent motivation to succeed and inspiring me to always try to be better. Lastly, I would like to thank my cousin for introducing me to the field, helping me see that there are scientists that are fun to be around and genuinely care about the science, and for being a continuous source of support.

TABLE OF CONTENTS

| | |
|---|-----|
| ACKNOWLEDGEMENTS | IV |
| LIST OF TABLES | XV |
| LIST OF FIGURES | XVI |
| LIST OF ABBREVIATIONS..... | XX |
| SUMMARY | XXI |
| CHAPTER 1 INTRODUCTION | 1 |
| 1.1 Cardiovascular Disease/Atherosclerosis Prevalence | 1 |
| 1.2 Normal Blood Vessel Architecture..... | 2 |
| 1.3 Atherosclerosis..... | 4 |
| 1.4 Coronary Artery Bypass Grafting..... | 6 |
| 1.5 Tissue Engineered Arteries | 7 |
| 1.5.1 Gel-derived Scaffolds | 7 |
| 1.5.2 Cell Self-Assembly | 8 |
| 1.5.3 Synthetic Biodegradable Scaffolds..... | 8 |
| 1.5.4 Decellularized Tissue Scaffolds..... | 9 |
| 1.6 Effects of Stresses on Remodeling | 10 |
| 1.7 Theoretical Modeling..... | 13 |
| 1.7.1 Modeling of Native Blood Vessels..... | 13 |
| 1.7.2 Mechanical Properties of Collagen-based TEBVs | 13 |
| 1.7.3 Necessity for Modeling of TEBVs | 16 |
| 1.8 Summary | 18 |
| 1.9 References..... | 18 |
| CHAPTER 2 SPECIFIC AIMS | 27 |
| 2.1 Project Significance | 27 |
| 2.2 Project Objective..... | 28 |
| 2.3 Specific Aims and Hypotheses | 29 |
| 2.3.1 Specific Aim 1 | 29 |
| 2.3.2 Specific Aim 2 | 29 |

| | | |
|-----------|--|-----|
| 2.3.3 | Specific Aim 3 | 29 |
| | | |
| CHAPTER 3 | A PHENOMENOLOGICAL MODEL FOR MECHANICALLY-MEDIATED GROWTH, REMODELING, DAMAGE, AND PLASTICITY OF GEL-DERIVED TISSUE ENGINEERED BLOOD VESSELS | 31 |
| 3.1 | Introduction..... | 31 |
| 3.2 | Theoretical Framework..... | 33 |
| 3.2.1 | Plasticity and Growth (Kinematics)..... | 34 |
| 3.2.2 | Damage and Remodeling (Constitutive Equations)..... | 36 |
| 3.3 | Illustrative Example | 39 |
| 3.3.1 | Kinematics | 39 |
| 3.3.2 | Constitutive Equation and Equilibrium | 42 |
| 3.3.3 | Evolution Equations for Plasticity, Growth, Damage, and Remodeling | 44 |
| 3.3.4 | Simulation Results | 51 |
| 3.4 | Discussion..... | 66 |
| 3.5 | References..... | 72 |
| | | |
| CHAPTER 4 | A PHENOMONOLOGICAL MODEL FOR COLLAGEN GEL DAMAGE UNDER UNIAXIAL LOADING | 75 |
| 4.1 | Introduction..... | 75 |
| 4.2 | Mathematical Model | 76 |
| 4.3 | Illustrative Examples | 83 |
| 4.3.1 | Monotonic Loading to Failure | 88 |
| 4.3.2 | Uniaxial Creep Testing | 90 |
| 4.3.3 | Uniaxial Fatigue Testing..... | 92 |
| 4.4 | Discussion..... | 97 |
| 4.5 | References..... | 99 |
| | | |
| CHAPTER 5 | EXPERIMENTAL FRAMEWORK TO STUDY THE EFFECTS OF PLASTICITY AND DAMAGE DURING UNIAXIAL LOADING OF COLLAGEN GELS | 102 |
| 5.1 | Introduction..... | 102 |
| 5.2 | Materials and Methods..... | 103 |
| 5.2.1 | Experimental Methods | 103 |
| 5.2.2 | Mathematical Modeling..... | 108 |

| | | |
|--|--|-----|
| 5.3 | Results and Discussion | 109 |
| 5.3.1 | Monotonic Tensile Testing | 109 |
| 5.3.2 | Uniaxial Creep Testing | 110 |
| 5.3.3 | DIC Verification | 111 |
| 5.3.4 | Fatigue Testing..... | 111 |
| 5.3.5 | Material and Damage Parameters | 116 |
| 5.4 | Conclusions..... | 120 |
| 5.5 | References..... | 122 |
| CHAPTER 6 A MECHANICAL TESTING SYSTEM TO CHARACTERIZE THE PLASTICITY AND DAMAGE OF TEBVS UNDER BIAXIAL LOADING | | 124 |
| 6.1 | Introduction..... | 124 |
| 6.2 | Materials and Methods..... | 125 |
| 6.2.1 | Experimental Methods | 125 |
| 6.2.2 | Mathematical Modeling | 129 |
| 6.3 | Results and Discussion | 137 |
| 6.3.1 | Simulation Results | 144 |
| 6.4 | Conclusions..... | 147 |
| 6.5 | References..... | 148 |
| CHAPTER 7 EFFECT OF CULTURE TIME AND CROSSLINKING ON TEBV DAMAGE | | 150 |
| 7.1 | Introduction..... | 150 |
| 7.2 | Materials and Methods..... | 151 |
| 7.2.1 | Experimental Methods | 151 |
| 7.3 | Results and Discussion | 152 |
| 7.3.1 | Change in Material Properties due to Time in Culture | 152 |
| 7.3.2 | Change in Material Properties with Tg Crosslinking | 157 |
| 7.4 | Conclusions..... | 161 |
| 7.5 | References..... | 164 |
| CHAPTER 8 CONCLUSIONS AND FUTURE DIRECTIONS..... | | 165 |
| 8.1 | References..... | 168 |

LIST OF TABLES

| | |
|---|-----|
| Table 4-1. List of simulated uniaxial mechanical tests..... | 87 |
| Table 5-1. List of uniaxial tests performed..... | 105 |

LIST OF FIGURES

| | |
|---|----|
| Figure 1-1. Anatomy of the artery. | 3 |
| Figure 1-2. Progression of atherosclerosis..... | 5 |
| Figure 1-3. Forces on the the vascular wall. | 11 |
| Figure 1-4. Typical nominal stress-Eulerian strain curve for uniaxial (ring) tests. | 14 |
| Figure 3-1. General schema for the kinematics of combined plasticity and volumetric growth. | 35 |
| Figure 3-2. Kinematics of growth and plasticity of a thick-walled axisymmetric tube... | 39 |
| Figure 3-3. Model predicted evolution of changes in the geometric properties. | 55 |
| Figure 3-4. Model predicted changes in mean mechanical properties..... | 57 |
| Figure 3-5. Evolution of mechanical properties over time in culture. | 59 |
| Figure 3-6. Model predicted changes in loaded and unloaded geometry. | 63 |
| Figure 3-7. Evolution of material properties..... | 65 |
| Figure 4-1. Uniaxial Kinematics..... | 77 |
| Figure 4-2. Comparison of theoretical and experimental stress-stretch curves prior to damage. | 86 |
| Figure 4-3. Comparison of theoretical and experimental stress-stretch curves following damage. | 88 |
| Figure 4-4. Modeling simulations of uniaxial tensile tests at different stretch rates. | 89 |
| Figure 4-5. Theoretical prediction of the a) apparent and b) effective stresses..... | 90 |
| Figure 4-6. Predicted UTS with increasing stretching rates. | 90 |
| Figure 4-7. Modeling simulations of uniaxial creep tests..... | 91 |
| Figure 4-8. Predicted time to failure with increasing applied nominal stress..... | 92 |
| Figure 4-9. Modeling simulations of uniaxial cyclic loading. | 94 |
| Figure 4-10. Apparent stress-stretch response during cyclic loading. | 95 |
| Figure 4-11. Nominal stress with increasing cycle number..... | 95 |

| | |
|--|-----|
| Figure 4-12. Effect of amplitude on the apparent a) stress and b) stretch ratio over the time of the test..... | 96 |
| Figure 4-13. Effect of frequency on the apparent a) stress and b) stretch ratio with increasing cycle number. | 96 |
| Figure 5-1. Image of the vessel during uniaxial testing..... | 105 |
| Figure 5-2. Tracking of the vessel using DIC during uniaxial testing..... | 107 |
| Figure 5-3. Manual tracking of the vessel during uniaxial testing. | 108 |
| Figure 5-4. Representative Cauchy stress-Green strain curves for monotonic uniaxial tests performed at stretch rates of.1 mm/s and 1 mm/s..... | 109 |
| Figure 5-5. Uniaxial test performed from the cross-sectional view..... | 110 |
| Figure 5-6. Representative change in green strain over time during creep tests performed at different stress magnitudes..... | 111 |
| Figure 5-7. Representative typical response during cyclic loading. | 112 |
| Figure 5-8. Typical monotonic stress-strain response following cyclic loading. | 113 |
| Figure 5-9. Response of TEBVs following cyclic loading. | 113 |
| Figure 5-10. Estimation of stretch ratio using hook displacement. | 114 |
| Figure 5-11. Effect of amplitude during cyclic loading..... | 115 |
| Figure 5-12. Effect of frequency during cyclic loading..... | 116 |
| Figure 5-13. Experimentally and theoretically predicted stress-strain response during monotonic loading. | 117 |
| Figure 5-14. Experimental and theoretically predicted creep testing. | 118 |
| Figure 5-15. Change in stretch ratio over the time course of cyclic loading. | 118 |
| Figure 5-16. Monotonic testing following cyclic loading. | 119 |
| Figure 6-1. Biomechanical Testing System..... | 127 |
| Figure 6-2. Image of a collagen gel TEBV undergoing biaxial mechanical testing..... | 128 |
| Figure 6-3. General kinematics for plastic deformation. | 131 |
| Figure 6-4. Kinematics of the plastic deformation of a thin-walled tube. | 133 |

| | |
|---|-----|
| Figure 6-5. Kinematics of growth and plasticity of a thick-walled axisymmetric tube.. | 135 |
| Figure 6-6. Biomechanical tests on collagen-based TEBVs..... | 139 |
| Figure 6-7. Axial force-pressure data with increasing cyclic pressure..... | 139 |
| Figure 6-8. Effect of axial extension on pressure and axial load..... | 140 |
| Figure 6-9. Axial force-length response at constant pressure..... | 141 |
| Figure 6-10. Functional testing of a collagen-based TEBV. | 141 |
| Figure 6-11. Representative burst pressure tests for collagen gel TEBVs. | 143 |
| Figure 6-12. Mean burst pressures at 0.4 mm Hg/s and 1.4 mm Hg/s..... | 143 |
| Figure 6-13. Representative isobaric tests of collagen gel TEBVs. | 144 |
| Figure 6-14. Representative fatigue test collagen gel TEBVs..... | 144 |
| Figure 6-15. Verification of the proposed strain energy function. | 145 |
| Figure 6-16. Predicted burst pressure test response..... | 146 |
| Figure 6-17. Predicted isobaric response of collagen gel TEBVs | 146 |
| Figure 6-18. Representative predicted fatigue response of a collagen gel TEBV..... | 147 |
| Figure 7-1. Uniaxial tensile tests performed at different times of static culture..... | 154 |
| Figure 7-2. Uniaxial creep tests performed at 2 and 7 days of static culture..... | 155 |
| Figure 7-3. Burst pressure tests performed at 2, 7, and 14 days of static culture. | 155 |
| Figure 7-4. Mechanical responses of TEBVs cultured statically for 2, 7, and 14 days.. | 156 |
| Figure 7-5. Differences in moduli between different time-points in culture. | 156 |
| Figure 7-6. Change in the volume of collagen-based TEBVs over time in culture..... | 157 |
| Figure 7-7. Uniaxial monotonic tensile tests performed on control and Tg-crosslinked TEBVs..... | 158 |
| Figure 7-8. Uniaxial creep tests performed on control and Tg-crosslinked TEBVs. | 159 |
| Figure 7-9. Burst pressure tests of control and Tg-treated collagen gel TEBVs. | 160 |
| Figure 7-10. Mechanical responses of control and Tg-treated TEBVs. | 160 |
| Figure 7-11. Changes in the geometric properties of control and Tg-treated collagen gel- based TEBVs. | 161 |

Figure 7-12. Theoretical change in the uniaxial tensile response between the control and Tg-crosslinked TEBVs..... 163

LIST OF ABBREVIATIONS

| | |
|------|---------------------------------|
| BP | Burst Pressure |
| CABG | Coronary Artery Bypass Grafting |
| CVD | Cardiovascular Disease |
| DTT | Dithiothreitol |
| ECM | Extracellular Matrix |
| EC | Endothelial Cell |
| ET-1 | Endothelin-1 |
| PGA | Polyglycolic Acid |
| SMC | Smooth Muscle Cell |
| Tg | Transglutaminase |

SUMMARY

The development of small diameter tissue engineered blood vessels (TEBVs) with low thrombogenicity, low immunogenicity, suitable mechanical properties, and a capacity to remodel to their environment could significantly advance the treatment of coronary and peripheral artery disease. Despite significant advances in the field of tissue engineering, autologous vessels are still primarily utilized as grafts during bypass surgeries. However, undamaged autologous tissue may not always be available due to disease or prior surgery. TEBVs lack long-term efficacy due to a variety of types of failures including aneurysmal dilations, thrombosis, and rupture; the mechanisms of these failures are not well understood. In vitro mechanical testing may help the understanding of these failure mechanisms. The typical mechanical tests lack standardized methodologies; thus, results vary widely.

The overall goal of this study is to develop novel experimental and mathematical models to study the mechanical properties and failure mechanisms of TEBVs. Our results suggest that burst pressure tests, the current standard, are not sufficient to assess a TEBVs' suitability as a coronary substitute; creep and/or cyclic loading tests are also required. Results from this model can help identify the most insightful experiments and quantities to be measured – ultimately reducing the overall number of experimental iterations. Improving the testing and characterization of TEBVs is critically important in decreasing the time necessary to validate the mechanical and functional responses of TEBVs over time, thus quickly moving TEBVs from the benchtop to the patient.

CHAPTER 1

INTRODUCTION

1.1 Cardiovascular Disease/Atherosclerosis Prevalence

Cardiovascular disease (CVD) is estimated to account for 32.8% of all deaths in the U.S. and estimated to cost \$297.7 billion in 2008 [1]. CVD includes coronary artery diseases, stroke, peripheral artery disease, heart failure, arrhythmia, and valve disease.

Atherosclerosis accounts for approximately 75% of CVD deaths. Complications due to atherosclerosis are projected to be the world's leading cause of death by 2020 [1]. Atherosclerosis occurs when lipids, cells, and extracellular matrix (ECM) buildup on the luminal surface of the arterial wall and form structures called plaques [2]. These plaques can rupture and result in blockage of the artery, which decreases blood flow to the distal tissues and leads to tissue ischemia and death. When atherosclerosis occurs in the coronary arteries (coronary artery disease) it leads to a decrease in the blood supply to the heart and can lead to myocardial infarction.

Coronary artery disease is estimated to account for 1 out of every 6 deaths in the U.S. and estimated to cost of \$156.4 billion in 2008 [1]. Coronary bypass surgery is a common form of treatment. Most often these surgeries use autologous saphenous vein or mammary artery as grafts. However, long-term complications still occur 30-50% of the time with the use of autologous grafts [3-5]. Patients with atherosclerosis frequently have inadequate amounts of undamaged tissue available for use as a graft because of

preexisting disease or previous surgery [6, 7]. An alternative method is ultimately necessary for these patients. Implantation of synthetic grafts, such as Dacron or PFTE, to replace large diameter vessels (>6mm) has had some success [8]. However, thrombus formation and intimal hyperplasia have caused these synthetic grafts to fail as replacements for small diameter arteries [9-12]. Thus, there is a great clinical need to develop a small diameter tissue engineered blood vessels (TEBVs) with low thrombogenicity and immune response, suitable mechanical properties, and a capacity to remodel to their environment.

1.2 Normal Blood Vessel Architecture

Blood vessels are composed of three layers: the tunica intima, tunica media, and tunica adventitia (Figure 1-1). The intima is the innermost layer and is comprised of a continuous monolayer of endothelial cells (ECs). The basal lamina, the outermost layer of the intima, separates the intima from the rest of the vessel wall, which consists of type IV collagen, laminin, elastin, and proteoglycans. ECs form a semi-permeable, non-thrombogenic layer on the lumen of the blood vessel wall and interact directly with the components in the blood, which allows the ECs to sense and respond to changes in blood flow. The intima contains a thick elastic layer called the internal elastic lamina. The middle layer, the media, is the thickest layer and consists predominantly of smooth muscle cells (SMCs), collagen, elastin, and proteoglycans. The media is thought to be the main load bearing layer over physiological conditions [13]. The SMCs' main functions are to maintain vascular tone and synthesize ECM. In elastic arteries, elastic laminae are concentrically located in between layers of smooth muscle cells. The elastic laminae are

more compliant than other ECM constituents and contribute to load bearing, primarily low loads, while collagen contributes to it at higher loads [14]. The adventitia, the outermost layer, is mainly composed of fibroblasts and collagen and is thought to provide a significant mechanical contribution over supraphysiological loads, thereby preventing over-distension of the vessel. The adventitia also tethers the vessel to surrounding connective tissue, and is vascularized to provide nutrients to the SMCs in the media of the vessel.

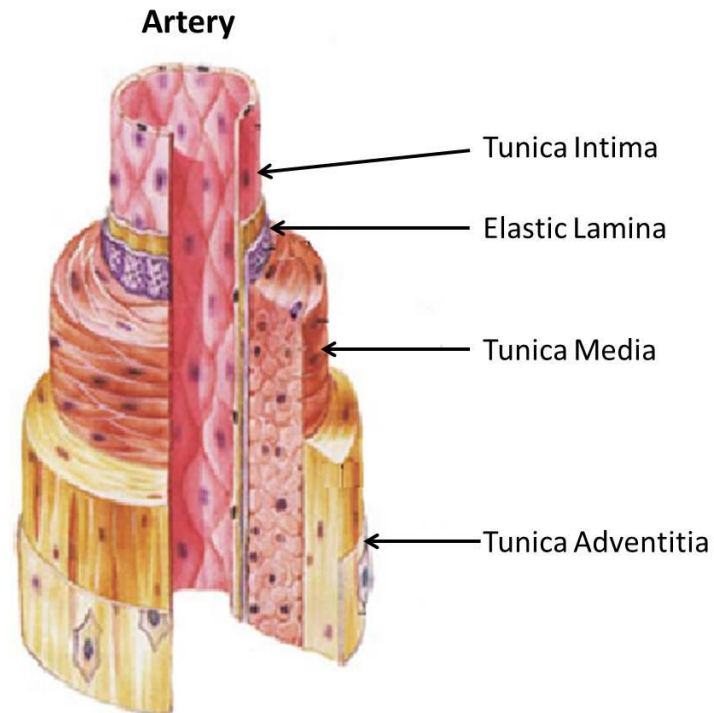


Figure 1-1. Anatomy of the artery. Adapted from [15].

The size and composition of each of the three layers in blood vessels depend on the location and function of the vessel. Arteries and veins differ significantly in their compositions. Since arteries are closer to the heart, arteries are exposed to much higher

pulsatile pressures and shear stresses than veins [16]. The mean pressures in arteries are 90 to 100 mm Hg, while the mean pressures in veins are 2 mm Hg. Arteries generally have a thicker media layer, have higher elastin and collagen content, and are stiffer than veins to compensate for the higher stresses [15]. Any changes in the content or organization of the blood vessel's ECM can result in significant changes in the mechanical properties of the vessel. Various pathological conditions, such as CVD, can affect the vessel's structure and negatively impact its mechanical environment.

1.3 Atherosclerosis

Atherosclerosis is major contributor to deaths worldwide [17]. It is characterized by the formation of plaques on the lumen of the vascular wall. A plaque is the accumulation of lipids, cells, and ECM on the lumen. Atherosclerosis is considered to be caused by a combination of genetic factors and lifestyle choices. It occurs predominantly in areas of disturbed flow of the vasculature. In response to disturbed flow or the accumulation of lipids in the vascular walls, the ECs begin expressing markers for the adherence of monocytes and T cells to the endothelium. Following adherence, monocytes differentiate into macrophages and start to migrate, into the subendothelial layer. As the macrophages internalize the lipids in the wall they transform into foam cells, which eventually rupture and contribute to plaque formation. The rupture also induces signals for the SMCs to start migrating towards the luminal surface, which synthesize fibrous tissue and start to form a fibrous cap. Under certain conditions the fibrous cap can rupture, releasing all the material from the necrotic core. This leads to thrombosis and blockage of the artery [18].

If the fibrous cap ruptures in a coronary artery, the artery needs to be replaced to provide adequate nutrients to the heart (Figure 1-2).

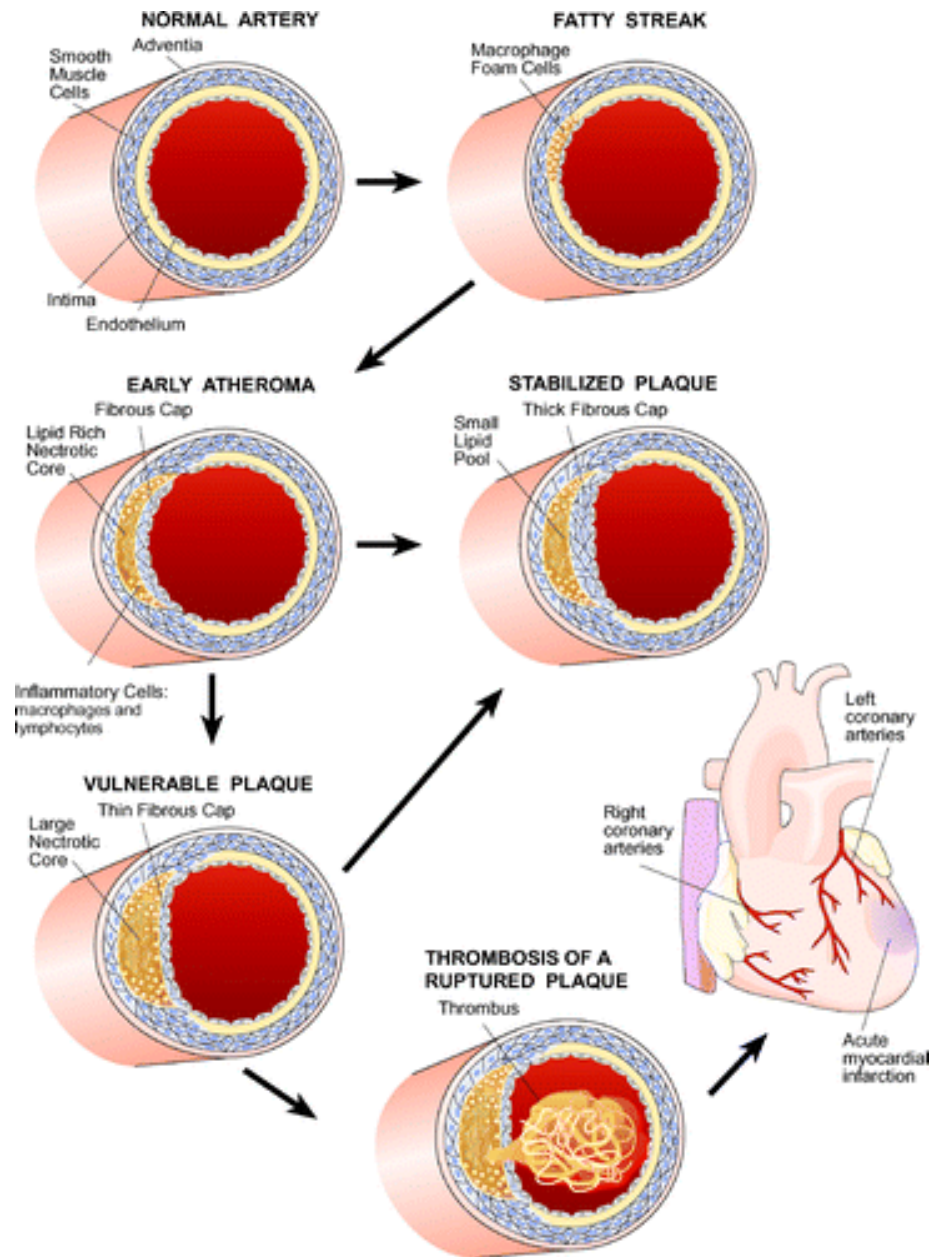


Figure 1-2. Progression of atherosclerosis. Taken from [19].

1.4 Coronary Artery Bypass Grafting

Coronary artery bypass grafting (CABG) has been a common surgical procedure since the 1960s [20]. CABG uses grafts to circumvent the occluded regions of the coronary arteries and restore the supply of nutrients to the heart. Currently, only autologous vessels—the saphenous veins, internal mammary arteries, or radial arteries—are used as grafts in this procedure. While the internal mammary arteries have been shown to be the most effective autologous graft with the longest patency and survival, most patients require supplemental graft sources because multiple vessels require grafts for treatment [21]. Following implantation, the veins are exposed to significantly different mechanical environments from their native state. The coronary artery is exposed to significantly higher mean pressures and shear stresses. Blood vessels generally adapt to their environment by remodeling the ECM to lessen the mechanical burden on the cells. The saphenous vein is under lower loading and is significantly thinner than the coronary artery; thus, when exposed to similar loading to that of the coronary arteries, saphenous veins experience significantly higher circumferential stresses across the wall. While the radial artery experiences less dramatic changes in mechanical loading following implantation, the flow rates are still much higher and there are still complications due to compliance mismatch and differences in the mechanical environment [21-23]. Therefore, long-term patency of autologous grafts still appears to be suboptimal due to unsuitable mechanical properties [3-5]. The development of a suitable tissue engineered graft serves as a promising alternative for autologous grafts during coronary bypass surgery [24-27].

1.5 Tissue Engineered Arteries

There have been many advances in the development a small diameter TEBV since the first report by Weinberg and Bell in 1986, which contained an adventitia layer of fibroblasts, a media with SMCs, and a lumen seeded with a monolayer of ECs in a collagen-based TEBV [28]. Even though these vessels were not able to withstand physiological conditions, the feasibility of developing a vascular replacement in vitro was demonstrated. Since then, there have been numerous advances in the field.

Several tissue engineering strategies show great promise for vascular applications, including TEBVs that are gel-derived [28], cell self-assembly derived [29], biodegradable scaffold-derived [30], and decellularized native tissue [31]. Each of these approaches has inherent advantages and disadvantages. For example, whereas gel-derived constructs can be molded into complex geometries and require relatively shorter culture times compared to other approaches, these constructs often have a lower strength compared to the synthetic biodegradable scaffold or self-assembly derived constructs.

1.5.1 Gel-derived Scaffolds

The gel-derived method involves the combination of reconstituted matrix with vascular cells. This solution of cells and ECM proteins is poured into a vascular mold and allowed to solidify. The gel is then cultured in cell culture media where the cells compact and reorient the existing matrix and synthesize new matrix, making the vessel stronger over time. Several attempts at increasing the strength of gel-derived TEBVs such as the use of

crosslinking agents, biochemical stimulation, and mechanical stimulation have been made [32-35]. While each of these methods lead to an increase in the overall mechanical properties, none are suitable for coronary replacement due to lack of strength.

1.5.2 Cell Self-Assembly

The cell self-assembly method involves the use of vascular cells, either fibroblasts or SMCs, grown to confluence and then cultured for several weeks. During this time, the cells synthesize ECM and start to form sheets. These sheets can then be peeled off and rolled up around an inner mandrel forming a tube. This tube is then cultured for approximately 8 weeks. During this time, the cells align circumferentially and synthesize more ECM, which leads to a fusion of the individual layers that forms a vessel [29]. These vessels have been demonstrated to have burst pressures and compliances comparable to those of native vessels [36]. However, additional mechanical testing [37], unfavorable initial clinical trial results [38, 39], and long culture times prior to implantation suggest that vessels made using the cell self-assembly method may not be a feasible replacement alternative to autologous grafts.

1.5.3 Synthetic Biodegradable Scaffolds

The scaffold-derived approach involves seeding vascular cells onto a synthetic biodegradable scaffold. As the scaffold degrades, the cells synthesize ECM, resulting in a final vessel consisting of mostly cells and cellular ECM [30]. The scaffold-derived approach is particularly attractive because of their tunable mechanical properties and the

potential for off the shelf-availability. However, there have been some issues arising from degradation byproducts and an immune response to the material.

Polyglycolic acid (PGA) is the most commonly used biodegradable scaffold, due to its high porosity and ease of use [40]. However, due to its rapid resorption rates, PGA is difficult to use because it can degrade before the cells have an opportunity to stabilize the vessel. In addition, the mechanical properties of PGA scaffold have been shown to be significantly lower than those of native tissues [41]. Various attempts have been made to combine other polymer with PGA to decrease its rate of resorption [35, 42-44]. There has been some success using PGA with ϵ -caprolactone or L-lactide in clinical trials in pediatric patients with congenital heart defects [45, 46]. However, these grafts were implanted in the low pressure system because they lack the mechanical properties to serve as a coronary replacement.

1.5.4 Decellularized Tissue Scaffolds

The use of decellularized tissues is one of the most common current approaches to tissue engineering. Removal of the cells reduces the potential of an immune response following implantation, while maintaining the native ECM structure of the tissue. Following decellularization, the tissue can then be reseeded with autologous cells for better immunocompatibility [47]. This method has been used on human saphenous veins to demonstrate feasibility and has been shown to have short term patency in vivo [48]. The use of decellularized tissue is a particularly promising approach because it does not require long waiting times while the vessel develops and the cells synthesize their own

matrix. This reduces the waiting time from months to days, making these grafts more likely candidates for CABG. However, it has also been shown that removal of the cells from the native vessels leads to an increase in the stiffness of the artery [49, 50], changes in the crimping and packing of collagen, and a decrease in proteoglycan density [51]. In addition, an immune response could possibly be elicited from the use of decellularized xenografts and the harsh chemicals used in the decellularization process can affect the mechanical properties of the vessel [52].

1.6 Effects of Stresses on Remodeling

In vivo, arteries are exposed to constant multi-axial mechanical loading. The vascular wall is exposed to cyclic circumferential stress and luminal shear stress due to pulsatile blood pressure and flow and an axial load due to tethering of the arterial wall to surrounding perivascular tissue (Figure 1-3). The values of these stresses can be estimated by assuming the vessel is a straight cylindrical segment [53]. The equations for the mean wall shear stress (τ_w), mean circumferential stress (σ_θ) and mean axial stress (σ_z), homeostatic values in humans are

$$\tau_w = \frac{4\mu Q}{\pi a^3} \approx 1.5 \text{ Pa} , \quad \sigma_\theta = \frac{Pa}{h} \approx 150 \text{ kPa} , \quad \text{and} \quad \sigma_z = \frac{f}{\pi h(2a+h)} \approx 150 \text{ kPa}$$

where Q is the luminal blood flow rate, P is the transmural pressure, f is the axial force, a is the luminal radius, h is the thickness of the vessel wall, and μ is the viscosity of blood.

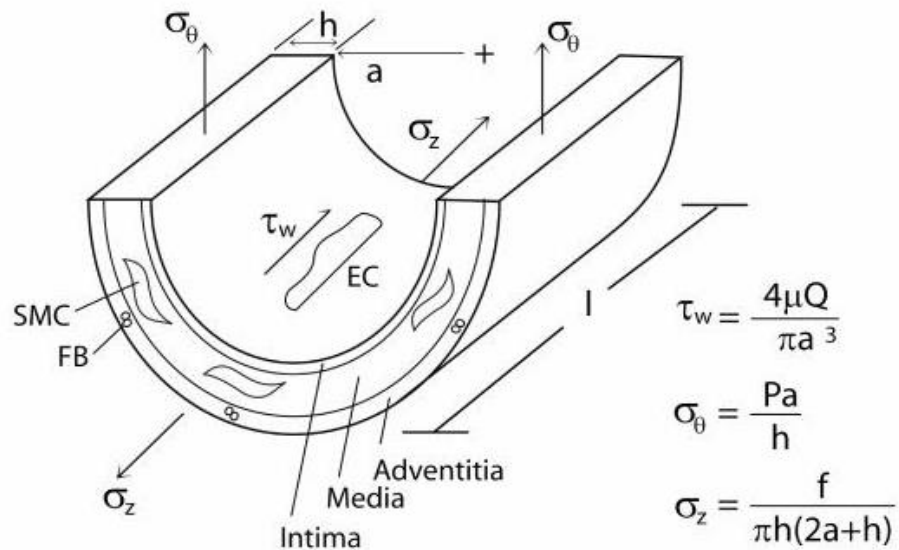


Figure 1-3. Forces on the the vascular wall. The blood vessel is exposed to three stresses: circumferential, axial, and shear. Taken from [53].

In healthy blood vessels, cells respond and remodel in response to mechanical forces including pulsatile pressure, flow, and axial load. These responses appear to be aimed towards maintaining a state of target local stress values [54]. Native arteries adjust to changes in their mechanical environment, such as changes in flow [55-59] and pressure [60, 61] by adjusting their inner diameter initially and intimal thickening long term, and axial stress by longitudinal lengthening [53, 62-65].

These responses can also be maladaptive in response to pathologic conditions. The remodeling that occurs in response to hypertension can lead to other secondary conditions, such as atherosclerosis or aneurysm formation [66]. It has also been shown that the compliance of native arteries significantly decreases with increasing heart rate

[67, 68], suggesting a critical role of cyclic strain frequency in the vascular adaptation response to mechanical loading [69].

While the mean stresses can be calculated using equations (1), constitutive equations are necessary to describe the stress distribution throughout the vessel wall. It appears that remodeling tends to be aimed towards maintaining homeostatic local stresses throughout the native blood vessel wall [70]. Cells sense changes in their mechanical environment through adhesive surface receptors [71] and respond to any perturbations in from the homeostatic environment through morphologic and functional changes [72]. For example, cellular responses to changes in mechanical stimuli include increased or decreased expression of ECM proteins, ECM degrading enzymes, and vasoactive molecules, which are all aimed at cellular adaptation to changes in the local stresses from the homeostatic values. While the mean stresses can be calculated using equations (1), it is ultimately necessary to include mathematical models to determine the local distribution of stresses across the vascular wall.

TEBVs appear to also respond to altered mechanical loads. Several studies have shown an increase in collagen production of TEBVs in response to cyclic strain as compared to unstrained or static strain [34, 73-75]. An increase in MMP-2 activity in response to cyclic strain was also seen. Even though MMP-2 activity is associated with ECM degradation, blocking MMP resulted in a block of compaction as well [32, 76], suggesting that MMP activity is necessary for remodeling and strengthening of the vessel. It has also been demonstrated that an incremental strain increase leads to a higher

UTS, modulus, and higher rates of collagen production as compared to cyclic strain of constant amplitude [35].

1.7 Theoretical Modeling

1.7.1 Modeling of Native Blood Vessels

It is well known that cells respond to changes in their local mechanical environment. Given that the local growth and remodeling response correlates well with the local stresses, which cannot be directly measured, models are necessary to describe the material behavior throughout the arterial wall and calculate these stresses. There are two general approaches to modeling the mechanical behavior of blood vessels – phenomenological and constitutive models. Phenomenological models take into account the bulk mechanical behavior of the tissue [77], while constitutive models take into account the microstructure of the artery and correlate physical attributes to the mechanical behavior of the artery [78]. While microstructural models are preferable to phenomenological models, it is difficult to design experiments to directly relate microstructural components with the mechanical properties of the tissue [79].

1.7.2 Mechanical Properties of Collagen-based TEBVs

While the mechanical properties of TEBVs are not yet suitable for implantation, it is important to characterize these properties to motivate strategies to improve the mechanical properties during TEBV development. The two most common methods for mechanical testing of vascular tissue are uniaxial ring tests and burst pressure testing.

1.7.2.1 Uniaxial Ring Tests

Uniaxial ring tests are more typically used to test the mechanical properties of TEBVs, since they are easier to run, require less tissue per experiment, and the results are easier to interpret. Typically, the vessel is cut into equal sized rings and the rings are mounted onto a testing device. The ring is then monotonically stretched until failure, while the force and extension are recorded [34, 74]. Since collagen gels undergo large deformations, it is necessary to track markers on the tissue to obtain accurate strain measurement. A typical nominal stress-strain curve for a collagen-based TEBV is shown in Figure 1-4, values for modulus, yield stress, and ultimate stress can be obtained from these tests. The modulus is defined as the slope of the linear stress-strain region, the yield stress is the point where the linear region changes by more than 10%, and the ultimate stress is the maximum stress. The test demonstrates a nonlinear loading profile to the ultimate stress, followed by a decrease in loading until failure.

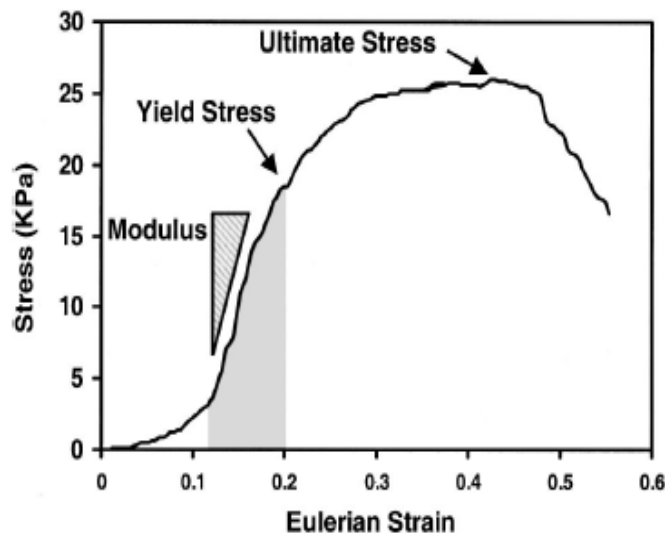


Figure 1-4. Typical nominal stress-Eulerian strain curve for uniaxial (ring) tests. Figure taken from Seliktar *et al* [74].

1.7.2.2 Burst Pressure Tests

Burst pressure testing of native blood vessels or vascular grafts is frequently performed to characterize the material properties of the vessel. While burst pressure can be a good indicator of the vessels' mechanical properties, the method of pressurization and the pressurization rate have a significant impact on the obtained burst pressure [80].

1.7.2.3 Biaxial Tests

Since uniaxial tests do not provide information on the mechanical properties in the axial direction and burst pressure tests typically only record the pressure at failure, biaxial tests are necessary to perform accurate stress analysis. Due to the cylindrical geometry of vessel, pressure-diameter and force-length data are typically obtained during biaxial tests [81, 82]. In native vessels, preconditioning is usually performed prior to testing. Preconditioning involves cycles of loading and unloading until the stress-strain response becomes repeatable [83]. This stress-strain response occurs due to internal structural changes that occur initially until eventually until steady state is reached when no further structural changes occur and the cycles become repeatable [84]. Collagen gels do not exhibit this same behavior; the stress-strain response does not become repeatable after cyclic loading, even under modest loads [85-87].

1.7.2.4 Changes in the Mechanical Properties of Collagen-based TEBVs over Time in Culture

Over the time course of development of cell-seeded collagen-based TEBVs the cells contract and orient the existing collagen matrix while synthesizing new matrix material, leading to a denser and stronger vessel [88]. Mechanical stimulation of the vessels induces cell and matrix alignment in the direction of applied the load [89-91].

Geometrically inducing circumferential cellular alignment by imposing boundary conditions increases the circumferential tensile strength and decreases the circumferential extensibility of the vessel [74, 82, 92].

1.7.3 Necessity for Modeling of TEBVs

Though it has been shown that mechanical conditioning, such as cyclic stretching, stimulates remodeling of collagen derived TEBVs and consequently improves their mechanical properties, mechanical loading of gel-derived TEBVs can also induce plastic deformations. In addition, interpretation of data in the literature is difficult due to the large number of factors that can be varied during collagen gel culture. For example, Isenberg and Tranquillo [34] demonstrated that the amplitude of strain, and parameters related to the pulse frequency and shape of the pulse waveform are important variables regulating cell-mediated changes in TEBV mechanical properties. These results suggest that modeling is ultimately necessary for understanding the combined and individual effects of all of these factors. Use of this model may be exploited to design loading strategies to allow for direct multi-axial stimulation of collagen gel-based TEBVs and reduce requisite culture times. While a microstructural model that could quantify the changes in the microstructural content and organization during damage and plastic deformation is ultimately necessary, obtaining the mechanical properties and microstructural properties simultaneously is very difficult. However, a phenomenological model that characterizes the mechanisms of damage and plasticity can help motivate new experiments to elucidate the effects of individual tissue components on the overall

mechanical properties of the tissue. The theoretical framework proposed in this work combines the concepts of volumetric growth and continuum damage mechanics.

1.7.3.1 Volumetric Growth

The volumetric growth approach, developed by Rodriguez et al. [93], describes growth (referring to any change in volume, i.e. compaction) via the evolution of the stress-free state. The original stress-free reference state is cut into discontinuous (and fictitious) elements and each element grows independently over time. When these elements are reassembled, they are not always compatible, which induces residual stresses. The elastic deformation gradient tensor is then referenced to the zero-stress configuration.

1.7.3.2 Damage Mechanics

Damage is the process of microstructural change of materials that leads to a loss in mechanical strength due to loading. Generally, materials can damage under monotonic loading, creep (when the load exceeds a critical value), or cyclic loading (fatigue) [94]. In this work, the theoretical framework of Kachanov [95, 96] and Rabotnov [97] is employed and anisotropic damage is considered. An effective stress is introduced, which accounts for the fact that damaged material cannot bear any loads. A damage variable is used to represent the loss in effective area due to anisotropic damage. It is assumed that the only effects of damage are on the effective stress, which can replace the undamaged stress in the constitutive laws [98]. Plasticity is the change in the stress-free geometric properties, which occurs as a result of permanent slips of molecules. Yield stress is defined as the stress beyond which plasticity ensues [94]. Since collagen gels are characterized by compaction (volume change), damage, and plasticity, a combination of

the concepts from volumetric growth and continuum damage mechanics are used in this study.

1.8 Summary

The design of a TEBV that can be successfully used as a bypass graft requires that the vessel have suitable mechanical properties, non-thrombogenic luminal surface, and low immunoreactivity or graft rejection. a compliance similar to that of native vessels to prevent compliance mismatch, not exhibit significant plastic deformation under loading, and be able to withstand the imposed mechanical loads without failure. To date, there is no tissue engineered vascular graft that meets these requirements. Appropriate experimental and mathematical models are necessary to better understand and predict these mechanical properties and ultimate graft failure.

1.9 References

1. Roger, V.L., et al., *Heart disease and stroke statistics--2012 update: a report from the American Heart Association*. Circulation, 2012. **125**(1): p. e2-e220.
2. Ross, R., *Atherosclerosis is an inflammatory disease*. Am Heart J, 1999. **138**(5 Pt 2): p. S419-20.
3. Alderman, E.L., et al., *Ten-year follow-up of survival and myocardial infarction in the randomized Coronary Artery Surgery Study*. Circulation, 1990. **82**(5): p. 1629-46.
4. Malenka, D.J., et al., *Comparing long-term survival of patients with multivessel coronary disease after CABG or PCI: analysis of BARI-like patients in northern New England*. Circulation, 2005. **112**(9 Suppl): p. I371-6.
5. Yusuf, S., et al., *Effect of coronary artery bypass graft surgery on survival: overview of 10-year results from randomised trials by the Coronary Artery Bypass Graft Surgery Trialists Collaboration*. Lancet, 1994. **344**(8922): p. 563-70.

6. Darling, R.C. and R.R. Linton, *Durability of femoropopliteal reconstructions. Endarterectomy versus vein bypass grafts*. Am J Surg, 1972. **123**(4): p. 472-9.
7. Clayson, K.R., et al., *Arm veins for peripheral arterial reconstruction*. Arch Surg, 1976. **111**(11): p. 1276-80.
8. Ku, D.N. and R.C. Allen, *128.1 History of Vascular Grafts*. 2000.
9. Klinkert, P., et al., *Saphenous vein versus PTFE for above-knee femoropopliteal bypass. A review of the literature*. European journal of vascular and endovascular surgery, 2004. **27**(4): p. 357-362.
10. Budd, J., et al., *Infrainguinal bypass surgery: factors determining late graft patency*. British journal of surgery, 2005. **77**(12): p. 1382-1387.
11. Plecha, E., et al., *Femoropopliteal bypass revisited: an analysis of 138 cases*. Cardiovascular Surgery, 1996. **4**(2): p. 195-199.
12. Mitchell, S.L. and L.E. Niklason, *Requirements for growing tissue-engineered vascular grafts*. Cardiovascular Pathology, 2003. **12**(2): p. 59-64.
13. Stergiopoulos, N., et al., *Assessing the homogeneity of the elastic properties and composition of the pig aortic media*. J Vasc Res, 2001. **38**(3): p. 237-46.
14. Roach, M.R. and A.C. Burton, *The reason for the shape of the distensibility curves of arteries*. Can J Biochem Physiol, 1957. **35**(8): p. 681-90.
15. Fox, S.I., *Human physiology*. 2004: McGraw-Hill.
16. Malek, A.M., S.L. Alper, and S. Izumo, *Hemodynamic shear stress and its role in atherosclerosis*. JAMA: the journal of the American Medical Association, 1999. **282**(21): p. 2035-2042.
17. Poole-Wilson, P.A., *Global Differences in Atherosclerosis*. Cardiovascular Medicine, 2007: p. 653-658.
18. Ross, R., *Atherosclerosis--an inflammatory disease*. N Engl J Med, 1999. **340**(2): p. 115-26.
19. Lusis, A.J., R. Mar, and P. Pajukanta, *Genetics of atherosclerosis*. Annu. Rev. Genomics Hum. Genet., 2004. **5**: p. 189-218.
20. Favaloro, R.G., *Saphenous vein autograft replacement of severe segmental coronary artery occlusion: operative technique*. The Annals of thoracic surgery, 1968. **5**(4): p. 334.

21. Athanasiou, T., et al., *Radial artery versus saphenous vein conduits for coronary artery bypass surgery: forty years of competition—which conduit offers better patency? A systematic review and meta-analysis*. European Journal of Cardio-Thoracic Surgery, 2011. **40**(1): p. 208-220.
22. Chamiot-Clerc, P., et al., *Comparative reactivity and mechanical properties of human isolated internal mammary and radial arteries*. Cardiovascular research, 1998. **37**(3): p. 811-819.
23. Cohen, G., et al., *The radial artery versus the saphenous vein graft in contemporary CABG: a case-matched study*. The Annals of thoracic surgery, 2001. **71**(1): p. 180-186.
24. Nerem, R.M. and D. Seliktar, *Vascular tissue engineering*. Annu Rev Biomed Eng, 2001. **3**: p. 225-43.
25. Isenberg, B.C., C. Williams, and R.T. Tranquillo, *Small-diameter artificial arteries engineered in vitro*. Circulation research, 2006. **98**(1): p. 25-35.
26. Cleary, M.A., et al., *Vascular tissue engineering: the next generation*. Trends in Molecular Medicine, 2012.
27. Peck, M., et al., *The evolution of vascular tissue engineering and current state of the art*. Cells Tissues Organs, 2012. **195**(1-2): p. 144-158.
28. Weinberg, C.B. and E. Bell, *A blood vessel model constructed from collagen and cultured vascular cells*. Science, 1986. **231**(4736): p. 397-400.
29. L'Heureux, N., et al., *A completely biological tissue-engineered human blood vessel*. FASEB J, 1998. **12**(1): p. 47-56.
30. Niklason, L.E., et al., *Functional arteries grown in vitro*. Science, 1999. **284**(5413): p. 489-93.
31. Quint, C., et al., *Decellularized tissue-engineered blood vessel as an arterial conduit*. Proceedings of the National Academy of Sciences, 2011. **108**(22): p. 9214-9219.
32. Seliktar, D., R.M. Nerem, and Z.S. Galis, *Mechanical strain-stimulated remodeling of tissue-engineered blood vessel constructs*. Tissue Eng, 2003. **9**(4): p. 657-66.
33. Stegemann, J.P. and R.M. Nerem, *Phenotype modulation in vascular tissue engineering using biochemical and mechanical stimulation*. Annals of biomedical engineering, 2003. **31**(4): p. 391-402.

34. Isenberg, B.C. and R.T. Tranquillo, *Long-term cyclic distention enhances the mechanical properties of collagen-based media-equivalents*. Ann Biomed Eng, 2003. **31**(8): p. 937-49.
35. Syedain, Z.H., J.S. Weinberg, and R.T. Tranquillo, *Cyclic distension of fibrin-based tissue constructs: Evidence of adaptation during growth of engineered connective tissue*. Proceedings of the National Academy of Sciences of the United States of America, 2008. **105**(18): p. 6537-6542.
36. Konig, G., et al., *Mechanical properties of completely autologous human tissue engineered blood vessels compared to human saphenous vein and mammary artery*. Biomaterials, 2009. **30**(8): p. 1542-1550.
37. Zaucha, M.T., et al., *Biaxial biomechanical properties of self-assembly tissue-engineered blood vessels*. Journal of The Royal Society Interface, 2011. **8**(55): p. 244-256.
38. L'Heureux, N., T.N. McAllister, and L.M. de la Fuente, *Tissue-engineered blood vessel for adult arterial revascularization*. New England Journal of Medicine, 2007. **357**(14): p. 1451-1453.
39. McAllister, T.N., et al., *Effectiveness of haemodialysis access with an autologous tissue-engineered vascular graft: a multicentre cohort study*. The Lancet, 2009. **373**(9673): p. 1440-1446.
40. Kakisis, J.D., et al., *Artificial blood vessel: the Holy Grail of peripheral vascular surgery*. Journal of vascular surgery, 2005. **41**(2): p. 349-354.
41. Dahl, S.L., et al., *Mechanical properties and compositions of tissue engineered and native arteries*. Annals of biomedical engineering, 2007. **35**(3): p. 348-355.
42. Kim, B.S., et al., *Engineered smooth muscle tissues: regulating cell phenotype with the scaffold*. Experimental cell research, 1999. **251**(2): p. 318-328.
43. Shum-Tim, D., et al., *Tissue engineering of autologous aorta using a new biodegradable polymer*. The Annals of thoracic surgery, 1999. **68**(6): p. 2298-2304.
44. Wake, M.C., P.K. Gupta, and A.G. Mikos, *Fabrication of pliable biodegradable polymer foams to engineer soft tissues*. Cell transplantation, 1996. **5**(4): p. 465-473.
45. Hibino, N., et al., *Late-term results of tissue-engineered vascular grafts in humans*. The Journal of thoracic and cardiovascular surgery, 2010. **139**(2): p. 431-436. e2.

46. Shin'oka, T., et al., *Midterm clinical result of tissue-engineered vascular autografts seeded with autologous bone marrow cells*. The Journal of thoracic and cardiovascular surgery, 2005. **129**(6): p. 1330-1338.
47. Gilbert, T.W., T.L. Sellaro, and S.F. Badylak, *Decellularization of tissues and organs*. Biomaterials, 2006. **27**(19): p. 3675-3683.
48. Schaner, P.J., et al., *Decellularized vein as a potential scaffold for vascular tissue engineering*. Journal of vascular surgery, 2004. **40**(1): p. 146-153.
49. Roy, S., P. Silacci, and N. Stergiopoulos, *Biomechanical properties of decellularized porcine common carotid arteries*. American Journal of Physiology-Heart and Circulatory Physiology, 2005. **289**(4): p. H1567-H1576.
50. Fitzpatrick, J.C., P.M. Clark, and F.M. Capaldi, *Effect of decellularization protocol on the mechanical behavior of porcine descending aorta*. International journal of biomaterials, 2010. **2010**.
51. Williams, C., et al., *Altered structural and mechanical properties in decellularized rabbit carotid arteries*. Acta biomaterialia, 2009. **5**(4): p. 993-1005.
52. Kurobe, H., et al., *Concise Review: Tissue-Engineered Vascular Grafts for Cardiac Surgery: Past, Present, and Future*. Stem cells translational medicine, 2012. **1**(7): p. 566-571.
53. Humphrey, J.D., et al., *Fundamental role of axial stress in compensatory adaptations by arteries*. J Biomech, 2009. **42**(1): p. 1-8.
54. Humphrey, J.D., *Continuum biomechanics of soft biological tissues*. Proceedings of the Royal Society a-Mathematical Physical and Engineering Sciences, 2003. **459**(2029): p. 3-46.
55. Glagov, S., et al., *Mechanical functional role of non-atherosclerotic intimal thickening*. Front Med Biol Eng, 1993. **5**(1): p. 37-43.
56. Langille, B.L. and F. O'Donnell, *Reductions in arterial diameter produced by chronic decreases in blood flow are endothelium-dependent*. Science, 1986. **231**(4736): p. 405-7.
57. Langille, B.L., M.P. Bendeck, and F.W. Keeley, *Adaptations of carotid arteries of young and mature rabbits to reduced carotid blood flow*. Am J Physiol, 1989. **256**(4 Pt 2): p. H931-9.

58. Sho, E., et al., *Arterial enlargement, tortuosity, and intimal thickening in response to sequential exposure to high and low wall shear stress*. J Vasc Surg, 2004. **39**(3): p. 601-12.
59. Kamiya, A. and T. Togawa, *Adaptive regulation of wall shear stress to flow change in the canine carotid artery*. Am J Physiol 1980. **239**.
60. Clark, J.M. and S. Glagov, *Structural integration of the arterial wall. I. Relationships and attachments of medial smooth muscle cells in normally distended and hyperdistended aortas*. Lab Invest, 1979. **40**(5): p. 587-602.
61. Matsumoto, T. and K. Hayashi, *Mechanical and dimensional adaptation of rat aorta to hypertension*. Journal of biomechanical engineering, 1994. **116**(3): p. 278.
62. Clerin, V., et al., *Tissue engineering of arteries by directed remodeling of intact arterial segments*. Tissue Eng, 2003. **9**(3): p. 461-72.
63. Jackson, Z.S., A.I. Gotlieb, and B.L. Langille, *Wall tissue remodeling regulates longitudinal tension in arteries*. Circ Res, 2002. **90**(8): p. 918-25.
64. Han, H.C., D.N. Ku, and R.P. Vito, *Arterial wall adaptation under elevated longitudinal stretch in organ culture*. Ann Biomed Eng, 2003. **31**(4): p. 403-11.
65. Cardamone, L., et al., *Origin of axial prestretch and residual stress in arteries*. Biomechanics and modeling in mechanobiology, 2009. **8**(6): p. 431-446.
66. Taylor, W.R., *Hypertensive vascular disease and inflammation: mechanical and humoral mechanisms*. Current hypertension reports, 1999. **1**(1): p. 96-101.
67. Mangoni, A.A., et al., *Heart rate-dependence of arterial distensibility in vivo*. Journal of hypertension, 1996. **14**(7): p. 897.
68. Mircoli, L., et al., *Heart rate-dependent stiffening of large arteries in intact and sympathectomized rats*. Hypertension, 1999. **34**(4): p. 598-602.
69. Zieman, S.J., V. Melenovsky, and D.A. Kass, *Mechanisms, pathophysiology, and therapy of arterial stiffness*. Arteriosclerosis, thrombosis, and vascular biology, 2005. **25**(5): p. 932-943.
70. Matsumoto, T. and K. Hayashi, *Stress and strain distribution in hypertensive and normotensive rat aorta considering residual strain*. Journal of biomechanical engineering, 1996. **118**(1): p. 62.
71. EGB, K.A. and C. Ingegneria Genetica, *Mechanotransduction across the cell surface and through the cytoskeleton*. Science, 1993. **260**: p. 21.

72. Davies, P.F., *Flow-mediated endothelial mechanotransduction*. *Physiological reviews*, 1995. **75**(3): p. 519.
73. Kim, B.S., et al., *Cyclic mechanical strain regulates the development of engineered smooth muscle tissue*. *Nat Biotechnol*, 1999. **17**(10): p. 979-83.
74. Seliktar, D., et al., *Dynamic mechanical conditioning of collagen-gel blood vessel constructs induces remodeling in vitro*. *Ann Biomed Eng*, 2000. **28**(4): p. 351-62.
75. Schutte, S.C., et al., *Cyclic strain improves strength and function of a collagen-based tissue-engineered vascular media*. *Tissue Engineering Part A*, 2010. **16**(10): p. 3149-3157.
76. Seliktar, D., R.M. Nerem, and Z.S. Galis, *The role of matrix metalloproteinase-2 in the remodeling of cell-seeded vascular constructs subjected to cyclic strain*. *Ann Biomed Eng*, 2001. **29**(11): p. 923-34.
77. Chuong, C. and Y. Fung, *On residual stresses in arteries*. *Journal of biomechanical engineering*, 1986. **108**(2): p. 189.
78. Holzapfel, G.A., T.C. Gasser, and R.W. Ogden, *A new constitutive framework for arterial wall mechanics and a comparative study of material models*. *Journal of elasticity*, 2000. **61**(1): p. 1-48.
79. Robertson, A.M., M.R. Hill, and D. Li, *Structurally motivated damage models for arterial walls. Theory and application*, in *Modeling of Physiological Flows*. 2012, Springer. p. 143-185.
80. Sarkar, S., et al., *Critical parameter of burst pressure measurement in development of bypass grafts is highly dependent on methodology used*. *Journal of vascular surgery*, 2006. **44**(4): p. 846-852.
81. Gleason, R., et al., *A multiaxial computer-controlled organ culture and biomechanical device for mouse carotid arteries*. *Journal of biomechanical engineering*, 2004. **126**(6): p. 787.
82. Wagenseil, J.E., E.L. Elson, and R.J. Okamoto, *Cell orientation influences the biaxial mechanical properties of fibroblast populated collagen vessels*. *Annals of biomedical engineering*, 2004. **32**(5): p. 720-731.
83. Humphrey, J.D., *Cardiovascular solid mechanics: cells, tissues, and organs*. 2002: Springer.
84. Fung, Y.C., *Biomechanics: Mechanical Properties of Living Tissues*. 1993: Springer.

85. Wagenseil, J., et al., *One-dimensional viscoelastic behavior of fibroblast populated collagen matrices*. Journal of biomechanical engineering, 2003. **125**(5): p. 719.
86. Wille, J.J., E.L. Elson, and R.J. Okamoto, *Cellular and matrix mechanics of bioartificial tissues during continuous cyclic stretch*. Annals of biomedical engineering, 2006. **34**(11): p. 1678-1690.
87. Zaucha, M.T., et al., *A novel cylindrical biaxial computer-controlled bioreactor and biomechanical testing device for vascular tissue engineering*. Tissue Eng Part A, 2009. **15**(11): p. 3331-40.
88. Feng, Z., et al., *Investigation on the mechanical properties of contracted collagen gels as a scaffold for tissue engineering*. Artificial organs, 2003. **27**(1): p. 84-91.
89. Kanda, K., T. Matsuda, and T. Oka, *Mechanical stress induced cellular orientation and phenotypic modulation of 3-D cultured smooth muscle cells*. ASAIO journal, 1993. **39**(3): p. M691.
90. Kanda, K., T. Matsuda, and T. Oka, *In Vitro Reconstruction of Hybrid Vascular Tissue Hierarchic and Oriented Cell Layers*. ASAIO journal, 1993. **39**(3): p. M566.
91. Vader, D., et al., *Strain-induced alignment in collagen gels*. PLoS One, 2009. **4**(6): p. e5902.
92. Girton, T., T. Oegema, and R. Tranquillo, *Exploiting glycation to stiffen and strengthen tissue equivalents for tissue engineering*. Journal of biomedical materials research, 1999. **46**(1): p. 87-92.
93. Rodriguez, E.K., A. Hoger, and A.D. McCulloch, *Stress-dependent finite growth in soft elastic tissues*. J Biomech, 1994. **27**(4): p. 455-67.
94. Lemaître, J., *A course on damage mechanics*. 2nd rev. and enl. ed. 1996, Berlin ; New York: Springer. xix, 228 p.
95. Kachanov, L.M., *Introduction to continuum damage mechanics*. Mechanics of elastic stability. 1986, Dordrecht ; Boston: M. Nijhoff. x, 135 p.
96. Kachanov, L., *Time of the rupture process under creep conditions*. Isv. Akad. Nauk. SSR. Otd Tekh. Nauk, 1958. **8**: p. 26-31.
97. Rabotnov, Y.N. *Creep rupture*. 1968.

98. Chaboche, J. and C.D. Mechanics, *Part I-General Concepts*. Journal of applied mechanics, 1988. **55**: p. 59-64.

CHAPTER 2

SPECIFIC AIMS

2.1 Project Significance

There is a pressing clinical need to develop tissue engineered blood vessels (TEBVs) to treat multi-occlusive coronary and peripheral artery diseases. While there have been significant advances in the field of tissue engineering, autologous vessels are still primarily utilized as grafts during bypass surgeries. TEBVs lack long-term efficacy due to a variety of types of failures including aneurysmal dilations, thrombosis, and rupture, but the mechanisms of these failures are not well understood. In vitro mechanical testing may help to better understand these failure mechanisms. However, the typical mechanical tests lack standardized methodologies, thus results vary widely. For instance, burst pressure, a standard metric for assessing ultimate failure is highly dependent on the pressurization or strain rates for the same vessel. However, the strain rate is frequently not reported and results cannot be compared between studies. In addition, effects due to creep are frequently overlooked. Moreover, mechanical tests have demonstrated that cell-seeded TEBVs exhibit plastic deformation and damage even under modest loads. These effects are decreased over time in culture due to cell-mediated remodeling of the ECM. Improving the testing and characterization of TEBVs is critically important in decreasing the time necessary to validate the mechanical and functional responses of TEBVs, thus quickly moving TEBVs from the benchtop to the patient.

2.2 Project Objective

The overall goal of this study is to develop novel methods and mathematical models to study the mechanical properties and failure mechanisms of TEBVs. Appropriate mathematical models will help to better understand and predict temporal, biologically-mediated changes in the mechanical (functional) responses of the TEBVs. Furthermore, understanding the underlying mechanisms of TEBV failure will lead to a better understanding of what is ultimately necessary to develop a more practical TEBV design. The collagen gel-based TEBVs was used as a platform for this study, as they are widely used for fabricating TEBVs.

Mathematical models are powerful tools for understanding the full complexities of the combined effects of mechanically-mediated growth, remodeling, damage, and plasticity of gel-derived TEBVs. One of the main goals of this work is to develop a phenomenological mathematical model that can capture the salient features of the geometry and material properties, as well as the complexity of mechanically-induced changes during culture of collagen-based TEBVs.

2.3 Specific Aims and Hypotheses

2.3.1 Specific Aim 1

Develop a phenomenological model to predict mechanically-mediated growth, remodeling, damage, and plasticity of gel-derived tissue engineered blood vessels.

Hypothesis: a model combining the effects of growth, remodeling, plasticity, and damage will capture the salient features of the geometry and material properties of collagen-based TEBVs as the material evolves and changes over time.

2.3.2 Specific Aim 2

Develop an experimental platform to quantify damage and plasticity in gel-derived tissue engineered blood vessels.

Hypothesis: multi-axial monotonic loading, creep, and fatigue testing are necessary to fully characterize damage and plasticity properties and can be successfully performed on collagen-based TEBVs.

2.3.3 Specific Aim 3

Study the role of tissue transglutaminase cross-linking in reducing damage and plasticity of collagen gels.

Hypothesis: the addition of tissue transglutaminase to collagen gel-based TEBVs will reduce damage and plasticity, improving the overall strength and quality of the TEBVs, while maintaining the necessary biological support of the cells on the TEBVs.

Successful realization of these aims will provide a theoretical-experimental approach for the development of TEBVs. Since development often requires weeks or even months of culture time to generate one set of TEBVs under one set of experimental conditions, a theoretical approach will help cut down on the number of experiments that need to be performed. The proposed model (1) can be used to integrate seemingly diverse sets of data; (2) can be used for parametric studies to compare the consequences of competing hypotheses through time- and cost-efficient simulations; and (3) can guide the identification, performance, and interpretation of revealing experiments. Thus, mathematical models can help identify the most insightful experiments and quantities to be measured; ultimately reducing the overall number of experimental iterations.

CHAPTER 3

A PHENOMENOLOGICAL MODEL FOR MECHANICALLY-MEDIATED GROWTH, REMODELING, DAMAGE, AND PLASTICITY OF GEL-DERIVED TISSUE ENGINEERED BLOOD VESSELS*

3.1 Introduction

There is a great unmet clinical need to develop small diameter tissue engineered blood vessels (TEBVs) with low thrombogenicity and immune response, suitable mechanical properties, and a capacity to adapt to their environment [1-3]. Since the pioneering work by Weinberg and Bell [4], there have been tremendous advances towards this pursuit. Nevertheless, the need for a TEBV suitable as a coronary by-pass graft remains unmet. Biomechanical stimuli, such as cyclic strain, have been shown to stimulate remodeling of collagen gel-derived TEBVs to greatly improve their mechanical behavior [5]. It is now becoming clear that tissue engineered constructs adapt synergistically to specific combinations of multidirectional loading [6]. A critical gap remains, however, in understanding the role of multidirectional loading on TEBV remodeling.

* Modified from: J Raykin, AI Rachev, RL Gleason Jr. A phenomenological model for mechanically mediated growth, remodeling, damage, and plasticity of gel-derived tissue engineered blood vessels.

Several tissue engineering strategies show great promise for vascular applications, including gel-derived [4], biodegradable scaffold-derived [7], and cell self-assembly-derived [8] TEBVs. This study focuses on the gel-derived approach. Weinberg and Bell [4] pioneered the gel-derived approach by combining collagen gels with a Dacron mesh and showed that the burst pressure increased with increasing collagen concentrations from 2 to 5 mg/ml and burst pressure was the maximum at 30 days in culture. Kanda *et al.* [9] observed that both isometric loading and cyclic dynamical loading of collagen gel rings showed cellular and extracellular matrix alignment in the direction of loading. Seliktar *et al.* [5] showed that circumferential distension increased modulus, yield stress, ultimate tensile stress, and rates of compaction compared to static cultures; Seliktar *et al.* [10] report that these responses can be blocked by inhibiting expression of matrix metalloproteinases, thus this is an active cell-mediated adaptive response. Isenberg and Tranquillo [11] demonstrated that the amplitude of strain and parameters related to the pulse frequency and shape of the pulse waveform are important parameters regulating these cell-mediated changes in TEBV mechanical properties.

Isenberg and Tranquillo [11] said well that, “[a]s promising as [gel-derived TEBV] results may be, their interpretation is difficult due to a number of confounding factors”; they cite confounding factors such as degree of compaction prior to mechanical stimulation and plastic deformation due to loading. Interpretation of data from experiments that contain such confounding factors requires a predictive mathematical model. Towards this end, the purpose of this paper is to describe a theoretical framework suitable for quantifying mechanically-mediated growth and remodeling of gel-derived

TEBVs, while considering that (even under modest loading) the TEBVs experience plastic deformations and damage. Although a microstructurally-motivated model is ultimately required to understand the full complexities for growth, remodeling, damage, and plasticity of gel-derived TEBVs at multiple length scales, a purely phenomenological model will provide important guidance for designing experiments, interpreting experimental data, and motivating more detailed models.

In this work, a theoretical framework that combines the concepts of volumetric growth, plasticity, and continuum damage mechanics is described and several illustrative examples that mimic typical experiments presented in the literature are compared to model prediction. Illustrative simulations are used to demonstrate the capability of the proposed modeling framework to capture the salient features of growth, remodeling, damage, and plasticity by comparing simulation results to data from the literature; this work focuses on the results of Seliktar et al. [5], which provides the most comprehensive set of mechanical data currently available. One of the main utilities of theoretical models is to motivate experiments; thus, these illustrative simulations are used to highlight data that are currently lacking in the literature and to motivate a new experimental approach to mechanical conditioning of gel-derived TEBVs that may be employed to improve mechanical properties and reduce requisite culture times for the development of TEBVs.

3.2 Theoretical Framework

The major hypothesis of this study is that changes in the geometrical dimensions and mechanical properties of the gel-derived TEBV depend on the magnitude of the local

stress experienced by the tissue and the amplitude of the periodic circumferential stretching during dynamic conditioning. To test this hypothesis some theoretical predictions of a proposed phenomenological model are compared to the available experimental data in the literature. To build the model the kinematics of the TEBV are first defined and subsequently describe the constitutive formulation of the mechanical response of the TEBV is described. The derived equations are used in an illustrative example for examining the behavior of a TEBV on a rigid mandrel and on an elastic sleeve of periodically varying diameter.

3.2.1 Plasticity and Growth (Kinematics)

Consider a stress-free body $\beta_o(0)$ at time $t=0$ that is loaded to the configuration $\beta_\ell(t)$; the deformation gradient for the mapping of points from $\beta_o(0)$ to $\beta_\ell(t)$ is denoted \mathbf{F} (Figure 3.1). The transformation from $\beta_o(0)$ to $\beta_\ell(t)$ results predominately from three processes that can occur simultaneously: (i) an elastic deformation; (ii) a deformation due to plasticity; and (iii) a change in the configuration of an infinitesimal element caused by processes termed generally as growth.

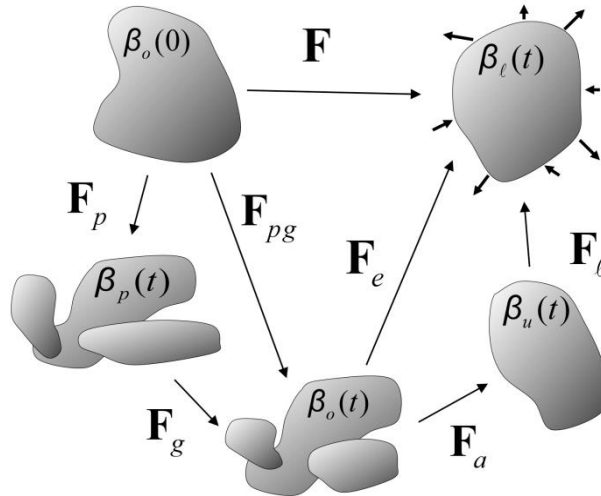


Figure 3-1. General schema for the kinematics of combined plasticity and volumetric growth.

If the applied loads induce stresses beyond the yield stress, *plasticity* will ensue. Plasticity is defined as a mechanically, but not biologically, mediated change in the stress-free (i.e., natural) configuration. Also, over time, these applied loads can induce a mechanically-mediated *growth*. Growth is defined as the mechano-biologically-mediated change of the stress-free configuration, including changes in volume (cf. [12]). Growth can occur via cell proliferation or hypertrophy and cell-mediated extracellular matrix production. More specifically the term growth refers to the case when the mass of the element increases, while the case of diminishing mass is considered as resorption. A special case of resorption can also occur via cell-mediated compaction; i.e., the rearrangement of cells and collagen or fibrin and extrusion of water from the construct that result in a diminishing of the volume. Thus, growth (or compaction) and plastic deformation may occur in parallel and result in an evolution of the natural configuration.

As plastic deformation and growth proceed in parallel, the traction-free (unloaded) configuration at time t denoted $\beta_u(t)$ is, in general, not stress-free; it contains residual stresses. However, $\beta_o(t)$ can be defined as the configuration wherein the local neighborhood about every point in the body is stress-free; this configuration consists of discontinuous (and fictitious) elements (see [12]). The mapping of points from $\beta_o(t)$ to $\beta_u(t)$, thereby assembling the discontinuous elements into the traction-free elements and producing residual stresses, has the deformation gradient \mathbf{F}_a . The mapping from the stress-free configuration $\beta_o(t)$ to the loaded configuration $\beta_\ell(t)$ has deformation gradient \mathbf{F}_e .

The mapping of points from $\beta_o(0)$ to $\beta_o(t)$, which defines the plastic deformation and the growth, can be decomposed into two deformations: the first accounting for the plastic deformation and the second accounting for the growth. Let the plastic deformation map points from the stress-free configuration $\beta_o(0)$ to an intermediate, stress-free configuration $\beta_p(t)$ (which consists of discontinuous (fictitious) elements) have deformation gradient \mathbf{F}_p . Let the growth deformation map points from $\beta_p(t)$ to $\beta_o(t)$ and have deformation gradient \mathbf{F}_g . Finally, $\mathbf{F}_{pg} = \mathbf{F}_g \mathbf{F}_p$ is defined, which accounts for the combined effect of growth and plastic deformations; therefore $\mathbf{F} = \mathbf{F}_e \mathbf{F}_g \mathbf{F}_p = \mathbf{F}_e \mathbf{F}_{pg}$.

3.2.2 Damage and Remodeling (Constitutive Equations)

In addition to growth (or compaction) and plastic deformations, mechanically-mediated mechanisms can result in the change in the local material response described by the

constitutive equation of the TEBV. It is well documented that mechanical stimuli can increase the effective elastic modulus of collagen gel-derived TEBVs [5, 11] through biological mechanisms; thus, *remodeling* is defined as mechano-biologically-mediated changes in material properties. In this phenomenological approach, such changes in material properties could be due to altered cellular contraction, altered mechanical properties of cells, extrusion of water leading to increased fraction of load bearing material, synthesis, degradation, or altered cross-linking of extracellular matrix, amongst many other mechanisms. In addition, if the applied loads produce stresses above some critical stress, local *damage* may occur. Damage is defined as the non-biologically, but mechanically-mediated, change in material properties.

3.2.2.1 Anisotropic Damage and Remodeling

With regard to changes in material behavior due to damage, the theoretical framework of Kachonov [13, 14] and Rabotnov [15] is employed here; anisotropic damage is considered. The Clausius-Duhem equation for isothermal mechanical processes requires that

$$-\frac{\partial W}{\partial t} + \frac{1}{2} \mathbf{S} \square \frac{\partial \mathbf{C}_e}{\partial t} = \Phi \geq 0, \quad (1)$$

where t is time, W is the strain energy density function (per unit volume), \mathbf{S} is the second Piola-Kirchhoff stress tensor, $\mathbf{C}_e = \mathbf{F}_e^T \mathbf{F}_e$ is the right Cauchy-Green strain tensor of the elastic deformation, and Φ is the local entropy production. Let $W = W(\mathbf{C}_e, \mathbf{D})$, where \mathbf{D} is a second order damage tensor; thus,

$$\left(-\frac{\partial W}{\partial \mathbf{C}_e} + \frac{1}{2} \mathbf{S} \right) \square \frac{\partial \mathbf{C}_e}{\partial t} + \frac{\partial W}{\partial \mathbf{D}} \square \frac{\partial \mathbf{D}}{\partial t} = \Phi \geq 0, \quad (1)$$

which is satisfied when

$$\mathbf{S} = 2 \frac{\partial W}{\partial \mathbf{C}_e} \quad \text{and} \quad \frac{\partial W}{\partial \mathbf{D}} \square \frac{\partial \mathbf{D}}{\partial t} \geq 0. \quad (2)$$

For $\partial W / \partial \mathbf{D} \geq 0$, equation (2) requires that $\partial \mathbf{D} / \partial t$ be non-negative; thus \mathbf{D} is constant or an increasing function.

With regard to changes in material behavior due to remodeling, a similar approach is used. Let $W = W(\mathbf{C}_e, \mathbf{M})$, where \mathbf{M} is a second order remodeling tensor; thus,

$$\left(-\frac{\partial W}{\partial \mathbf{C}_e} + \frac{1}{2} \mathbf{S} \right) \square \frac{\partial \mathbf{C}_e}{\partial t} + \frac{\partial W}{\partial \mathbf{M}} \square \frac{\partial \mathbf{M}}{\partial t} = \Phi \quad (3)$$

where, since remodeling is a biologically mediated process, the tissue is modeled as an open thermodynamical system; thus, the local entropy production need not be greater than or equal to zero. Let $\mathbf{S} = 2 \partial W / \partial \mathbf{C}_e$ with no constraint on the sign of $\partial \mathbf{M} / \partial t$.

In general, damage and remodeling may occur simultaneously; thus, let

$$W = W(\mathbf{C}_e, \mathbf{D}, \mathbf{M}) = W(\mathbf{C}_e, \Gamma), \quad (4)$$

where Γ is a tensor that accounts for the net effect of damage and remodeling. In this case equation **Error! Reference source not found.** becomes

$$\left(-\frac{\partial W}{\partial \mathbf{C}_e} + \frac{1}{2} \mathbf{S} \right) \square \frac{\partial \mathbf{C}_e}{\partial t} + \frac{\partial W}{\partial \mathbf{D}} \square \frac{\partial \mathbf{D}}{\partial t} + \frac{\partial W}{\partial \mathbf{M}} \square \frac{\partial \mathbf{M}}{\partial t} = \Phi, \quad (5)$$

which is satisfied with equations (2), with no constraint on the sign of $\partial \mathbf{M} / \partial t$. An illustrative functional form and material parameters of $W = W(\mathbf{C}_e, \Gamma)$ and $\Gamma(\mathbf{M}, \mathbf{D})$ are prescribed below.

3.3 Illustrative Example

Here culture of long, straight, thick-walled, incompressible, cylindrical gel-derived TEBVs under two different loading scenarios are considered; namely, static culture on a rigid mandrel and culture on a distensible tube. There is significant experimental data available in the literature, to which simulation results are compared. At any moment the TEBV is considered to be in an axisymmetric state of stress and strain which produce axisymmetric, but radially variable, plastic, growth, damage and remodeling responses. The general description of the geometrical and material alterations described above for the case when the introduced configurations $\beta_o(0)$ and $\beta_\ell(t)$ are referred to appropriate cylindrical coordinate systems (Figure 3.2).

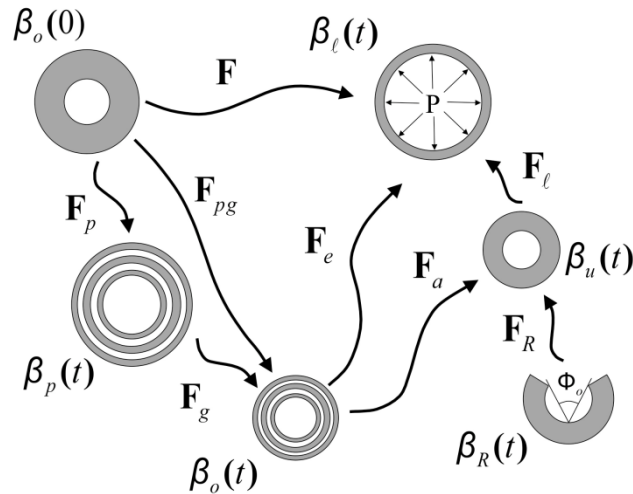


Figure 3-2. Kinematics of growth and plasticity of a thick-walled axisymmetric tube. Note that the configurations $\beta_p(t)$ and $\beta_o(t)$ consist of infinitesimally thin rings (each with thickness $dR_p(t)$) that pass through radial location $R(0)$ in $\beta_o(0)$; since each ring is infinitesimally thin and cannot support a residual stress.

3.3.1 Kinematics

The TEBV is modeled as a thick-walled tube with initial axial length $L(0)$ and initial radius $R(0) \in [A(0), B(0)]$, where $A(0)$ and $B(0)$ are the inner and outer radii. The plastic deformation gradient has components $[\mathbf{F}_p] = \text{diag}[\lambda_{pr}, \lambda_{p\theta}, \lambda_{pz}]$ where

$$\lambda_{pr} = \frac{\partial R_p(t)}{\partial R(0)}, \quad \lambda_{p\theta} = \frac{R_p(t)}{R(0)}, \quad \lambda_{pz} = \frac{L_p(t)}{L(0)}, \quad (6)$$

$L_p(t)$ is the length and $R_p(t)$ is the radius in β_p of the infinitesimally thin ring (with thickness $dR_p(t)$) that passes through radial location $R(0)$ in $\beta_o(0)$; since each ring is infinitesimally thin, they cannot support a residual stress. Note that $L_p(t)$ and $R_p(t)$ are functions of $R(0)$. In addition, the plastic deformation is considered isochoric; thus, $\det[\mathbf{F}_p] = 1$. The growth deformation gradient has components $[\mathbf{F}_g] = \text{diag}[\lambda_{gr}, \lambda_{g\theta}, \lambda_{gz}]$, where

$$\lambda_{gr} = \frac{\partial R(t)}{\partial R_p(t)}, \quad \lambda_{g\theta} = \frac{R(t)}{R_p(t)}, \quad \lambda_{gz} = \frac{L(t)}{L_p(t)}, \quad (7)$$

where $L(t)$ is the length and $R(t)$ is the radius of the cylindrical shell that passes through radial location $R_p(t)$ in $\beta_p(t)$ and $R(0)$ in $\beta_o(0)$; $L(t)$ and $R(t)$ are functions of $R_p(t)$ and thus functions of $R(0)$. The growth deformation from $\beta_o(0)$ to $\beta_o(t)$ is not isochoric; thus, $\det[\mathbf{F}_g] \neq 1$. By combining equations (6) and (7), the components of the deformation gradient combining plasticity and growth, $[\mathbf{F}_{pg}] = \text{diag}[\lambda_{pgr}, \lambda_{pg\theta}, \lambda_{pgz}]$, are given as

$$\lambda_{pgr} = \frac{\partial R(t)}{\partial R(0)}, \quad \lambda_{pg\theta} = \frac{R(t)}{R(0)}, \quad \lambda_{pgz} = \frac{L(t)}{L(0)}. \quad (8)$$

The elastic deformation gradient has components $[\mathbf{F}_e] = \text{diag}[\lambda_{er}, \lambda_{e\theta}, \lambda_{ez}]$, where

$$\lambda_{er} = \frac{\partial r(t)}{\partial R(t)}, \quad \lambda_{e\theta} = \frac{r(t)}{R(t)}, \quad \lambda_{ez} = \frac{\ell(t)}{L(t)}, \quad (9)$$

where $\ell(t)$ is the loaded length and $r(t)$ is the loaded radius in $\beta_\ell(t)$ of the cylindrical shell that passes through radial location $R(0)$ in $\beta_o(0)$. Finally, the constraint that the elastic deformation is assumed to be isochoric $\det(\mathbf{F}_e) = 1$, i.e. $\lambda_{er}\lambda_{e\theta}\lambda_{ez} = 1$, is enforced.

Thus, the overall deformation, from $\beta_o(0)$ to $\beta_\ell(t)$, is $[\mathbf{F}] = \text{diag}[\lambda_r, \lambda_\theta, \lambda_z]$, where

$$\lambda_r = \frac{\lambda_{gr}}{\lambda_{p\theta}\lambda_{pz}\lambda_{e\theta}\lambda_{ez}}, \quad \lambda_\theta = \lambda_{p\theta}\lambda_{g\theta}\lambda_{e\theta}, \quad \text{and} \quad \lambda_z = \lambda_{pz}\lambda_{gz}\lambda_{ez}, \quad (10)$$

which leads to an ordinary differential equation for $r(t)$ having solution

$$r^2 = \frac{2}{\lambda_z} \int_{R_i(0)}^{R(0)} \lambda_{pgr} \lambda_{pg\theta} \lambda_{pgz} R(0) dR(0) + \mu^2 R_i(0)^2. \quad (11)$$

where $R_i(0)$ is the initial stress-free inner radius and $\mu(t) = r(t)/R_i(0)$ is the ratio of the inner radii in the current loaded and the original stress-free configurations, respectively.

Given (11), the circumferential elastic stretch is

$$\lambda_{e\theta}^2 = \frac{1}{\lambda_{pg\theta}^2} \frac{r^2(t)}{R^2} = \frac{2}{\lambda_z \lambda_{pg\theta}^2 R^2} \int_{R_i(0)}^{R(0)} \lambda_{pgr} \lambda_{pg\theta} \lambda_{pgz} R(0) dR(0) + \frac{\mu^2 R_i(0)^2}{\lambda_{pg\theta}^2 R(0)^2}. \quad (12)$$

Finally, whereas $\beta_o(t)$ is truly stress-free and thus an appropriate configuration for stress analysis, it is not experimentally tractable. Thus, a nearly stress-free configuration that is experimentally tractable is considered here; namely, $\beta_R(t)$ which represents an unloaded ring with a single radial cut that relieves much of the residual stress present in the traction-free configuration. Typically, this configuration is characterized by its axial

length $L_R(t)$, the radius of the arch $R_R(t) \in [A_R(t), B_R(t)]$, where $A_R(t)$ and $B_R(t)$ are the inner and outer radii of the open arch, and an opening angle. Let the opening angle be denoted as Φ_o (Figure 3.2).

3.3.2 Constitutive Equation and Equilibrium

For these simulations, at any time, let the strain energy density function be

$$W(\mathbf{C}_e, \Gamma) = \frac{c}{2} (\Gamma : \mathbf{E}^2) \quad (13)$$

where c is a material parameter and $\mathbf{E} = (\mathbf{C}_e - \mathbf{I})/2$ is the Green strain; thus,

$$W = \frac{c}{2} (\Gamma_{rr} E_{rr}^2 + \Gamma_{\theta\theta} E_{\theta\theta}^2 + \Gamma_{zz} E_{zz}^2), \quad (14)$$

which is similar to the approach proposed by Fung *et al.* [16]. Let the net effect of damage and remodeling be given as the difference between remodeling and damage:

$$2\Gamma = (\mathbf{M} - \mathbf{D}). \quad (15)$$

At time $t = 0$, let $\mathbf{M} = \mathbf{I}$ and $\mathbf{D} = \mathbf{0}$; thus, $2\Gamma(t = 0) = \mathbf{I}$. The components of the Cauchy stress are

$$T_{ii} = -p + \hat{T}_{ii} \quad \text{where} \quad \hat{T}_{ii} = 2c\Gamma_{ii}(\lambda_{ei})^2[(\lambda_{ei}^2 - 1)/2], \quad (16)$$

where $i = r, \theta$, or z , p is a Lagrange multiplier that follows from incompressibility, and \hat{T}_{ii} are the components of the ‘extra’ stress due to the deformation; no summation is implied in equation (16). Thus, let

$$c_i = 2c\Gamma_{ii}; \quad (17)$$

c_i may be considered as a material parameter that evolves with remodeling and damage. In general, $\Gamma_{ii} \in [0, \Gamma_{\max}]$, where $\Gamma_{ii} = 0$ corresponds to completely damaged material and Γ_{\max} is an upper limit of Γ_{ii} associated with the maximum possible increase in material parameters.

Given axisymmetry, the linear momentum balance under quasi-static conditions in the absence of body forces requires that $T_{r\theta} = T_{rz} = 0$ (neglecting frictional loads between the mandrel or distensible tube and the vessel wall) and that $\partial T_{rr} / \partial r + (T_{rr} - T_{\theta\theta}) / r = 0$. Noting that $T_{rr}(r_i) = -P$ and $T_{rr}(r_o) = 0$, where P is the luminal pressure, equilibrium requires that

$$P = \int_{r_i}^{r_o} \frac{\hat{T}_{\theta\theta} - \hat{T}_{rr}}{r} dr \quad \text{and} \quad p(r) = \hat{T}_{rr} + P - \int_{r_i}^r \frac{(\hat{T}_{\theta\theta} - \hat{T}_{rr})}{r} dr. \quad (18)$$

where \hat{T}_{ii} depends on Γ_{ii} according to equation (16). Axial equilibrium requires that the magnitude of the axial force, f , maintaining the in vivo axial extension on a glass mandrel or silicone sleeve in the bioreactor be

$$f = 2\pi \int_{r_i}^{r_o} T_{zz} r dr, \quad (19)$$

where $T_{zz} = -p + \hat{T}_{zz}$; $p(r)$ is given by equation (18)₂ and \hat{T}_{zz} is given by equation (16). Note that f is the axial force borne by the vessel wall; since frictional forces between the rigid mandrel or distensible tube and the vessel are neglected, the axial force due to the internal pressure acting on the closed ends of the tube is borne entirely by the silicone sleeve.

3.3.3 Evolution Equations for Plasticity, Growth, Damage, and Remodeling

As for any objective constitutive law, an evolution equation for the time course of parameters that describe plasticity, growth, damage, or remodeling has to be formulated from the results of simple experiments or on the basis of comparison between model predictions using a priori postulated equations and available experimental data. In this study, the second approach was used. The analytical form of the postulated equations must satisfy certain conditions that follow from some mechanical and thermodynamical considerations.

In general, the rate of change of the plastic deformation may be a function of many factors, including current growth and plastic deformations \mathbf{F}_g and \mathbf{F}_p , the Cauchy stress \mathbf{T} above the yield stress, the rate of change of Cauchy stress $d\mathbf{T}/dt$, the amplitude of the pulsatile strain $\Delta\mathbf{E}$ (or pulsatile stress), amongst many others; thus, in general, $\partial\lambda_{pi}/\partial t = f(\mathbf{F}_g, \mathbf{F}_p, \mathbf{T}, \partial\mathbf{T}/\partial t, \dots)$. It is assumed that there is no axial force applied to the vessel; thus, $f = 0$ from equation (19). For the case of the silicone sleeve, this requires that all of the axial force associated with mounting the silicone sleeve and internal end cap pressure are borne by the silicone sleeve. This assumption may differ from the experimental case in which the vessel becomes adhered to the mandrel or silicone tube; here the existence of possible axial traction was neglected.

Because the inner diameter of the vessel is prescribed by the diameter of the rigid mandrel or silicone tube, as a result of compaction, a compressive radial stress (i.e., a

compaction-induced pressure) develops at the inner wall. Note that the radial stress at the outer wall is zero. Consequently, the vessel experiences circumferential tensile stresses which appear to be the maximum principal stress in the arterial wall. A linear dependence between the rate of change of $\lambda_{p\theta}$ and $T_{\theta\theta}$ is assumed:

$$\frac{\partial \lambda_{p\theta}}{\partial t} = a_{p\theta} \lambda_{p\theta} \hat{p}_\theta, \quad \text{where} \quad \hat{p}_\theta = \begin{cases} 0 & \text{for } T_{\theta\theta} < T_{\theta\theta}^Y \\ \frac{T_{\theta\theta} - T_{\theta\theta}^Y}{T_{\theta\theta}^Y} & \text{for } T_{\theta\theta} \geq T_{\theta\theta}^Y \end{cases} \quad (20)$$

where $a_{p\theta}$ is a kinetic parameter and $T_{\theta\theta}^Y$ is the yield stress at which plastic deformation occurs; if $T_{\theta\theta} < T_{\theta\theta}^Y$, then no plastic deformation exists. Given that $T_{rr} \ll T_{\theta\theta}$ and $T_{zz} \ll T_{\theta\theta}$ for this loading, plastic deformation is considered as in the case of uniaxial loading in the circumferential direction. Thus, incompressibility requires that $\lambda_{pr} \lambda_{pz} = 1/\lambda_{p\theta}$. For the case of a material that plastically deforms isotropically, $\lambda_{pr} = \lambda_{pz} = 1/\sqrt{\lambda_{p\theta}}$. Therefore, in this isotropic case, it is postulated

$$\frac{1}{\lambda_{pr}} \frac{\partial \lambda_{pr}}{\partial t} = \frac{1}{\lambda_{pz}} \frac{\partial \lambda_{pz}}{\partial t} = -\frac{1}{2\lambda_{p\theta}} \frac{\partial \lambda_{p\theta}}{\partial t} \quad (21)$$

In general, however, given that material anisotropies may develop and the applied loading is not truly uniaxial, assuming that the plastic deformation is isotropic may not be justified. Rather, motivated by equation (20) and (21), the following are prescribed

$$\frac{\partial \lambda_{pr}}{\partial t} = -a_{pr} \frac{\lambda_{pr}}{\lambda_{p\theta}} \frac{\partial \lambda_{p\theta}}{\partial t} = \lambda_{pr} (-a_{pr} a_{p\theta} \hat{p}_\theta) \quad (22)$$

and

$$\frac{\partial \lambda_{pz}}{\partial t} = -a_{pz} \frac{\lambda_{pz}}{\lambda_{p\theta}} \frac{\partial \lambda_{p\theta}}{\partial t} = \lambda_{pz} (-a_{pz} a_{p\theta} \hat{P}_\theta) \quad (23)$$

where a_{pr} and a_{pz} are kinetic parameters and $a_{pr} = a_{pz} = 0.5$ corresponds to an isotropic plastic deformation. Note that incompressibility ($\lambda_{pr}\lambda_{p\theta}\lambda_{pz}=1$) requires that $\partial(\lambda_{pr}\lambda_{p\theta}\lambda_{pz})/\partial t=0$ which requires that $a_{pr}+a_{pz}=1$ for incompressible plastic deformations given kinetic equations (20), (22), and (23).

In general, the rate of change of the growth deformation may be a function of many factors including current growth and plastic deformations \mathbf{F}_g and \mathbf{F}_p , the Cauchy stress \mathbf{T} , the rate of change of Cauchy stress $d\mathbf{T}/dt$, the amplitude of the pulsatile strain $\Delta\mathbf{E}$ (or pulsatile stress), amongst many others; thus, in general, $\partial\lambda_{gi}/\partial t = f(\mathbf{F}_g, \mathbf{F}_p, \mathbf{T}, \partial\mathbf{T}/\partial t, \Delta\mathbf{E}, \dots)$. Based on the notion that healthy arteries grow in response to stress- and cyclic strain-mediated enhanced mitosis and synthetic activity of the vascular smooth muscle cells which are oriented predominantly in the circumferential direction it is assumed that the compaction is also circumferential stress- and strain-mediated and postulate the following evolution equation.

$$\frac{\partial \lambda_{g\theta}}{\partial t} = a_{g\theta} \lambda_{g\theta} \hat{g}_\theta, \quad \text{where} \quad \hat{g}_\theta = \left(\frac{T_{\theta\theta} - T_{\theta\theta}^T}{T_{\theta\theta}^T} + b_{g\theta} (\Delta E_{\theta\theta}) \right) \quad (24)$$

where $a_{g\theta}$ and $b_{g\theta}$ are kinetic parameters and $T_{\theta\theta}^T$ are ‘target’ stresses (i.e., the stress at which the tissue is in biological equilibrium (homeostasis)) at which no net growth occurs.

The factor $\lambda_{g\theta}$ in equation (24) accounts for the fact that as compaction progresses the smooth muscle cells tend to align in the circumferential direction and the contribution of $T_{\theta\theta}$ as a driving stimulus increases. Similarly, circumferential stress and cyclic strain can mediate changes in vessel wall thickness. Thus, let

$$\frac{\partial \lambda_{gr}}{\partial t} = a_{gr} \lambda_{gr} \hat{g}_r, \quad (25)$$

where a_{gr} is a kinetic parameter and $\hat{g}_r = \hat{g}_r(T_{\theta\theta}, \dots)$ is a function of the circumferential stress amongst other factors; the functional form for \hat{g}_r is defined below.

It is less clear from experimental data what factors control the axial growth. If there is a target axial stress T_{zz}^T and if the vessel remains axially unloaded throughout culture, then one would expect the vessel to continually shorten axially; experimentally, the vessel does shorten axially, both under static and cyclic loading; however, this shortening in the axial directions asymptotically approaches a steady-state value. Indeed, it is argued that much of this axial shortening is due to the plastic deformation associated with circumferential loading.

Growth in the circumferential and radial directions necessarily affects growth in the axial direction; e.g., fiber realignment and loss of water due to circumferential stress-mediated remodeling. Thus, for the illustrations herein, let

$$\frac{\partial \lambda_{gz}}{\partial t} = a_{gz} \lambda_{gz} \hat{g}_z, \quad (26)$$

where a_{gz} is a kinetic parameter and $\hat{g}_z = \hat{g}_z(T_{\theta\theta}, \dots)$ is a function of the circumferential stress amongst other factors; the functional form for \hat{g}_z is defined later in the text (equation(34)).

Combining equations (20) and (24), the combined plastic and growth deformations,

$[\mathbf{F}_{pg}] = \text{diag} \{ \lambda_{pgr}, \lambda_{pg\theta}, \lambda_{pgz} \}$ yield the evolution equations

$$\frac{\partial \lambda_{pgr}}{\partial t} = \frac{\partial}{\partial t} (\lambda_{pr} \lambda_{gr}) = \lambda_{pgr} [a_{gr} \hat{g}_r + a_{pr} \hat{p}_r] \quad (27)$$

$$\frac{\partial \lambda_{pg\theta}}{\partial t} = \frac{\partial}{\partial t} (\lambda_{p\theta} \lambda_{g\theta}) = \lambda_{pg\theta} [a_{g\theta} \hat{g}_\theta + a_{p\theta} \hat{p}_\theta] \quad (28)$$

$$\frac{\partial \lambda_{pgz}}{\partial t} = \frac{\partial}{\partial t} (\lambda_{pz} \lambda_{gz}) = \lambda_{pgz} [a_{gz} \hat{g}_z + a_{pz} \hat{p}_z]. \quad (29)$$

Considering the matter of convergence and the steady state conditions of growth and plasticity (without damage and remodeling), the kinetic constants and functional forms for \hat{g}_i and \hat{p}_i should be chosen such that, as $t \rightarrow \infty$, the evolution equations for $(\partial \lambda_{pgr} / \partial t)$, $(\partial \lambda_{pg\theta} / \partial t)$, and $(\partial \lambda_{pgz} / \partial t)$ approach zero. By setting equation (28), with equations (20)₂ and (24)₂ to zero. It follows that, at steady state,

$$a_{g\theta} \left(\frac{T_{\theta\theta}|_{ss} - T_{\theta\theta}^T}{T_{\theta\theta}^T} + b_{g\theta} \Delta E_{\theta\theta} \right) + a_{p\theta} \left(\frac{T_{\theta\theta}|_{ss} - T_{\theta\theta}^Y}{T_{\theta\theta}^Y} \right) = 0 \quad (30)$$

where $T_{\theta\theta}|_{ss}$ is the steady-state value for $T_{\theta\theta}$. One way to enforce that $(\partial \lambda_{pgr} / \partial t)$ and $(\partial \lambda_{pgz} / \partial t)$ approach zero as $(\partial \lambda_{pg\theta} / \partial t)$ approaches zero is to require that

$$\frac{\partial \lambda_{pgr}}{\partial t} = a_{pgr} \frac{\lambda_{pgr}}{\lambda_{pg\theta}} \frac{\partial \lambda_{pg\theta}}{\partial t} \quad \text{and} \quad \frac{\partial \lambda_{pgz}}{\partial t} = a_{pgz} \frac{\lambda_{pgz}}{\lambda_{pg\theta}} \frac{\partial \lambda_{pg\theta}}{\partial t}. \quad (31)$$

That is, it is assumed that the rate of change of λ_{pgr} and λ_{pgz} are proportional to the rate of change of $\lambda_{pg\theta}$. The consequence of this assumption, employing equations (22) and (23), is that

$$\frac{1}{\lambda_{gr}} \frac{\partial \lambda_{gr}}{\partial t} = a_{pgr} \frac{1}{\lambda_{g\theta}} \frac{\partial \lambda_{g\theta}}{\partial t} + (a_{pgr} + a_{pr}) \frac{1}{\lambda_{p\theta}} \frac{\partial \lambda_{p\theta}}{\partial t} \quad (32)$$

$$\frac{1}{\lambda_{gz}} \frac{\partial \lambda_{gz}}{\partial t} = a_{pgz} \frac{1}{\lambda_{g\theta}} \frac{\partial \lambda_{g\theta}}{\partial t} + (a_{pgz} + a_{pz}) \frac{1}{\lambda_{p\theta}} \frac{\partial \lambda_{p\theta}}{\partial t} \quad (33)$$

or that,

$$a_{gr} \hat{\mathbf{g}}_r = a_{pgr} a_{g\theta} \hat{\mathbf{g}}_\theta + (a_{pgr} + a_{pr}) a_{p\theta} \hat{\mathbf{p}}_\theta \quad \text{and}$$

$$a_{gz} \hat{\mathbf{g}}_z = a_{pgz} a_{g\theta} \hat{\mathbf{g}}_\theta + (a_{pgz} + a_{pz}) a_{p\theta} \hat{\mathbf{p}}_\theta. \quad (34)$$

Thus, a consequence of prescribing equation (31) is that the growth rates in the r and z directions are not only functions of the difference between $T_{\theta\theta}$ and $T_{\theta\theta}^T$, but also functions of the difference between $T_{\theta\theta}$ and $T_{\theta\theta}^Y$.

The rate of change of the damage may also be a function of many factors, including current value of remodeling and damage \mathbf{M} and \mathbf{D} , the Cauchy stress \mathbf{T} , the rate of change of Cauchy stress $d\mathbf{T}/dt$, amongst many others; thus, in general, $\partial D_{ii}/\partial t = f(\mathbf{M}, \mathbf{D}, \mathbf{T}, \partial \mathbf{T}/\partial t, \dots)$. For these illustrative simulations, a linear dependence between D_{ii} and W is considered

$$\frac{dD_{ii}}{dt} = \alpha_{D1} \left(\frac{W - W_{cr}}{W_{cr}} \right) \quad (35)$$

where and a_{D1} is a kinetic parameter and W_{cr} is the critical strain energy above which damage occurs; if $W < W_{cr}$, then no damage occurs and let $\alpha_{D1} = 0$. Note that equation (35) models isotropic damage.

Similarly, in general, $\partial M_{ii}/\partial t = f(\mathbf{M}, \mathbf{D}, \mathbf{T}, \partial \mathbf{T}/\partial t, \Delta \mathbf{E}, \mathbf{F}_{gp}, \dots)$. For these illustrative simulations, let

$$\frac{dM_{\theta\theta}}{dt} = (a_{R\theta} + b_{R\theta} \Delta E) \frac{\partial \lambda_{gp\theta}}{\partial t} \quad (36)$$

where $a_{R\theta}$ is a kinetic parameter. That is, it is assumed that the rate of remodeling is linearly related to the rate of compaction of the tissue. Also, let

$$\frac{dM_{rr}}{dt} = a_{Rr} \frac{dM_{\theta\theta}}{dt} \quad \text{and} \quad \frac{dM_{zz}}{dt} = a_{Rz} \frac{dM_{\theta\theta}}{dt} \quad (37)$$

where a_{Rr} and a_{Rz} are kinetic parameters. Therefore, it is assumed that the material remodels in an orthotropic manner.

Finally, for these illustrative simulations, let

$$\frac{\partial T_{\theta\theta}^Y}{\partial t} = \frac{a_{Y\theta}}{2} \left(\frac{\partial M_{\theta\theta}}{\partial t} - \frac{\partial D_{\theta\theta}}{\partial t} \right) = a_{Y\theta} \frac{\partial \Gamma_{\theta\theta}}{\partial t}, \quad (38)$$

where $a_{Y\theta}$ is a kinetic parameter; thus, the change in yield stress is proportional to the change in the ‘stiffness’ defined by equation (17). The rationale for this assumption is that the same structural changes that lead to stiffening of the material most likely elevate the stress level at which the tissue manifests plasticity.

3.3.4 Simulation Results

The gel-derived approach to vascular tissue engineering consists of vascular cells embedded in a reconstituted gel matrix, typically of collagen or fibrin. These TEBVs are formed by pouring the solutions of vascular cells, collagen and/or fibrin, and supplemented cell culture media into a cylindrical mold. The suspension is allowed to polymerize (usually for ~1 hour), then the mandrel with the gel are removed and placed in tissue culture dishes containing supplemented cell culture media.

Two culture scenarios are considered: (i) culture of the vessel on the rigid mandrel, providing a circumferential constraint and radial loading and (ii) culture of the vessel on a distensible membrane that allows for displacement control of the inner radius. The goal of this paper is to illustrate that this modeling framework is sufficient to capture many of the salient features of growth, remodeling, damage, and plasticity of gel-derived TEBVs and to highlight data that is currently lacking in the literature.

The governing equations are the kinematic equations (8), (9), and (11), the constitutive equation (16)₂, equilibrium equations (18)₁, (18)₂, and (19), and the kinetic equations are (28), (31), and (35)-(38). The initial values were defined as $r_i(0) = R_i(0) = 1.775$ mm, $r_o(0) = R_o(0) = 5.25$ mm, $\ell(0) = 38$ mm, $T_{\theta\theta}^y(0) = 5$ kPa, $\Gamma_{ii}(0) = 1$. The following parameters were prescribed: $a = 1.0$, $c = 0.5$ kPa, $a_{g\theta} = 0.12/\text{day}$, $b_{g\theta} = 0.01/\text{day}$, $a_{p\theta} = 0.60/\text{day}$, $T_{\theta\theta}^T = 150$ kPa, $a_{pgr} = 1.4$, $a_{pgr} = 0.5$, $a_{R\theta} = 100$ kPa, $b_{R\theta} = 200$ kPa, $a_{Rz} = 0.5$,

$a_{y\theta} = 1.5$ and $W_{cr} = 10 \text{ kJ/m}^3$. This system of equations was solved numerically by discretizing the radius and using an implicit time-step, using MATLAB 7.1.

Given the initial values the Cauchy stress was calculated, employing the evolution equations for growth and plasticity to determine the stress-free configurations for the subsequent time step, and the evolution equations for remodeling and damage to determine values for Γ_{ii} at the subsequent time step. For all time-steps, the inner radius was explicitly prescribed in the loaded configuration and the axial force $f = 0$; thus, equation (19) was solved to determine the loaded length $\ell(t)$ and equation (12)₁ yielded the loaded radius for the current time-step.

Given the loaded configuration $(dr(t), r(t), \ell(t))$ and the stress-free configuration $(dR(t), R(t), L(t))$, the elastic stretches and the Cauchy stress was calculated and evolution equations evaluated for the subsequent time step. This iterative procedure was continued for a defined time interval. For the set of selected model functions and parameters the asymptotic solution was unique and stable. In addition, results from these numerical simulations showed that small variations of a single input parameter or combinations of parameters cause small changes in the output parameters, proving the necessary requirement for robustness of the model.

Note, for these illustrative parameters and loading scenarios, $W_{cr} = 10 \text{ kJ/m}^3$ was not exceeded in any simulations below and therefore mechanical conditioning did not cause tissue damage in these simulations. Nevertheless, damage was included in the general

theoretical framework, since damage mechanisms with other parameter sets or under other loading and testing scenarios (e.g., ring tests or burst pressure tests) are critical for interpreting such experimental results.

3.3.4.1 Static Culture on a Rigid Mandrel

The most widely reported experimental data for gel-derived TEBVs involves long-term culture (days to weeks) on a rigid mandrel. Seliktar *et al.*, [5] report the evolution of compaction and material properties at 2 days, 6 days, and 10 days of static culture. Collagen gels were molded around a glass mandrel covered with a silicone sleeve with outer radius 1.775 mm and length 38 mm; the inner radius of the test tube was 5.75 mm; it was assumed, however, that the outer radius of the vessel following the initial gelling process, which occurred in ~1 hour, was 5.25 mm. Thus, the initial volume of the cells, collagen, and culture media was approximately 3,500 mm³; the vessel volume immediately after gelling was approximately 2,900 mm³.

Seliktar *et al.*, performed two different static cultures: one in which the vessel was allowed to adhere to the silicone sleeve, impairing compaction in the axial direction and one in which the silicone sleeve was coated with Vaseline petroleum jelly, allowing the vessel to freely compact in the axial direction. These experiments are referred to as the ‘constrained static’ and ‘unconstrained static’ culture in this text. Since the traction force applied to the vessel on the luminal surface in the axial direction by the adherence to the silicone sleeve in the constrained static culture cannot be measured, below the unconstrained static culture where this traction force is negligible is simulated.

In Seliktar *et al.*[5], the total volume of the TEBVs decreased to approximately 620 and 510 mm³ after 6 and 10 days, respectively. The length decreased to 23 and 25 mm after 6 and 10 day, respectively; thus, the outer radius decreased to 3.4 and 3.1 after 6 and 10 days, respectively. The inner radius was constrained to remain at 1.775 mm throughout culture. Although they did not report the yield stress or modulus for the unconstrained static culture, they reported yield stresses of ~ 4 kPa and 8 kPa and material moduli of ~40 and 63 kPa at 6 and 10 days for the constrained static case. They also reported that the ultimate tensile stress was 1.24 and 1.55 times higher for the unconstrained versus constrained static culture at 6 and 10 days, respectively; thus, it may be reasonable to assume that the yield stress and (perhaps) the modulus for the unconstrained static culture are above that of the constrained static case.

Motivated by these experimental results, for these simulations, let $r_i(t)=1.775$ and $\Delta E(t) = 0$ for all time. As the local stress-free configurations and material parameters evolved, the vessel outer radius, thickness, and axial length became $r_o(t) = 4.7, 3.7, 3.0,$ and 2.8 mm and $\ell(t) = 34, 28, 24,$ and 23 mm at 2, 6, 10, and 20 days, respectively; these are comparable to those reported by Seliktar *et al.* (Figure 3.3a and 3.3b). The unloaded radii, thickness, and length in the traction-free configuration β_u decreased monotonically to $R_i^u(t \rightarrow \infty) = 1.1$ mm, $R_o^u(t \rightarrow \infty) = 2.4$ mm, $H^u(t \rightarrow \infty) = 1.3$ mm, and $L^u(t \rightarrow \infty) = 22$ mm. The opening angle in the reference configuration β_r initially decreased to -22 degrees, then began to increase at time $t = 5.3$ days towards a steady state value of 96 degrees (Figure 3.3c). Note that experimental values of the unloaded radii and axial length and the stress-free radii, length and opening angle are not reported in Seliktar *et*

al., nor are these values typically reported in the literature for TEBVs; the time course of these values, however, are necessary to quantify the three-dimensional evolution of strain and to predict the evolution of stress throughout culture.

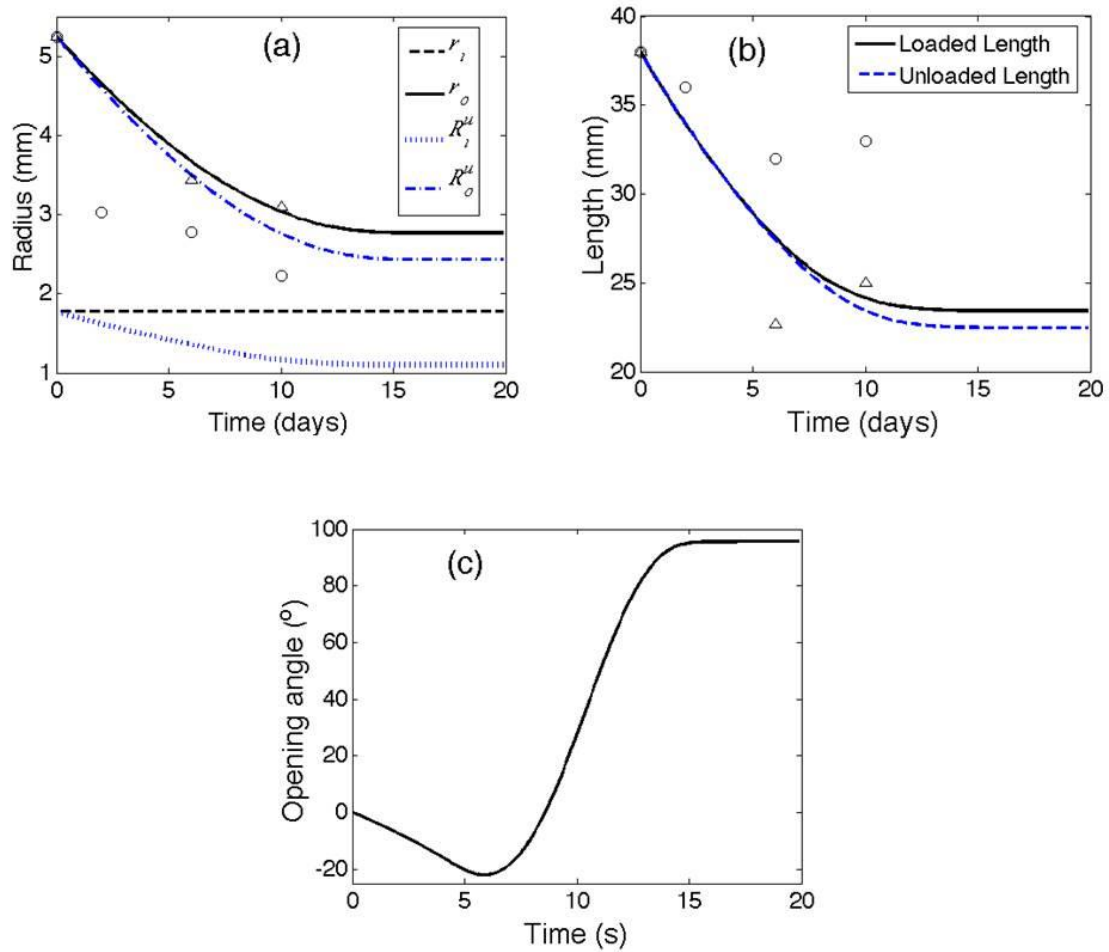


Figure 3-3. Model predicted evolution of changes in the geometric properties. Changes in the loaded and unloaded radii (a), axial length (b), and opening angle (c) for static culture on a mandrel. Data from Seliktar *et al.* [5] from constrained (open circles) and unconstrained (solid triangles) static culture are included for comparison to modeling results.

Fixed length pressure-diameter testing results were simulated for the model artery at different time-points and mean nominal stress-engineering strain curves were generated (Figure 3.4a). These curves were generated by fixing the length at L_u , increasing the

pressure at increments of 0.5 mmHg, and solving for the inner radius via regression. The pressure was increased until the yield stress was reached. The mean nominal stress (with respect to the undeformed area) and engineering strain were calculated as

$$\sigma_{\theta} = \frac{Pa}{\lambda_{\theta}h} \quad \text{and} \quad \varepsilon_{\theta\theta} = \frac{r_{mid}}{(R_u)_{mid}} - 1 \quad (39)$$

where r_{mid} and $(R_u)_{mid}$ are the loaded and unloaded radii at the middle of the wall, a is the inner radius, and h is the thickness. An ‘effective’ modulus as the slope of the nominal stress-engineering strain curve over the final five data points was calculated. The modulus was 15 kPa, 49 kPa, 69 kPa, and 72 kPa on Day 2, 6, 10, and 20, respectively (Figure 3.4b).

Note that the definition of modulus calculated from these pressure-diameter tests (i.e., slope of the stress-strain curve from a fixed length pressure-diameter test) is quantitatively different from that defined from uniaxial ring testing data by Seliktar *et al.* (i.e., slope of the stress-strain curve from a uniaxial ring test). One difference is that in the uniaxial ring test the vessel is free to retract axially, whereas in the pressure-diameter test the length is held fixed. Nevertheless, these different approaches to measuring modulus may be qualitatively compared.

The trends of the effective modulus from these simulations compare well to those of Seliktar *et al.* The mean yield stress was initially 0.2 kPa and evolved according to equation (38) to 3, 8, 12, and 13 kPa at $t = 2, 6, 10,$ and 20 days, respectively; the trends of the mean yield stress from these simulations compare well to those of Seliktar *et al.* (Figure 3.4c).

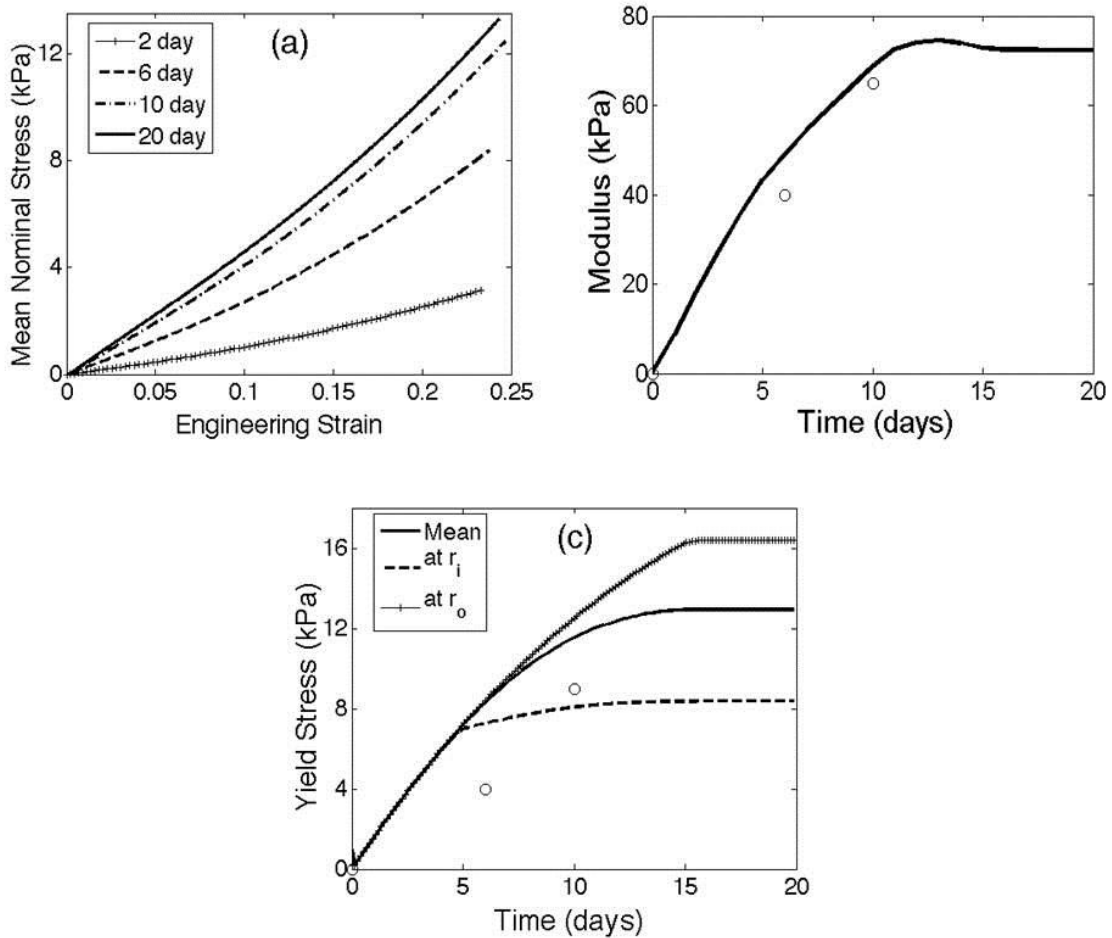


Figure 3-4. Model predicted changes in mean mechanical properties. Nominal stress-engineering strain curves that would result from fixed length pressure-diameter testing (a), evolution of modulus (b), and yield stress (c) for static culture on a mandrel. Data from Seliktar *et al.* [5] from constrained static culture (open circles) are included for comparison to modeling results.

In addition to predicting measurable quantities such as changes in geometry, residual stress, material response curves, and yield stress, an important utility of modeling is to predict quantities that are not experimentally measurable, such as the *local* stresses and strains and *local* material properties. Circumferential stress and cyclic circumferential strain are the driving stimuli for the evolution equations; however, since $\Delta E = 0$ in this simulation, cyclic strain does not contribute to the evolution equations.

The circumferential stress, initially zero at all locations across the wall, began to increase at different rates at each radial location (Figure 3.5a and 3.5b). The evolution of the circumferential stress is governed by the evolution of the material parameters (c_o , Γ_{rr} , $\Gamma_{\theta\theta}$ (Figure 3.5c), and Γ_{zz}) and the evolution of the circumferential stretch ($\lambda_{e\theta}$, Figure 3.5d); the evolution of the circumferential stretch is governed by the evolution of the stress-free and loaded configuration, as governed by the plastic-growth stretches (λ_{pgi} , Figure 3.5e and 3.5f). The plastic-growth stretches on the inner wall decreased monotonically until $t = 4.6$ days. Before $t = 4.6$ days the circumferential stress $T_{\theta\theta}$ was below the yield stress $T_{\theta\theta}^Y$ for all radii (Figure 3.4c). When the stress on the inner wall reached the yield stress, plastic deformation ensued near the inner wall and the rate of change of λ_{pgi} decreased according to equations (27), with (20) and (24)₂, and equations (31). Thus, after $t = 4.6$ days, the values $\partial\lambda_{pgi}/\partial t$ at the inner wall decreased and the values for λ_{pgi} at the inner wall asymptotically approached the values $\lambda_{pgr} = 0.61$, $\lambda_{pg\theta} = 0.70$, and $\lambda_{pgz} = 0.73$. Notice that the yield stress varied across the wall; the yield stresses at inner locations were lower than those at outer locations of the wall (Figure 3.4b). As a result, the steady state circumferential stress varied across the wall (Figure 3.5a and 3.5b); the steady state value of $T_{\theta\theta}$ may be found directly via equation (30) and is between $T_{\theta\theta}^Y$ and $T_{\theta\theta}^T$ when $T_{\theta\theta}^Y < T_{\theta\theta}^T$. The circumferential elastic stretch $\lambda_{e\theta}$, which was initially 1.0 across the wall, increased non-uniformly, but monotonically, across the wall as stress-mediated compaction was initiated via equation (27), with (20) and (24)₂; after $t = 4.6$ days, however, the elastic stretch varied non-monotonically across the wall, as inner

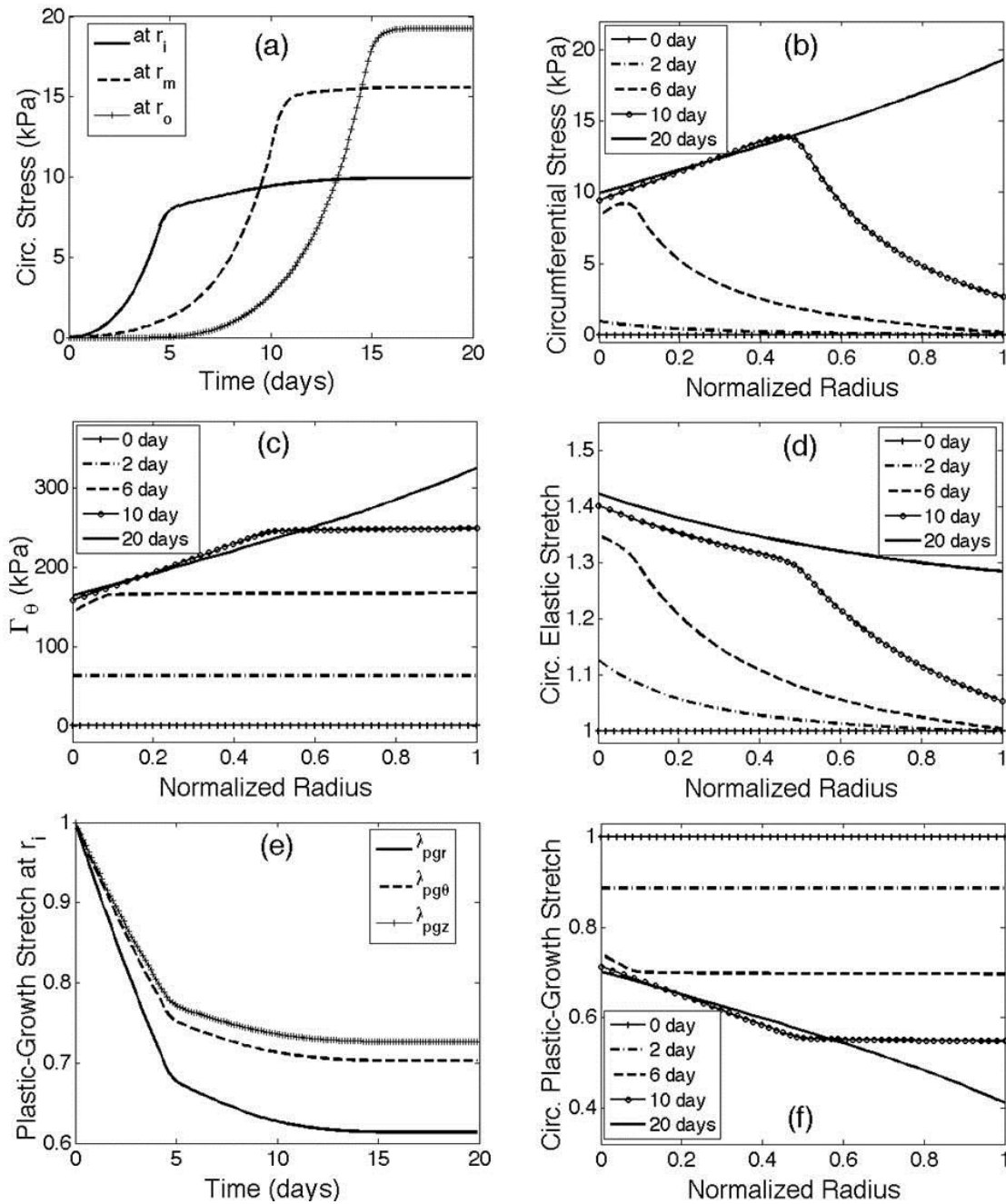


Figure 3-5. Evolution of mechanical properties over time in culture. Evolution of the local circumferential stress (a,b), circumferential damage and remodeling parameter Γ_θ (c), distribution of the elastic stretch (d), plastic-growth stretches in the radial, circumferential, and axial directions (e), and distribution of the circumferential plastic-growth stretch versus radius at different time-points (f) for static culture on a mandrel.

radial locations experienced plastic deformation, but outer radial locations remained in the elastic regime (below the yield stress). Eventually, as compaction proceeded at outer wall locations, the yield stress was reached at all radial locations and the distribution of elastic stretches became monotonic. Notice, however, that whereas the circumferential stress was highest at the outer wall, the circumferential elastic stretch was highest at the inner wall. The stress was higher at the outer wall because the material properties were highest on the outer wall (Figure 3.5c).

3.3.4.2 Culture on a Distensible Tube

Seliktar *et al.*, demonstrated that the elastic modulus and rate of compaction increase in response to cyclic strain. In their experimental approach, they cultured collagen gel-derived TEBVs on a distensible elastic membrane that allowed for the cyclic control of the inner radius. Collagen gels were again molded around a glass mandrel covered with a silicone sleeve with outer radius 1.775 mm and length 38 mm; the inner radius of the test tube was 5.75 mm; it was assumed, that the outer radius was ~5.25 mm after gelling for 1 hour. Thus, the initial volume immediately after gelling was ~2,900 mm³. Vessels were statically cultured on a rigid mandrel for 2 days, and then exposed to 10% cyclic strain for an additional 4 days or 8 days.

Seliktar *et al.*, attempted to culture vessels under cyclic loading both with and without Vaseline to account for the role of adhesion of the gel to the silicone tube. The tests with Vaseline, however, resulted in constructs that were visibly detached from the sleeve throughout the experiment; thus, these vessels did not receive the specified cyclic loading. Thus, the results from the experiments without Vaseline were considered.

In their experiment, the total volume of the TEBVs decreased to approximately 295 and 190 mm³ after 6 and 10 days (i.e., 2 days under static culture and 4 and 8 days under cyclic strain), respectively. The length decreased to 23 mm and 10 mm after 6 and 10 day, respectively; thus, the outer radius decreased to 2.7 mm and 3.0 mm after 6 and 10 days, respectively. The inner radius was constrained to cycle between 1.775 and 1.953 mm throughout culture. The yield stresses were ~8 kPa and 27 kPa and material moduli were ~40 and 135 kPa at 6 and 10 days, respectively.

Motivated by these experiments, for these simulations, let

$$r_i(t) = \begin{cases} 1.775 \text{ mm} & t \in [0, 2] \text{ days} \\ \frac{R_o^M \Delta \varepsilon}{2} \sin(2\pi\omega t - \pi / 2) + \frac{R_o^M (2 + \Delta \varepsilon)}{2} & t \in [2, 10] \text{ days} \end{cases} \quad (40)$$

where $R_o^M = 1.775$ mm is the outer diameter of the silicone sleeve, prior to inflation, $\Delta \varepsilon = 0.10$ is the fractional change in inner radius, and ω is the angular frequency. Note that most experiments were performed at a frequency of 1 Hz, which corresponds to 1.7×10^6 cycles over 20 days.

As the local stress-free configurations and material parameters evolve, the vessel outer radius, thickness, and axial length (when $r_i = 1.775$) evolve to $r_o(t) = 4.7, 3.1, 2.5,$ and 2.5 mm and $\ell(t) = 31, 25, 24,$ and 24 mm at 2, 6, 10, and 20 days, respectively. Whereas the radii were comparable to those reported by Seliktar *et al.* (Figure 3.6a), the axial length predicted in these simulations was significantly higher than their experimental value.

The unloaded radii and length in the traction-free configuration β_u decrease monotonically to $R_i^u = 1.6, 1.2, 1.0,$ and 1.0 mm, $R_o^u = 4.6, 2.8, 2.1,$ and 2.1 mm, $H^u = 3.0, 1.6,$ and 1.1 mm, and $L^u = 34, 24, 21,$ and 21 mm on 2, 6, 10, and 20 days, respectively (not shown).

The opening angle in the reference configuration β_r initially decreased from 0 to 2 days to -7.5 degrees as in the static case. After Day 2, cyclic stretching begins and the opening angle decreases at a faster rate to -85 degrees at $t=4.7$ days, after which the opening angle increases towards a steady state value of 104 degrees; steady state is reached at $t=10.5$ days (Figure 3.6b). Again, experimental values of the unloaded radii and axial length and the stress-free radii, length, and opening angle are not available in the literature.

The ‘effective’ modulus increased monotonically from 15 kPa, 170 kPa, 242 kPa, and 242 kPa at 2, 6, 10, and 20 days, respectively (not shown). These trends of the effective modulus from these simulations are qualitatively comparable to those of Seliktar *et al.* The mean yield stress was initially 0.2 kPa and evolved according to equation (38) to 3, 16, 20, and 20 kPa at $t = 2, 6, 10,$ and 20 days, respectively; the trends of the mean yield stress from these simulations compare well to those of Seliktar *et al.* (Figure 3.7a).

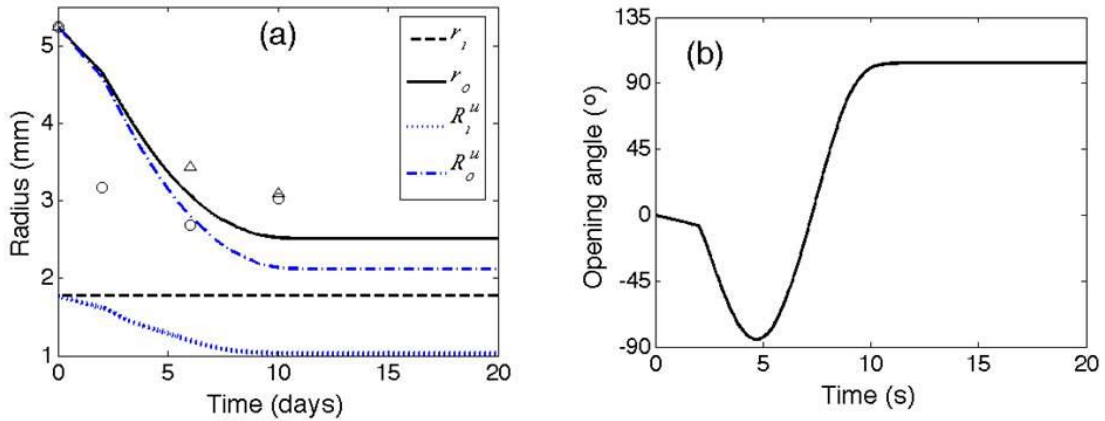


Figure 3-6. Model predicted changes in loaded and unloaded geometry. Model predicted evolution of loaded and unloaded radii (a) and opening angle (b) for culture on a distensible tube with 10% cyclic strain. Data from Seliktar *et al.* [5] from constrained (open circles) and unconstrained (solid triangles) static culture are included for comparison to modeling results.

The circumferential stress evolved at different rates across the thickness of the vessel (Figure 3.7b). At 6 days, there was a highly non-uniform distribution of circumferential stress across the wall, including both tensile stresses at inner wall locations and compressive stresses at outer wall locations. By 20 days, however, the transmural circumferential stress was nearly uniform.

Since the evolution of material properties (e.g., $\Gamma_{\theta\theta}$) is negatively proportional to the evolution of compaction and directly proportional to the local cyclic strain ΔE the distribution of material parameters versus radius was nearly uniform, with $\Gamma_{\theta\theta} \in [350, 410]$ kPa at steady state (Figure 3.7c); c.f., Figure 3.5c, for the static case $\Gamma_{\theta\theta} \in [160, 350]$ kPa at steady state.

The circumferential elastic stretch $\lambda_{e\theta}$ evolved from a uniform distribution of $\lambda_{e\theta} = 1.0$ across the wall to a highly non-uniform distribution (Figure 3.7d). At 6 days, for example, the inner wall experienced tensile elastic stretch $\lambda_{e\theta} = 1.47$, whereas the outer wall experienced compressive elastic stretch $\lambda_{e\theta} = 0.94$. The elastic stretch eventually evolved to a non-uniform distribution, with $\lambda_{e\theta} \in [1.35, 1.50]$.

The circumferential plastic-growth stretch $\lambda_{pg\theta}$ remains uniform across the wall until $t = 2$ days (Figure 3.7e), when cyclic stretching began and the circumferential stress $T_{\theta\theta}$ reached the yield stress $T_{\theta\theta}^Y$ at the inner wall at the highest radius of the cyclic loading (Figure 3.7d). The yield stress is a function of radial location when cyclic strain is initiated ($t > 2$ days).

The cyclic strain is both a function of radius and time (Figure 3.7f). Notice that, even though the displacement is the same for all time at the inner radius, the cyclic strain evolves with time, since the stress-free reference configuration evolves with time.

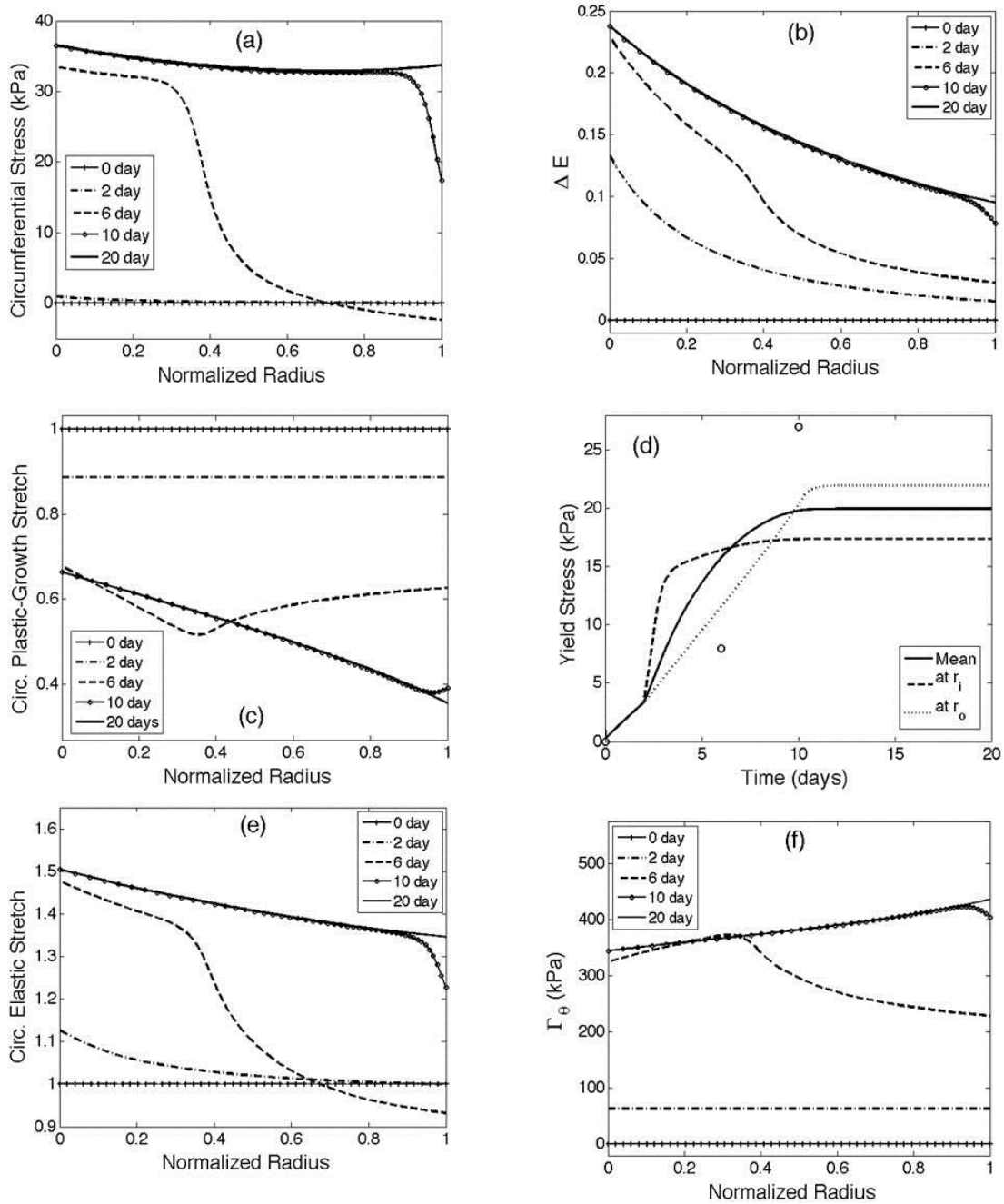


Figure 3-7. Evolution of material properties. Evolution of the yield stress (a), the local circumferential stress (b), the circumferential damage and remodeling parameter Γ_θ (c), the distribution of the elastic stretch (d), distribution of the circumferential plastic-growth stretch versus radius (e), and the amplitude of cyclic Green strain (f).

3.4 Discussion

In this work, a modeling framework and simulations for mechanically-mediated growth, remodeling, plasticity, and damage of gel-derived TEBVs was proposed. The results obtained suggest that the model framework can qualitatively predict the evolution of geometry and material behavior under common experimental loading scenarios. There remains, however, a need for additional data to identify specific functional forms for constitutive and evolution equations, ultimately leading to a model with predictive capabilities.

The results from Seliktar *et al.* [5] were used as a guide for choosing material and evolution equations. Of course many factors can effect these parameters, as well as the functional analytical forms for constitutive and evolution equations; these factors include cell source, extracellular matrix (e.g., collagen versus fibrin), media supplements, cross-linking [17, 18], amongst many others. Whereas such confounding factors make it difficult to quantify individual and synergistic effects, modeling can guide the interpretation of data and the design of experiments to optimize vessel geometry and material behavior and minimize requisite culture time.

Towards the end of guiding experimental design, the model framework and simulations presented here illustrate the need to make experimental measurements that are currently lacking in the literature. For example, to quantify the kinematics and perform stress analyses, it is useful to identify the evolution of the traction-free configuration (β_u) and

is necessary to identify the evolution of a (at least nearly) stress-free configuration (β_o); following Chuong and Fung [19] the stress-free configuration may be approximated by quantifying the radius, length, and opening angle of a radially-cut vessel ring. These data can provide insight towards the evolution of λ_{pgi} .

Also, whereas uniaxial (ring) tests provide information on the material response in the circumferential direction, including an effective modulus, yield stress, ultimate tensile stress, a predictive model requires a constitutive equation, which is valid for multiaxial loading. Given that these TEBVs are clearly anisotropic, multiaxial mechanical testing is required; see [20, 21].

Although this work focused on the results of Seliktar et al., the modeling framework and illustrative results are consistent with other reports in the literature. For example, Syedain *et al.* [22] showed that incrementally increasing the amplitude of cyclic distention of gel-derived tissue engineered vessels grown on a distensible elastic sleeve improved mechanical properties beyond that of vessels exposed to an unchanging amplitude of cyclic strain. The model predicts similar results (not shown).

This model suggests that one key advantage of incrementally increasing the amplitude of the strain on gel-derived TEBVs is to reduce the overall plastic deformation at early time-points (day 2-3); at early time points the yield stress is low, thus, lower amplitude of cyclic strain causes less plastic deformation. At later time points, the yield stress is higher; thus, higher amplitudes of cyclic strain may be applied without introducing

significant plastic deformation. The current mathematical model could be used to optimize the time course of cyclic strain to maximize growth and remodeling mechanisms and minimize plasticity and damage. Essential data on the evolution of geometry and material properties, however, are currently lacking from the report from Syedain *et al.* [22] that prevent a direct comparison of simulation results to their experimental data.

The common approaches of culture of gel-derived TEBVs; namely, static culture on a rigid mandrel and culture on a distensible tube with cyclic circumferential distension were simulated. The advantage of these experimental approaches is the capability to deliver precise cyclic circumferential displacements. In addition, given that the distensible tube is impermeable to fluid, this tube also prevents leakage; a particularly significant challenge for gel-derived constructs at very early time-points in culture.

There are several disadvantages with these approaches as it relates to quantifying mechanically-mediated remodeling of TEBVs. First, whereas the change in circumferential distension (i.e., change in inner diameter) is known, the circumferential strain (defined with respect to an appropriate stress-free configuration) is not known and likely changes during culture. Consider the circumferential component of Green strain, $E_{\theta\theta} = (\lambda_\theta^2 - 1)/2$, where $\lambda_\theta(r) = \pi r / ((\pi - \Phi_o)R)$ (in 3D) where r and R are radial locations in the current and stress-free configurations, respectively, and Φ_o is the opening angle (see [23]) or $\lambda_\theta = r / R$ (in 2D) if variations across the vessel wall are neglected. In both the 3D and the 2D case, although this approach carefully controls r ,

since the stress-free diameter R of the vessel can change during culture, via growth and plasticity mechanisms, the circumferential strain can change. In 3D, these changes are more pronounced; for example, as the vessel thickens or compacts, or as the opening angle changes with remodeling.

Second, although the pressure applied to the distensible sleeve is known, the pressure applied to the luminal surface of the TEBV is not known; thus, the circumferential stress is variable and is not known during culture.

Third, in most cases the vessels are adhered to the glass or silicone and partially constrained from retracting axially; this applied load, too, is unknown. It is well argued that cells sense and respond to their local mechanical environment (i.e., the local stress and strain); thus, evolution equations for growth and remodeling should be functions of the local stress or strain. In these experimental approaches, however, neither the stress nor the strain is known throughout the experiment. Load controlled (e.g., pressure, flow, and axial force controlled) experiments are better suited for quantifying growth, remodeling, plasticity, and damage of gel-derived TEBVs. Such experiments allow for the control of mean components of the stress tensor, thereby allowing for a more direct comparison between experimental stimuli and the evolution of geometry, reference states, and material behavior.

The evolution equations proposed in this study combine the effects of growth and plasticity into a set of equations and the effects of remodeling and damage into a set of

equations. Given that plasticity and damage typically occur over shorter time-scales than growth and remodeling, it is necessary to consider the effects separately. The effect of plasticity and damage can be experimentally quantified independent of those of growth and plasticity by performing acute tests to failure; such tests do not allow enough time for significant growth and remodeling, thereby isolating the non-cell-mediated mechanisms of damage and plasticity. Tests such as uniaxial creep, fatigue, and monotonic loading to failure and cylindrical biaxial isobaric, fatigue, and burst pressure testing can be sufficient to quantify evolution equations for damage and plasticity. Once the evolution equations and kinetic parameters are specified for damage and plasticity, culture experiments can be used to identify growth and remodeling equations and parameters.

Limitations of the proposed theoretical approach originate from the adopted assumptions. First, the modeling framework that was employed combines ideas from volumetric growth, plasticity, and continuum damage mechanics; these frameworks track changes at the tissue level, without quantification of changes in the underlying microstructure. Future refinement of this modeling framework could employ microstructurally motivated constitutive and evolution equations to capture such microstructural changes [24]. Indeed, Feng et al. [25] showed well that even acute mechanical testing, in the absence of growth and remodeling, induced significant realignment of collagen fibrils.

Second, evolution equations were chosen as linear functions of stress and strain amplitude and a simple quadratic constitutive equation for the stress response; presumably, growth, remodeling, plasticity, and damage are related in some, yet to be

determined, non-linear manner; data to prescribe such functional forms is currently lacking. Similarly, the damage and plasticity equations are also linear functions of stress and strain amplitude. Literature from native soft tissues [26] and unpublished data from our lab on collagen gel-derived TEBVs suggest that plasticity and damage are functions both of stress and rate of change of stress; again, more data are needed to assess their relative contribution and identify appropriate evolution equations.

Third, these simulations have focused on compaction of TEBVs in the first 10 days; however, it is more likely that there are two different mechanisms associated with growth of TEBVs: a short-term (0-14 day) compaction response and a long-term (>1 week) growth response, including cell proliferations/apoptosis, and extracellular matrix synthesis/degradation. These different responses will require different sets of evolution equations.

In conclusion, a phenomenological model has been developed for the growth, remodeling, damage, and plasticity of gel-derived tissue engineered blood vessels. Illustrative simulations suggest that this model has the capability of capturing the salient features of mechanically-induced changes in TEBV development. Simulations also highlight the need for additional experimental measurements (e.g., evolution of traction-free and stress-free configurations) and the need to perform additional theoretically-motivated experiments to quantify analytical forms and parameters for constitutive and evolution equations. Once quantified, use of such a predictive model may be exploited to

design loading strategies to improve the mechanical properties of TEBVs and reduce requisite culture times for TEBV development.

3.5 References

1. Nerem, R.M. and D. Seliktar, *Vascular Tissue Engineering*. Ann Rev Biomed Eng, 2001. **3**: p. 225-243.
2. Isenberg, B.C., C. Williams, and R.T. Tranquillo, *Small-diameter artificial arteries engineered in vitro*. Circulation Research, 2006. **98**: p. 25-35.
3. Ku, D.K. and H.-C. Han, *Assessment of function in tissue-engineered vascular grafts*, in *Functional tissue engineering*, F. Guilak, et al., Editors. 2003, Springer-Verlag: New York. p. 258-267.
4. Weinberg, C.B. and E. Bell, *A blood vessel model constructed from collagen and cultured vascular cells*. Science, 1986. **231**: p. 397-400.
5. Seliktar, D., et al., *Dynamic mechanical conditioning of collagen-gel blood vessel constructs induces remodeling in vitro*. Annals of Biomedical Engineering, 2000. **28**: p. 351-362.
6. Engelmayer, G.C., et al., *Cyclic flexure and laminar flow synergistically accelerate mesenchymal stem cell-mediated engineered tissue formation: Implications for engineered heart valve tissues*. Biomaterials, 2006. **27**(36): p. 6083-6095.
7. Niklason, L.E., et al., *Functional arteries grown in vitro*. Science, 1999. **284**: p. 489-493.
8. L'Heureux, N., et al., *A completely biological tissue-engineered human blood vessel*. FASEB Journal, 1998. **12**: p. 47-56.
9. Kanda, K., T. Matsuda, and T. Oka, *Mechanical stress induced cellular orientation and phenotypic modulation of 3-D cultured smooth muscle cells*. ASAIO Journal, 1993. **39**: p. M686-M690.
10. Seliktar, D., R.M. Nerem, and Z.S. Galis, *Mechanical strain-stimulated remodeling of tissue-engineered blood vessels constructs*. Tissue Engineering, 2003. **9**(4): p. 657-666.
11. Isenberg, B.C. and R.T. Tranquillo, *Long-term cyclic distention enhances the mechanical properties of collagen-based media-equivalents*. Annals of Biomedical Engineering, 2003. **31**: p. 937-949.

12. Rodriguez, E.K., A. Hoger, and A.D. McCulloch, *Stress-dependent finite growth in soft elastic tissues*. Journal of Biomechanics 1994. **27**: p. 455-467.
13. Kachanov, L., *Time of the rupture process under creep conditions*. Izvestija Akademii Nauk Sojuza Sovetskich Socialisticeskich Respubliki (SSSR) Otdelenie Techniceskich Nauk (Moskra), 1958. **8**: p. 26-31.
14. Kachanov, L., *Introduction to continuum damage mechanics*. 1986, Dordrecht, The Netherlands: Martinus Nijhoff Publishers.
15. Rabotnov, Y., *Creep Rupture*. Proceedings of the XII International Congress on Applied Mechanics, 1968.
16. Fung, Y.C., S.Q. Liu, and J.B. Zhou, *Remodeling of the constitutive equation while a blood vessel remodels itself under stress*. Journal of Biomechanical Engineering, 1993. **115**: p. 453-459.
17. Girton, T., T. Oegema, and R.T. Tranquillo, *Exploiting glycation to stiffen and strengthen tissue equivalents for tissue engineering*. Journal of Biomedical Materials Research, 1999. **46**: p. 87-92.
18. Elbjeirami, W.M., et al., *Enhancing mechanical properties of tissue-engineered constructs via lysyl oxidase crosslinking activity*. Journal of Biomedical Materials Research, 2003. **66A**: p. 513-521.
19. Chuong, C.J. and Y.C. Fung, *On residual stress in arteries*. Journal of Biomechanical Engineering, 1986. **108**: p. 189-192.
20. Wagenseil, J.E., E. Elson, and R.J. Okamoto, *Cell orientation influences the biaxial mechanical properties of fibroblast populated collagen vessels*. Annals of Biomedical Engineering, 2004. **32**(5): p. 720-731.
21. Zaucha, M.T., et al., *A novel cylindrical biaxial computer-controlled bioreactor and biomechanical testing device for vascular tissue engineering*. Tissue Eng Part A, 2009. **15**(11): p. 3331-40.
22. Syedain, Z.H., J.S. Weinberg, and R.T. Tranquillo, *Cyclic distension of fibrin-based tissue constructs: evidence of adaptation during growth of engineered connective tissue*. Proceedings of the National Academy of Sciences of the United States of America, 2008. **105**(18): p. 6537-6542.
23. Humphrey, J.D., *Cardiovascular Solid Mechanics: Cells, Tissues, Organs*. 2002, New York: Springer-Verlag.

24. Gleason, R.L. and J.D. Humphrey, *A 2-D constrained mixture model for arterial adaptations to large changes in flow, pressure, and axial stretch*. *Mathematical Medicine and Biology*, 2005. **22**(4): p. 347-369.
25. Feng, Z., et al., *Investigation of the mechanical properties of contracted collagen gels as a scaffold for tissue engineering*. *Artificial Organs*, 2003. **27**(1): p. 84-91.
26. Stemper, B.D., N. Yoganandan, and F.A. Pintar, *Mechanics of arterial subfailure with increasing loading rate*. *Journal of Biomechanics*, 2007. **40**(8): p. 1806-1812.

CHAPTER 4

A PHENOMONOLOGICAL MODEL FOR COLLAGEN GEL

DAMAGE UNDER UNIAXIAL LOADING

4.1 Introduction

In this study a phenomenological model for the damage of collagen-based TEBVs is proposed. A non-linear, incompressible, isotropic material under a uniaxial load is considered. Following the continuum damage mechanics approach [1], the basic hypothesis of this chapter is that damage is the process of accumulation and growth of microdefects that can be described via the evolution of an internal scalar parameter over time.

In general, materials can fracture: i) under monotonic loading at a constant loading rate; ii) under creep-fracture tests when the magnitude of the constant load exceeds a certain value, and iii) under cyclic loading. The latter case is termed fatigue. The main characteristics that distinguish fatigue fracture from other types of fracture are a) an increase in stress (or strain) stress results in a decrease in the number of cycles to failure for the material; this is usually typified in an S-N graph, which plots the nominal stress against the number of cycles to failure; and b) there is a concomitant increase in the extension (development of a plastic deformation) with increasing cycle number at any given stress. In most cases there exists an endurance amplitude stress at or below which the material does not fracture and does not change its mechanical properties regardless of the number of cycles. Cyclic loading is a typical physiological event in many biological tissues, especially in arterial tissue.

In this study, a theoretical framework for the evolution of damage in collagen gel-derived TEBVs is described. Data was obtained from Seliktar et al. [2] to determine necessary parameters for the model. The model is then used to present illustrative examples of monotonic loading, creep-fracture tests, and cyclic loading until failure tests.

4.2 Mathematical Model

Consider a strip made of a nonlinear elastic, homogeneous, isotropic and incompressible material. In the unloaded state, denoted by B_0 , it has an initial length L_0 and cross-sectional area A_0 , (Fig.1). At time $t=0$, the strip is subjected to a uniaxial tensile force and experiences large strains which produce nominal stresses (force per unit undeformed area A_0) that are defined by:

$$P(t) = P_s + \dot{P}t + P_d \sin^2 2\pi ft, \quad (4.1)$$

where P_s is the constant nominal stress, \dot{P} is the rate of change of the nominal stress, $P_d \sin^2 2\pi ft$ is the cyclic nominal stress of amplitude P_d and frequency f .

Because the material is elastic, the strip undergoes an instantaneous finite deformation to the deformed state b_0 (Figure 4-1), with length $L(0)$ and cross-sectional area $A(0)$. The

longitudinal stretch ratio is

$$\lambda(0) = \frac{l(0)}{L_0} \quad (4.2)$$

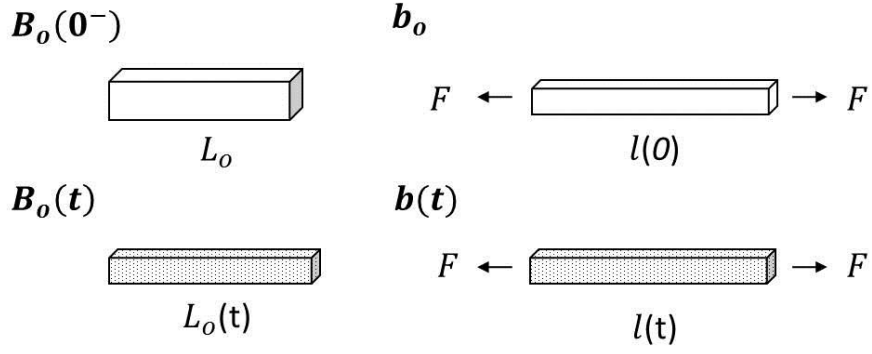


Figure 4-1. Uniaxial Kinematics. Schematic of the initial unloaded state $B_o(0)$, the deformed state b_o due to the instantaneous elastic deformation, the deformed state $b(t)$ that results from the accumulation of damage, and the unloaded state $B_o(t)$ after the load in $b(t)$ is removed.

Due to the material incompressibility assumption, the right Green strain tensor is

$$\begin{pmatrix} \frac{1}{2}(\lambda(0)^2 - 1) & 0 & 0 \\ 0 & \frac{1}{2}\left(\frac{1}{\lambda(0)} - 1\right) & 0 \\ 0 & 0 & \frac{1}{2}\left(\frac{1}{\lambda(0)} - 1\right) \end{pmatrix} \quad (4.3)$$

and the only non-zero Cauchy (or true) stress component is

$$\sigma(0) = 2\left(\lambda(0)^2 - \frac{1}{\lambda(0)}\right)\left(\frac{\partial W}{\partial I_1} + \frac{1}{\lambda_1} \frac{\partial W}{\partial I_2}\right), \quad (4.4)$$

where $W(I_1, I_2)$ is the strain energy density function of the elastic material and

$$I_1 = \lambda^2 + \frac{2}{\lambda} \quad \text{and} \quad I_2 = 2\lambda + \frac{1}{\lambda^2} \quad (4.5)$$

are strain invariants of the Green strain tensor E .

Consistent with experimental observations in soft biological tissue and collagen gels [3-9], it is hypothesized that if the magnitude of the stress (or strain) exceeds a certain critical value the tissue becomes partially damaged, which causes i) a gradual reduction in the effective load bearing capacity of the material and ii) an increase in the unloaded length of the strip. Denoting the unloaded and deformed length as $L_o(t)$ and $l(t)$ at time t , respectively (Fig.1), the longitudinal ratio stretch,

$$\lambda(t) = \frac{l(t)}{L_o} \quad (4.6)$$

can be decomposed as follows

$$\lambda(t) = \lambda_p(t)\lambda_s(t), \quad (4.7)$$

$$\text{where } \lambda_p(t) = \frac{L_o(t)}{L_o} \text{ and } \lambda_s(t) = \frac{l(t)}{L_o(t)} \quad (4.8)$$

where $\lambda_p(t)$ and $\lambda_s(t)$ are the irreversible (plastic) and reversible stretch ratios, respectively.

It is assumed that the state $B_o(t)$ is stress-free both locally and globally. Since the tissue represents a mixture of damaged and undamaged material, this assumption is valid provided that the damaged material is not capable of bearing any load; only the stretch $\lambda_s(t)$ produces a stress. The stress, defined per unit current area of undamaged material is the *effective stress* at time t and is denoted by $\sigma_{ef}(t)$. This way the contribution of the damage is separated from the deformation that induces the stress field.

Since the material is assumed to be elastic, the stress configuration $B_o(t)$ is unique and this decomposition can be performed. It is assumed that the material remains elastic, isotropic and incompressible and the constitutive equations remain unchanged over time. The stress-strain relation at any time t is given by equation (4.4) when $\sigma(0)$ is replaced by $\sigma_{sf}(t)$ and $\lambda(0)$ by $\lambda_s(t)$.

It is assumed in this study that the mechanical properties of the undamaged material are not affected by the damage of the rest of material. A plausible justification of this assumption is based on the structure of most soft tissues and tissue engineered constructs, fibers or long chain collagen molecules are gradually recruited during load bearing [10-14]. The breakage of certain fibers might lead to a redistribution of the load and rearrangement of the fibers in a manner such that the intrinsic structure of the tissue is preserved. The gradual fiber recruitment and failure can justify the introduced assumption for the evolution of the unloaded configuration.

Following the continuum damage mechanics approach proposed by Kachanov [1] and Rabotnov [15], the decrease in load bearing capacity of a material is considered to be due to a loss in the load-bearing area due to the accumulation and growth of microdefects. The ratio between the damaged deformed area $A_D(t)$ and total deformed area $A(t)$ is assumed to be an internal scalar damage parameter. The damage parameter, D , is defined

as one minus this ratio, which gives the ratio of undamaged area to the total deformed area. Assuming that the damaged material remains incompressible, the damage parameter can be defined through the ratios of the undeformed areas:

$$D(t) = 1 - \frac{A_{D_o}(t)}{A_o}. \quad (4.9)$$

Since the undeformed damaged area $A_{D_o}(t)$ cannot be measured experimentally, the damage parameter $D(t)$ ¹ is not known. D varies from $D = 1$ to $D = 0$, when the material is not damaged and when the material has failed (the entire cross-section is damaged), respectively.

The relationship between the nominal stress and the effective stress, assuming quasistatic deformation and accounting for material incompressibility, is

$$P = \frac{D\sigma_{ef}}{\lambda_p\lambda_e}. \quad (4.10)$$

Equation (4.10) and the constitutive equation (4.4) contain four unknown scalar functions: σ_{ef} , λ_e , λ_p , and D . To complete the system of equations it is necessary to prescribe i) an evolution equation for the damage parameter D and ii) an evolution equation for the irreversible stretch ratio λ_p .

The evolution of the damage parameter is postulated to have following general form

¹ The argument t will be omitted for the rest of this chapter.

$$\frac{dD}{dt} = \phi(\sigma_{ef}) + \phi_2\left(\frac{d\sigma_{ef}}{dt}\right) + \phi_3(D). \quad (4.11)$$

The functions $\phi(\sigma_{ef}) \geq 0$ and $\phi_2(d\sigma_{ef}/dt) \geq 0$ account for the contribution of the current effective stress and the stress rate to damage accumulation, respectively. Both functions are equal to zero when $\sigma_{ef} \leq \sigma_{cr}$, where σ_{cr} is the critical stress that initiates damage. Though the mechanical response of the undamaged material is purely elastic, it is assumed that the process of damage might depend on the rate of stress and its effects are additive to the effect of the stress itself. $\phi_2(d\sigma_{ef}/dt)$ is zero when $d\sigma_{ef}/dt \leq d\sigma_{cr}/dt$, where $d\sigma_{cr}/dt$ is a critical stress rate that initiates damage. The third term in equation (4.11) accounts for a possible coupling between in vivo damage accumulation and the biological repair processes that takes place in living tissues. A similar mechanism was proposed for the damage-adaptive remodeling of bones [16]. The function $\phi_3(D)$ is less than 0 if $D < 0$, and zero if $D = 1$. In this study, ϕ_3 is assumed to be zero because the tests are performed rapidly and with not enough time for biological repair to take place.

Finally, it is assumed that the rate of change of the rate of change of the irreversible stretch ratio, λ_p , depends on effective stress, σ , and the current λ_p :

$$\frac{d\lambda_p}{dt} = \psi(\sigma, \lambda_p) \quad (4.12)$$

The functional form of ϕ_1 , ϕ_2 , ϕ_3 , and ψ must be determined on the basis of some heuristic considerations and appropriately designed experiments that will be discussed later.

At the moment the load is applied, $t=0$, no part of the material is damaged, i.e. $D(0) = 1$ and $\lambda_p(0) = 1$. Equations (4.4), (4.10), (4.11), and (4.12) are coupled and have to be solved simultaneously. At time t , let the solution of the system of the governing equations be $D(t) = D$, \bar{D} and $\lambda_p(t) = \bar{\lambda}_p$. If the loading process is interrupted and no biological repair has taken place, the strip takes the unloaded configuration $B_0(t)$ (Fig. 1) and has length $L_o(t) = \bar{\lambda}_p L_o$ and cross-sectional area $A_o(t) = A_o / \bar{\lambda}_p$. Let the strip be subjected to a quasistatic load that produces an effective stress that does not cause any damage. Since the mechanical properties of the undamaged part of the material are assumed to be identical to those of the material before the damage occurred, with fixed values for \bar{D} and $\bar{\lambda}_p$, the relationship between any nominal stress P and a corresponding elastic stretch ratio λ_e can be calculated using equation (4.10). The $P - \lambda_e$ relation can be converted into the “apparent true stress”, σ_{app} , - “apparent stretch ratio”, λ_{app} , relation using the expressions

$$\begin{aligned}\sigma_{app} &= \lambda_e P \\ \lambda_{app} &= \lambda_e\end{aligned}\tag{4.13}$$

This $\sigma_{app}-\lambda_{app}$ relationship is analogous to the stress-stretch relationship that follows from the one-dimensional constitutive equation (4.4) for an undamaged, intact strip. The relation $\sigma_{app}-\lambda_{app}^2$ describes the theoretically predicted mechanical response of a partially damaged strip at time t . It is important to obtain this relationship for different stages of damage, so that the predicted variation of the irreversible stretch ratio can be compared with experimental data for the damage-induced residual elongation of the strip and the mechanical response under uniaxial tensile testing.

4.3 Illustrative Examples

Applications of the proposed model requires a specification of the functional form of the constitutive equations of the material, the kinetic equations for evolving the damage parameter and irreversible deformation, as well as the values of all model parameters. This information must come from relevant experimental data. Reliable constitutive equations for most biological soft tissues can be found in the literature [17, 18]. However, the available experimental data on fracture and fatigue of gel-based tissues are insufficient for identification of model functions and parameters. To illustrate the theoretical predictions of the proposed model several illustrative examples are considered based on *a priori* selection of the evolution equations and from general results from the literature.

² The subscript *app* will be omitted for the rest of this chapter.

In general, the one-dimensional constitutive equation is a function of two response functions (equation 4.4) and uniaxial tests are not sufficient to determine the form of the strain energy function. In this study, however, it is assumed that the strain energy is only a function of the first Green strain invariant, I_1 . This assumption has been shown to be reasonable for various materials such as rubber, elastin, and certain hydrogels [19-21].

Based on this relationship, the one-dimensional stress-stretch relationship (equation (4.4) for any time t) becomes

$$\sigma = 2 \left(\lambda^2 - \frac{1}{\lambda} \right) \frac{dW}{dI_1} \quad (4.14)$$

It then follows that $\partial W / \partial I_1$ is a function of measurable parameters:

$$\frac{dW}{dI_1} = \frac{\sigma \lambda}{2(\lambda^3 - 1)} \quad (4.15)$$

where $\sigma = f/A = f\lambda/A_o$, f is the measured force, A is the deformed area, and A_o is the initial, undeformed area, for an incompressible material. The expressions for I_1 (given by equation (4.5)) and dW/dI_1 can now be expressed in terms of measurable quantities that can be obtained during any state of the experiment and the analytical form of strain energy function can be derived from this relationship. In the particular case for the collagen gel, the relationship between I_1 and $\ln dW/dI_1$ is linear and the straight line can be expressed as

$$\ln dW/dI_1 = A I_1 + B, \quad (4.16)$$

where A and B are constants that can be determined using linear regression. Integration of equation (4.16) and the application of the boundary condition that under no load $I_1 = 3$ and $W = 0$ yields the following strain energy function

$$W = \frac{c}{a} \exp[a(I_1 - 3) - 1] \quad (4.17)$$

where $a = A$ and $c = e^{3a+b}$ are material constants. These material constants were determined by using data obtained from Seliktar *et al.* [2] using the nominal stress-strain curve provided, where $a = 29.158$ and $c = 1.413$. For this form of the strain energy function the stress-stretch relationship (equation (4.4)) is

$$\sigma = 2c \left(\lambda^2 - \frac{1}{\lambda} \right) \exp \left[a \left(\lambda^2 + \frac{2}{\lambda} - 3 \right) \right] \quad (4.18)$$

The stress-stretch curve obtained using equation 4.18 prior to damage or plastic deformation yields a good fit to the experimental data obtained by Seliktar *et al.* [2] (Figure 4-2).

The kinetic equation (4.11) is postulated to have the following form

$$\frac{dD}{dt} = \begin{cases} \alpha_1(\sigma - \sigma_{cr})^{\beta_1} + \alpha_2 \left(\frac{d\sigma}{dt} - \frac{d\sigma_{cr}}{dt} \right)^{\beta_2} & \text{if } \sigma > \sigma_{cr} \text{ and } \frac{d\sigma}{dt} > \frac{d\sigma_{cr}}{dt} \\ \alpha_1(\sigma - \sigma_{cr})^{\beta_1} & \text{if } \sigma > \sigma_{cr} \text{ and } \frac{d\sigma}{dt} < \frac{d\sigma_{cr}}{dt} \\ 0 & \text{if } \sigma < \sigma_{cr} \end{cases} \quad (4.19)$$

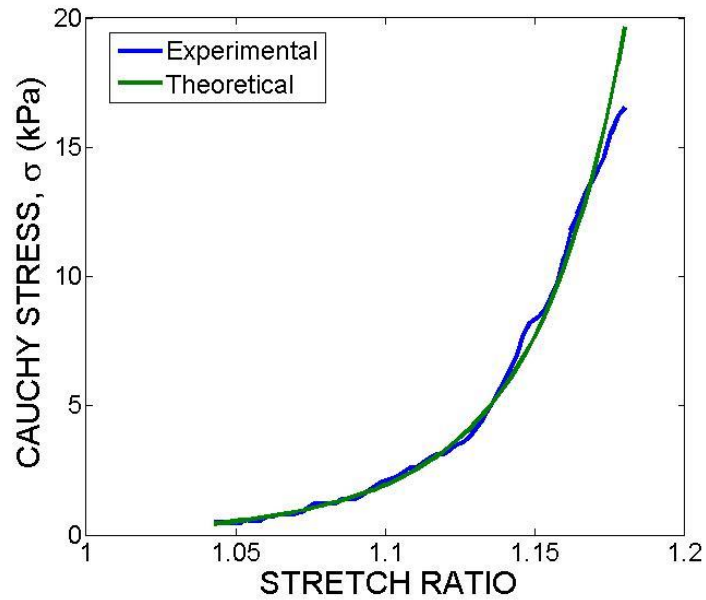


Figure 4-2. Comparison of theoretical and experimental stress-stretch curves prior to damage.

where $\alpha_1, \alpha_2, \beta_1, \beta_2, \sigma_{cr}$, and $d\sigma_{cr}/dt$ are constants that need to be determined experimentally. The constants σ_{cr} and $d\sigma_{cr}/dt$ are threshold values below which the stress and stress rate do not affect the continuity of the material. It is assumed that the deviations of stress and stress rate drive the accumulation of damage accumulation, while the constants $\alpha_1, \alpha_2, \beta_1$, and β_2 control the sensitivity of these processes. Since no biological repair mechanisms take place the model function α_3 in equation (4.11) is set equal to zero.

The evolution of the irreversible stretch ratio (equation (4.12)) is postulated to have the following form:

$$\frac{d\lambda_p}{dt} = \alpha_p \lambda_p \frac{\sigma - \sigma_y}{\sigma_y} \quad (4.20)$$

where σ_y is the yield stress after which plastic deformation ensues ($\alpha_p = 0$ if $\sigma < \sigma_y$).

In this study, the uniaxial loading conditions of collagen gels in vitro are simulated. Since most ‘uniaxial’ experiments in the literature are ring tests, the θ -direction from cylindrical coordinates corresponds to the uniaxial tensile loading direction. Note that gradients in strain across the wall that will develop as a circular ring is deformed to a uniaxial strip are neglected; i.e., the mean stresses across the wall are considered.

The load is specified to produce i) nominal stresses of 10 -100 kPa , ii) stress rates imposed by specifying the stretch rate to be 0.1- 10 mm/s, and iii) cyclic stresses of amplitudes 10-100 kPa at frequencies of 0.1-100 Hz. The governing equations of the model were solved numerically using MATLAB to simulate the following experimental conditions i) fracture due to monotonic loading at a constant loading rate, ii) creep-fracture tests, and iii) fatigue tests of different stress amplitudes and frequencies. The prescribed loads for the cases simulated are given in Table 4-1.

Table 4-1. List of simulated uniaxial mechanical tests.

| Type of Test | Nominal Stress | Values |
|--------------|-----------------------------------|---|
| Monotonic | $P(t) = \dot{P}t$ | $\dot{P} = 0.5, 1, 5, 10/s$ |
| Creep | $P(t) = P_s$ | $P_s = 40, 60, 80, 100 kPa$ |
| Fatigue | $P(t) = P_s + P_d \sin^2 2\pi ft$ | $P_s = 0$ $P_d = 0, 10, 20, 30, 40 kPa$ $f = 1, 2, 3, 4, 5/s$ |

4.3.1 Monotonic Loading to Failure

Uniaxial (ring) tests on collagen-based TEBVs have been presented by several groups in the literature [2, 22, 23]; a typical nominal stress (P) versus stretch curve shows a non-linear loading profile to the ultimate (nominal) stress, followed by a decrease in loading until failure (Figure 4-3). The parameters in equations (4.19) and (4.20) were determined using data obtained by Seliktar et al. [2] to be $\alpha_p = 0.25$, $\alpha_1 = 10^{-3.4}$, $\alpha_2 = 10^{-6.5}$, $a_1 = 1 \text{ kPa}$, $a_2 = 0.1 \text{ kPa/s}$, $\beta_1 = 1.96$, $\beta_2 = 1.2$, and $\sigma_y = 15 \text{ kPa}$. Simulations run at a stretch rate of $\dot{\lambda}=0.2/\text{s}$ are shown in Figure 4-3 and demonstrate a reasonable fit.

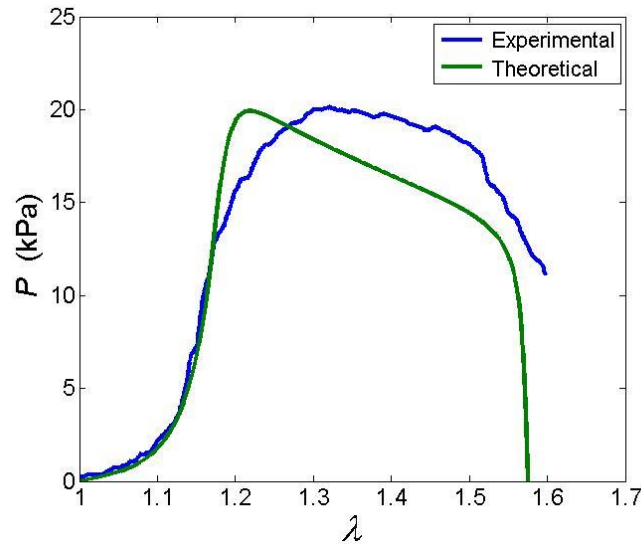


Figure 4-3. Comparison of theoretical and experimental stress-stretch curves following damage.

Modeling simulations performed at stretch rates of 0.5, 1, 5, and 10 /s are shown in. In agreement with results from the literature in native biological tissues [7] and collagen gels [6, 8, 9], different stretch rates result in different nominal stress-stretch curves and

ultimate stresses (Figure 4-4a). The damage parameter is initially 1 (no damage) and decreases over time as damage accumulates in the material (Figure 4-4b). The irreversible stretch ratio, λ_p , starts out at 1 (no plastic deformation) and increases as plasticity ensues, when the effective stress, σ_{ef} , exceeds the yield stress, σ_y (Figure 4-4c).

In addition, these simulations were used to predict the effective (Figure 4-5a) and apparent stresses (Figure 4-5b), which are non-measurable quantities that can help predict the mechanical environments that the cells in the gel experience. Figure 4-6 is a parametric study on the effects of strain rate on the ultimate stress. The ultimate stress increases with increasing strain rate, rapidly at first but starts to plateau as the strain rate exceeds 200/s.

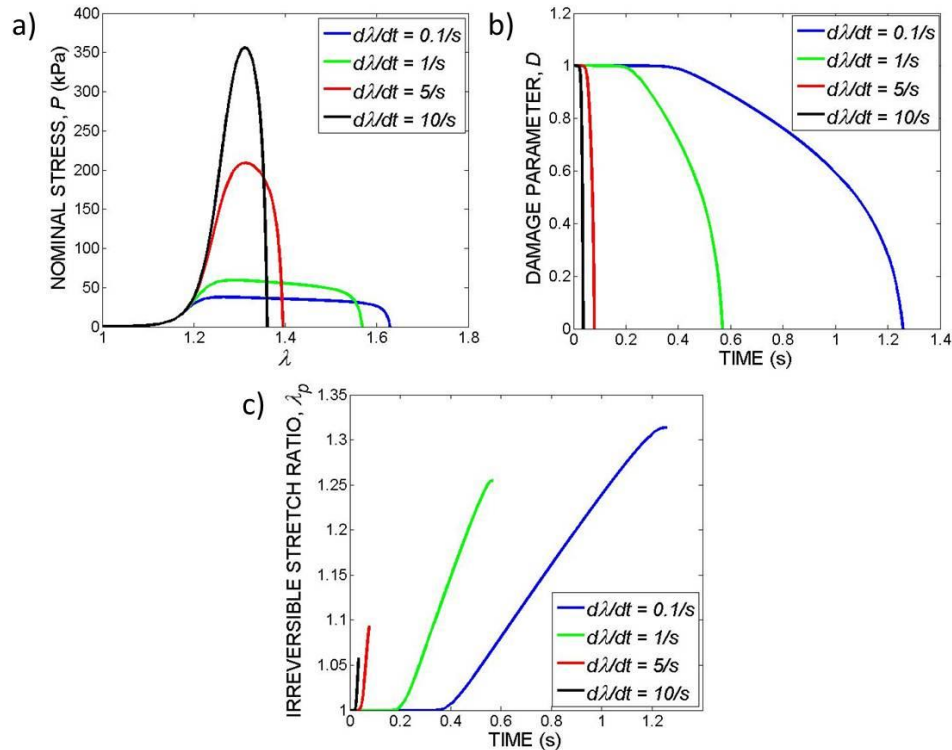


Figure 4-4. Modeling simulations of uniaxial tensile tests at different stretch rates.

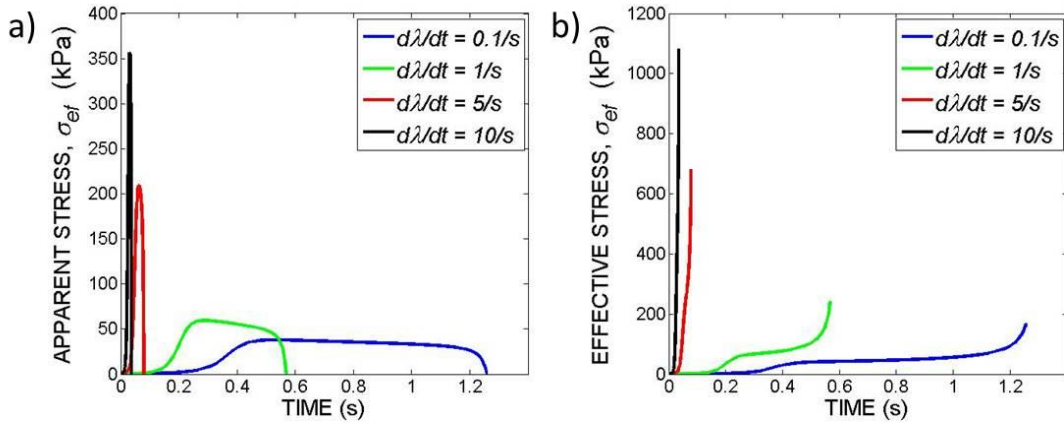


Figure 4-5. Theoretical prediction of the a) apparent and b) effective stresses.

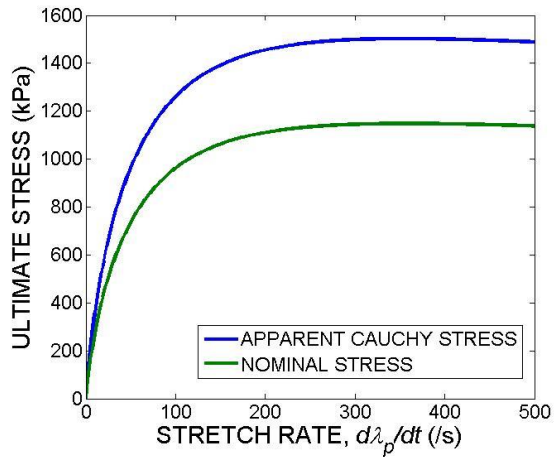


Figure 4-6. Predicted UTS with increasing stretching rates.

4.3.2 Uniaxial Creep Testing

Uniaxial creep tests have also been presented in the literature [6, 24-26]. Using the parameters obtained above, the general trends are the same as those observed in the literature. The exact magnitudes can be adjusted based on experiment and material parameters. The apparent Cauchy stress, σ , and the apparent stretch ratio, λ , increase gradually at first, then rapidly near the time of failure (Figure 4-7a-b). The residual stretch increases non-monotonically as the applied load increases (Figure 4-7c). The

damage parameter decreases faster with increasing applied load (Figure 4-7d). A parametric study of the effect of the applied load during uniaxial creep testing revealed that the stretch at failure increases as the applied load increases, while the time to failure decreases as the load increases (Figure 4-8). Experimental results of varying loads during creep tests were not available in the literature but the results are as intuitively expected.

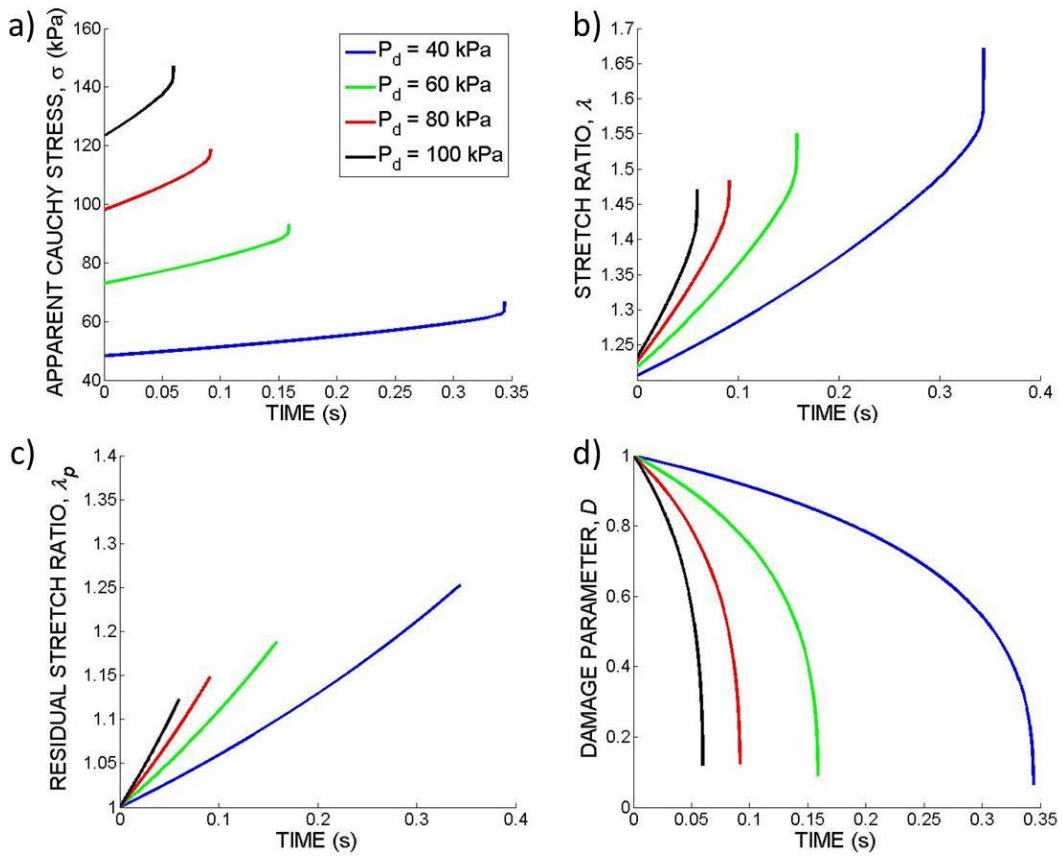


Figure 4-7. Modeling simulations of uniaxial creep tests. a) Change in the apparent stress, b) apparent stretch ratio, c) residual stretch ratio, and d) damage parameter over time.

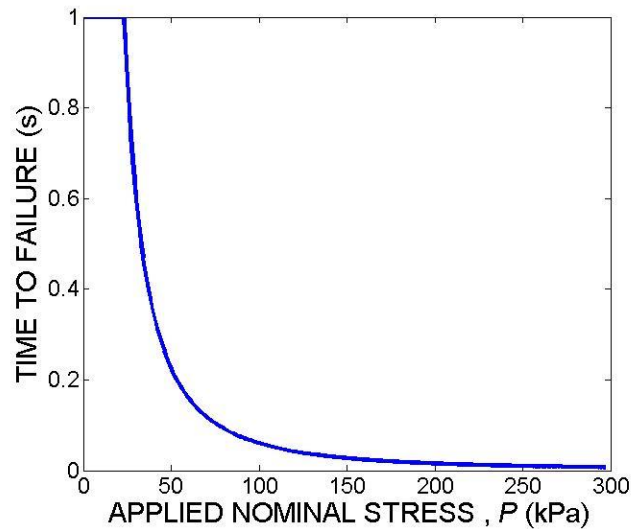


Figure 4-8. Predicted time to failure with increasing applied nominal stress.

4.3.3 Uniaxial Fatigue Testing

Fatigue testing on rings of gel-derived TEBV have also been performed [27-29]. These tests, however, were not performed until failure. Simulations were performed using the parameters obtained from uniaxial monotonic testing and therefore assume a stretch and stress behavior at failure. Simulations were performed with the inputs listed in table 4.1. In addition, two parametric studies of uniaxial fatigue testing were simulated: variable amplitudes at a constant frequency and variable frequencies at a constant amplitude.

To demonstrate the general trends during fatigue testing $P_d = 20 \text{ kPa}$ and $f = 2 \text{ Hz}$ were used. The mean and cyclic values of stretch and stress evolve as damage proceeds (Figure 4-9). The apparent Cauchy stress versus stretch curves shift to the right for each cycle (the unloaded stretch increases with each cycle), until failure (

Figure 4-10). This is consistent with results from the literature and biaxial fatigue experiments performed in our lab [30].

4.3.3.1 Effects of Strain Amplitude

The effect of varying the amplitude in the theoretical model was tested. Figure 4-11 is a parametric study of the effects of the amplitude of the applied load on the number of cycles. The number of cycles prior to failure (and time to failure) decreases as the amplitude of the applied load increases (Figure 4-12). The overall behavior is consistent with results from the literature [9, 27], however the behavior of the collagen gel failure was not determined in these studies and could not be compared to any simulations.

4.3.3.2 Effects of Frequency

Some tests on the effects of different frequencies have been reported in the literature [6, 9, 31], but the results are difficult to interpret because only the change in maximum force or stiffness were recorded and experiments were not performed to failure. In addition, most of these tests were performed long term, where biological remodeling could have taken place. Apparent stress-cycle number and apparent stretch ratio-cycle number curves for frequencies of 1-5 Hz at $P_d = 20 \text{ kPa}$ are shown in Figure 4-13. No differences in the time to failure were seen between different frequencies. The maximum apparent stress and strain gradually increase with each cycle (Figure 4-13) for each frequency, which is consistent with results obtained by Achilli et al [27]. The number of cycles prior to failure increases with increasing frequency, but the maximum stress remains approximately the same (Figure 4-13a), which is consistent with fatigue

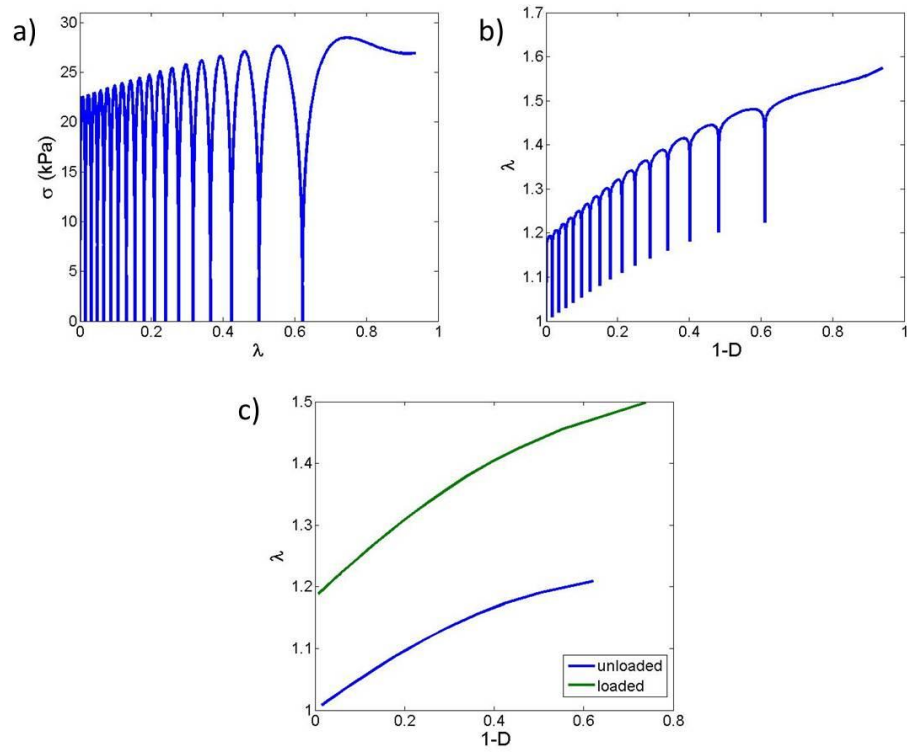


Figure 4-9. Modeling simulations of uniaxial cyclic loading. a) Stress-stretch response. b) Change in apparent stretch ratio and c) the loaded and unloaded stretch during the accumulation of damage.

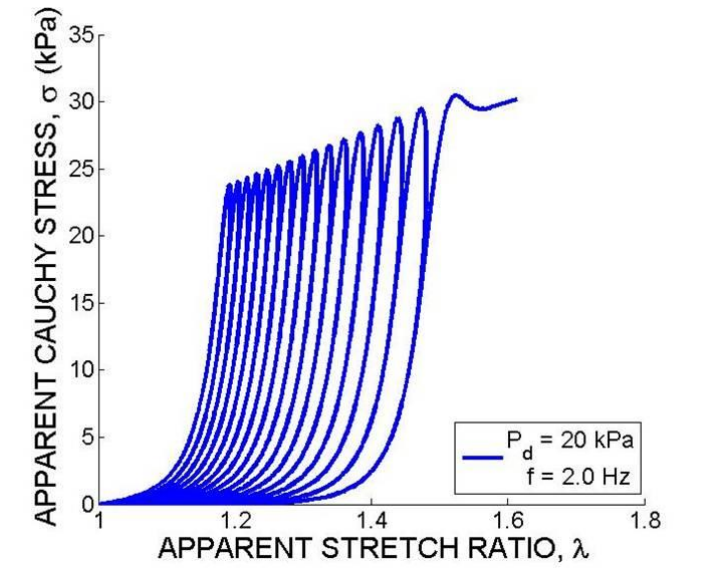


Figure 4-10. Apparent stress-stretch response during cyclic loading.

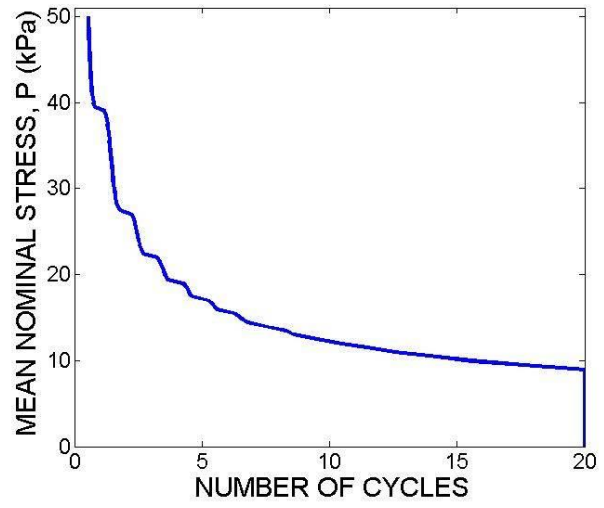


Figure 4-11. Nominal stress with increasing cycle number.

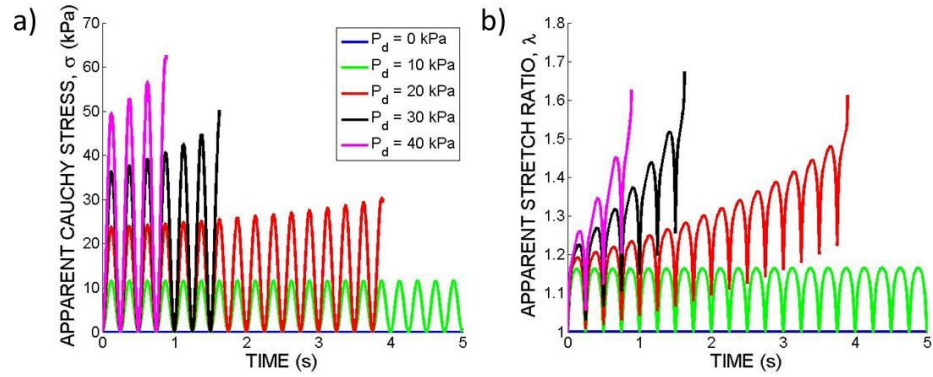


Figure 4-12. Effect of amplitude on the apparent a) stress and b) stretch ratio over the time of the test.

experiments performed on bone [32]. The variations in the maximum stress and strain in Figure 4-13 in the end are due to the vessel failing at different points of the final cycle. These results appear to be consistent with the observations by Wille et al [9]. When CytoD was added to the tissue, to disrupt the cellular cytoskeletal, the maximum force recorded with each cycle was not frequency-dependent.

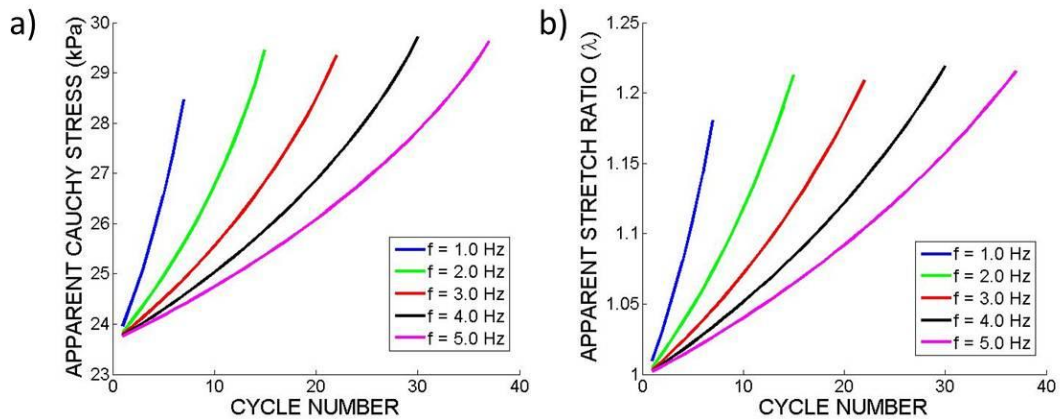


Figure 4-13. Effect of frequency on the apparent a) stress and b) stretch ratio with increasing cycle number.

4.4 Discussion

It is well known that collagen gels plastically deform [2, 23, 25] in response to applied loads. In this chapter, it is assumed that the vessel also undergoes structural damage as has been suggested through microstructural imaging of collagen gels after mechanical loading [29, 33, 34]. The objectives of this study were to predict the failure response of uniaxially tested collagen gel-based TEBVs and to motivate necessary experiments for quantifying the plastic and damage response of the TEBVs. It was assumed that damage is stress and stress rate dependent.

In this chapter, the damage of collagen-derived gels was considered under conditions that guarantee the elimination of non-mechanical factors on the mechanical properties and strength of the material. Experiments considered in this chapter are run *in vitro* and hence the tissue is not capable of biological repair.

The limitations of this study are due to the proposed simplifying assumptions. Only uniaxial data is taken into account. Extending the model to include biaxial mechanical testing is necessary to predict changes in the axial direction in addition to the circumferential direction. In addition, the model proposed does not take into account microstructural changes that occur during mechanical testing. Future extension of this model can include microstructurally-motivated constitutive and evolution equations [35-37].

The mechanical properties of the material were assumed from experiments presented in the literature. Additional experiments are necessary to verify the results of these simulations. Monotonic tensile tests run at different rates, creep tests performed at different loads, and fatigue loading until failure performed on the same set of TEBVs are necessary to identify the parameters presented in this model. In addition, since none of the results obtained from the literature performed all three mechanical tests on their vessels, results could not be verified between the different tests. A comparison of model predictions with data from experiments that were not used for parameter identification is needed to verify the accuracy of the model. The experiments proposed in this chapter are relatively simple and can be performed in most labs that test the mechanical properties of TEBVs.

In summary, a phenomenological model to predict the failure of collagen-based TEBVs under uniaxial loading was developed. In comparison with available literature, the simulations presented in this chapter suggest that the model captures the overall features of plastic deformation and damage of the collagen gel. The overall theoretical approach can be applied to other types of vessels. The constitutive equations can be modified to account for material differences and experiments motivated by this study can be performed to determine necessary parameters for the evolution equations prescribed. The model can then be used as a predictive tool to determine graft quality and give valuable insight into the response of the vessel following implantation.

4.5 References

1. Kachanov, L.M., *Introduction to continuum damage mechanics*. Mechanics of elastic stability. 1986, Dordrecht ; Boston: M. Nijhoff. x, 135 p.
2. Seliktar, D., et al., *Dynamic mechanical conditioning of collagen-gel blood vessel constructs induces remodeling in vitro*. Ann Biomed Eng, 2000. **28**(4): p. 351-62.
3. Avolio, A., D. Jones, and M. Tafazzoli-Shadpour, *Quantification of alterations in structure and function of elastin in the arterial media*. Hypertension, 1998. **32**(1): p. 170-175.
4. Mohan, D. and J.W. Melvin, *Failure properties of passive human aortic tissue. I—uniaxial tension tests*. Journal of biomechanics, 1982. **15**(11): p. 887-902.
5. Mohan, D. and J.W. Melvin, *Failure properties of passive human aortic tissue. II—biaxial tension tests*. Journal of biomechanics, 1983. **16**(1): p. 31-44.
6. Wagenseil, J., et al., *One-dimensional viscoelastic behavior of fibroblast populated collagen matrices*. Journal of biomechanical engineering, 2003. **125**(5): p. 719.
7. Stemper, B.D., N. Yoganandan, and F.A. Pintar, *Mechanics of arterial subfailure with increasing loading rate*. Journal of biomechanics, 2007. **40**(8): p. 1806-1812.
8. Kokini, K., et al., *Tensile mechanical properties of three-dimensional type I collagen extracellular matrices with varied microstructure*. 2002.
9. Wille, J.J., E.L. Elson, and R.J. Okamoto, *Cellular and matrix mechanics of bioartificial tissues during continuous cyclic stretch*. Annals of biomedical engineering, 2006. **34**(11): p. 1678-1690.
10. Burton, A.C., *Relation of structure to function of the tissues of the wall of blood vessels*. Physiological reviews, 1954. **34**(4): p. 619-642.
11. Roach, M.R. and A.C. Burton, *The reason for the shape of the distensibility curves of arteries*. Can J Biochem Physiol, 1957. **35**(8): p. 681-90.
12. Niklason, L.E., et al., *Functional arteries grown in vitro*. Science, 1999. **284**(5413): p. 489-93.
13. Thornton, G., N. Shrive, and C. Frank, *Ligament creep recruits fibres at low stresses and can lead to modulus-reducing fibre damage at higher creep stresses:*

- a study in rabbit medial collateral ligament model*. Journal of orthopaedic research, 2002. **20**(5): p. 967-974.
14. Wagenseil, J.E. and R.J. Okamoto, *Modeling cell and matrix anisotropy in fibroblast populated collagen vessels*. Biomechanics and modeling in mechanobiology, 2007. **6**(3): p. 151-162.
 15. Rabotnov, Y.N. *Creep rupture*. 1968.
 16. Carter, D. and W. Caler, *A cumulative damage model for bone fracture*. Journal of orthopaedic research, 1985. **3**(1): p. 84-90.
 17. Fung, Y.C., *Biomechanics: Mechanical Properties of Living Tissues*. 1993: Springer.
 18. Humphrey, J.D., *Cardiovascular solid mechanics: cells, tissues, and organs*. 2002: Springer.
 19. Elshazly, T.H., *Characterization of PVA hydrogels with regards to vascular graft development*. 2004.
 20. Rachev, A., T. ElShazly, and D.N. Ku. *Constitutive formulation of the mechanical properties of synthetic hydrogels*. 2004. ASME.
 21. Rachev, A., L. Felden, and D.N. Ku, *Design and Fabrication of a Mechanically Matched Vascular Graft*. Journal of biomechanical engineering, 2011. **133**(9).
 22. Cummings, C.L., et al., *Properties of engineered vascular constructs made from collagen, fibrin, and collagen-fibrin mixtures*. Biomaterials, 2004. **25**(17): p. 3699-3706.
 23. Isenberg, B.C. and R.T. Tranquillo, *Long-term cyclic distention enhances the mechanical properties of collagen-based media-equivalents*. Ann Biomed Eng, 2003. **31**(8): p. 937-49.
 24. Berglund, J.D., R.M. Nerem, and A. Sambanis, *Viscoelastic testing methodologies for tissue engineered blood vessels*. Journal of biomechanical engineering, 2005. **127**(7): p. 1176-1184.
 25. Tranquillo, R., et al., *Magnetically orientated tissue-equivalent tubes: application to a circumferentially orientated media-equivalent*. Biomaterials, 1996. **17**(3): p. 349-357.
 26. Barocas, V.H., A.G. Moon, and R.T. Tranquillo, *The fibroblast-populated collagen microsphere assay of cell traction force--Part 2: Measurement of the cell traction parameter*. Journal of biomechanical engineering, 1995. **117**(2): p. 161.

27. Achilli, M., S. Meghezi, and D. Mantovani, *On the Viscoelastic Properties of Collagen-Gel-Based Lattices under Cyclic Loading: Applications for Vascular Tissue Engineering*. *Macromolecular Materials and Engineering*, 2012. **297**(7): p. 724-734.
28. Chaudhry, B., et al., *Nanoscale viscoelastic properties of an aligned collagen scaffold*. *Journal of Materials Science: Materials in Medicine*, 2009. **20**(1): p. 257-263.
29. Feng, Z., et al., *Investigation on the mechanical properties of contracted collagen gels as a scaffold for tissue engineering*. *Artificial organs*, 2003. **27**(1): p. 84-91.
30. Zaucha, M.T., et al., *A novel cylindrical biaxial computer-controlled bioreactor and biomechanical testing device for vascular tissue engineering*. *Tissue Eng Part A*, 2009. **15**(11): p. 3331-40.
31. Krishnan, L., et al., *Design and application of a test system for viscoelastic characterization of collagen gels*. *Tissue engineering*, 2004. **10**(1-2): p. 241-252.
32. Caler, W.E. and D.R. Carter, *Bone creep-fatigue damage accumulation*. *Journal of biomechanics*, 1989. **22**(6): p. 625-635.
33. Raub, C.B., et al., *Noninvasive assessment of collagen gel microstructure and mechanics using multiphoton microscopy*. *Biophysical journal*, 2007. **92**(6): p. 2212-2222.
34. Raub, C., et al., *Predicting bulk mechanical properties of cellularized collagen gels using multiphoton microscopy*. *Acta biomaterialia*, 2010. **6**(12): p. 4657-4665.
35. Gleason, R.L., L.A. Taber, and J.D. Humphrey, *A 2-D model of flow-induced alterations in the geometry, structure, and properties of carotid arteries*. *J Biomech Eng*, 2004. **126**(3): p. 371-81.
36. Hansen, L., W. Wan, and R.L. Gleason, *Microstructurally motivated constitutive modeling of mouse arteries cultured under altered axial stretch*. *J Biomech Eng*, 2009. **131**(10): p. 101015.
37. Wan, W., J.B. Dixon, and R.L. Gleason, *Constitutive modeling of mouse carotid arteries using experimentally measured microstructural parameters*. *Biophysical journal*, 2012. **102**(12): p. 2916-2925.

CHAPTER 5

EXPERIMENTAL FRAMEWORK TO STUDY THE EFFECTS OF PLASTICITY AND DAMAGE DURING UNIAXIAL LOADING OF COLLAGEN GELS

5.1 Introduction

Collagen gel-based vascular scaffolds have been widely studied due to ease of fabrication, ability to support cell growth, and lack of immunogenicity [1, 2]. However, suboptimal mechanical properties have prevented the successful use of these grafts [3, 4]. Collagen-based scaffolds have been shown to undergo plastic deformation even under modest loads, which often leads to tissue damage and eventual failure [5-7]. A constitutive model that describes the response of these vessels to applied loads is necessary to understand and predict failure. Due to the plasticity and damage experienced by TEBVs in general, standard testing of compliance and burst pressure are not enough to determine graft quality. It is important to quantify the reduction in plasticity and damage in the production and evaluation of graft quality.

In chapter 4, a theoretical model was developed to describe the response of collagen-based TEBVs to uniaxial mechanical testing. It was postulated that monotonic tensile, creep, and fatigue tests are necessary in order to accurately describe the damage and plasticity response of the hydrogel. The goal of the current study is to develop an experimental framework to perform these tests, validate the proposed mechanisms of failure, and to determine the parameters of the prescribed evolution equations.

In addition, a new method for quantifying strain fields across the length of the ring during the mechanical test was developed by speckling the tissue with carbon markers and using digital image correlation (DIC). The results provide valuable information of the subfailure mechanisms of collagen-based TEBVs that could not be obtained by individual marker tracking alone.

5.2 Materials and Methods

5.2.1 Experimental Methods

5.2.1.1 Rat Aortic Smooth Muscle Cells

RASMCs were isolated from Sprague-Dawley rats. The cells were expanded and used at passages between 6 and 10. RASMC cell culture medium consisted of Dulbecco's modified Eagle's medium (DMEM; Mediatech Cellgro) supplemented with 10% FBS (Hyclone), 1% L-glutamine (Mediatech Cellgro), and 1% penicillin-streptomycin (Mediatech Cellgro).

5.2.1.2 Collagen Gel-derived TEBV Fabrication

Collagen constructs were made with type I bovine collagen (MP Biomedicals) at 2 mg/mL collagen. The lyophilized collagen was dissolved in 0.02 N acetic acid and neutralized with 0.1 M NaOH. RASMCs were added to this solution at a concentration of 1×10^6 cells/mL. This solution was then poured into a tubular mold, placed at 37°C to allow the collagen to polymerize and form a tubular gel. Following gel formation, the TEBVS were removed from the mold and placed in a tissue culture dish containing 120

mL of the RASMC cell culture medium. The culture medium was changed weekly, if necessary depending on the time-point tested.

5.2.1.3 Uniaxial Ring Tests

An Instron single-column test system (Instron Corporation, Canton, MA) was used to obtain the uniaxial mechanical properties of the TEBV. Each TEBV was cut into 4 mm long rings, which yielded approximately 6 rings per construct. The rings were mounted onto two hooks in a PBS bath. One hook was attached to a static plate and the other was attached to a 5N load cell and actuator, to allow for stretching of the tissue and measurement of the force. Instron Merlin software was used to prescribe the different testing protocols and to record the force and displacement during the duration of the test. The tissue was imaged from the side and the images were recorded using a digital video camera (Allied Marlin F131B IRF) in a custom written Labview (National Instruments v7.1, Austin, TX) program at a rate of about 10 images per second. Prior to the test, the rings were dipped in small particles (30- to 90- μ m diameter) of activated charcoal (Sigma, St. Louis, MO), which stick to the tissue without the use of any adhesives, to enable tracking of the tissue during the tests (Figure 5-1). The hook diameter was used as a reference to calibrate the images from pixels to millimeters. The rings were then tested accordingly (Table 5-1).

5.2.1.3.1 Monotonic Tensile Testing

Uniaxial tensile tests were performed at different strain rates to elucidate the effect of strain rate on collagen gel plasticity and damage. The rings were mounted onto the hooks of the Instron system and stretched at rates of 0.1 mm/s and 1 mm/s until failure. The tests were performed both with preconditioning and without preconditioning. Since

preconditioning did not produce a reproducible stress-strain curve and seemed to damage the tissue, preconditioning was not performed in most of the tests. The UTS and modulus were calculated from the Green strain-Cauchy stress curve.

Table 5-1. List of uniaxial tests performed.

| Test | Loading Regimes | Measurement |
|-----------|--|--|
| Monotonic | 0.1 and 1 | UTS, modulus |
| Creep | 60% and 80% of the UTF | Time to failure |
| Fatigue | 8 mm at 1mm/s (30 cycles) Then monotonic at 1mm/s | Strain after 30 cycles UTS, modulus |

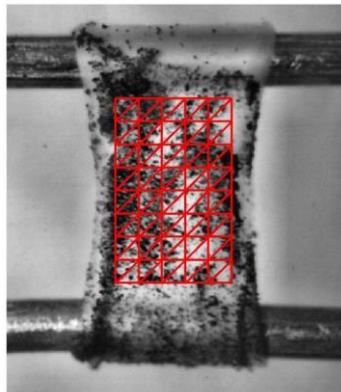


Figure 5-1. Image of the vessel during uniaxial testing. The vessel is speckled with activated charcoal. The region of interest is divided into a mesh grid and is shown in red.

5.2.1.3.2 Creep Testing

Uniaxial creep tests were performed to determine the effects of load amplitude on the plasticity of the tissue. The magnitude of the applied loads for the creep tests were chosen as percentages of the UTS at 1 mm/s to normalize for differences between constructs. Each ring was stretched until it reached a prescribed load and then further incrementally

stretched to maintain that load. Since the magnitude of the applied loads were so low, it was difficult to maintain the constant load throughout the experiment. The loads were frequently overshoot or undershot, producing noisy data. However, the mean load remained constant.

5.2.1.3.3 Fatigue Testing

Fatigue tests were performed to determine the effects of both the load and strain rate on the mechanical properties of the TEBV. Due to the plasticity of the TEBV it was impossible to stretch the tissue to the same load every time; instead the tissue had to be strained to a particular stretch every cycle. Since the tissue relaxed with every cycle, fatigue tests could not be performed to failure. Following 30 cycles of repeated stretching to 8 mm at 1mm/s, the ring was monotonically stretched at 1mm/s and compared to rings monotonically tested without cyclic pre-stretching.

5.2.1.4 Marker Tracking

Displacements of the particles between consecutive images were determined using a DIC program written in MATLAB (Mathworks, Inc., Natick, MA). An algorithm modified from Zamir et al. [8] was used. Briefly, a region of interest from the final image (image prior to failure) of each test was selected from the center of the tissue and divided into sub-regions (Figure 5-1). Normalized cross-correlation (normxcorr2 in MATLAB) was used to correlate pixels in the region of interest between consecutive images and find the best match for each sub-region. Displacements were determined and then fitted with a thin-plate spline approximation. The region of interest was divided into a 20x10 rectangle of vertices and tracked through every frame (Figure 5-2). The components of the

deformation gradient \mathbf{F} were determined by calculating the displacements of the tracked markers in the images. The Green strain, given by $\mathbf{E} = (\mathbf{C}_e - \mathbf{I})/2$, was calculated for each point (in the direction of the stretch), where $\mathbf{C}_e = \mathbf{F}_e^T \mathbf{F}_e$ is the right Cauchy-Green strain tensor. The strains at each point were then averaged to give the final Green strain average.

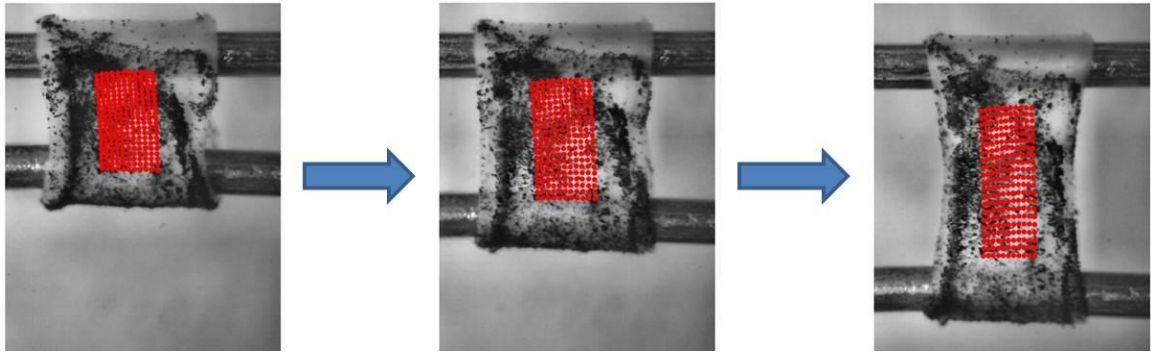


Figure 5-2. Tracking of the vessel using DIC during uniaxial testing.

5.2.1.5 DIC Verification

In order to validate the DIC method for tracking strains, 4 particles were tracked by hand (Figure 5-3) in 10 separate tests. The deformation gradient was then calculated using the isoparametric interpolation method described by Humphrey *et al* [9].

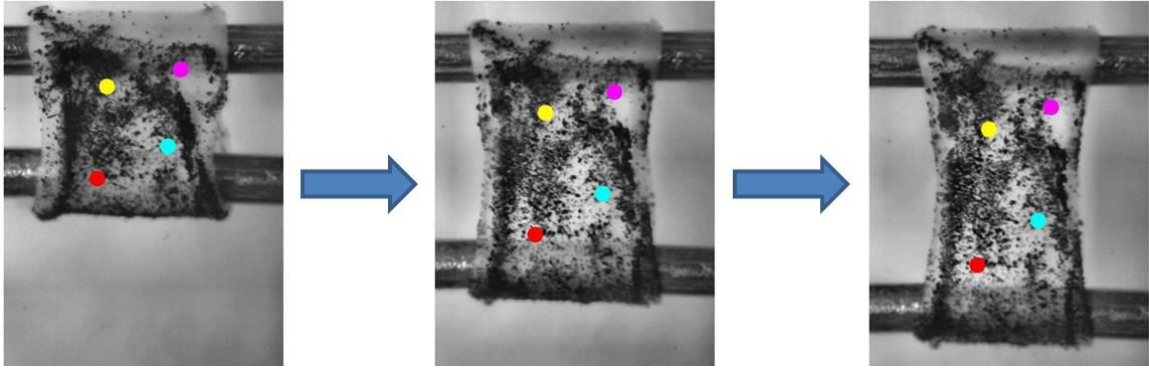


Figure 5-3. Manual tracking of the vessel during uniaxial testing.

5.2.1.6 Statistical Analysis

Statistical significance was established using a one way ANOVA with a post hoc tukey's t-test. $p < 0.05$ was considered significant.

5.2.2 **Mathematical Modeling**

The results from the uniaxial mechanical tests were fit to the theoretical model described in chapter 4. A representative set of experiments were chosen to determine the material constants and the parameters in the evolution equations for damage and plasticity.

$a = 20$, $c = 0.2$, $\alpha_p = 0.25$, $\alpha_1 = 10^{-3.4}$, $\alpha_2 = 10^{-6.5}$, $a_1 = 1 \text{ kPa}$, $a_2 = 0.1 \text{ kPa/s}$,

$\beta_1 = 1.96$, $\beta_2 = 1.2$, and $\sigma_y = 15 \text{ kPa}$ were approximated by minimizing the error

between experimentally and theoretically determined values for σ and λ for the representative 1 mm/s monotonic tensile test.

5.3 Results and Discussion

5.3.1 Monotonic Tensile Testing

Uniaxial monotonic tensile tests were performed to determine the effects strain rates on the mechanical properties of the collagen gel TEBVs. Initially, strain rates of 0.1 mm/s, 1 mm/s, and 10 mm/s were chosen to ensure a wide range of strain rates. However, due to the slow frame rates of our cameras, strain analysis could not be performed on rings stretched at 10 mm/s. Initial tests were performed by gluing 4 markers to the cross-section of the tissue as described by Seliktar et al [5]. Representative Cauchy stress-Green strain curves for 0.1 mm/s and 1 mm/s are shown in Figure 5-4. The stress-strain curve had the typical toe, heel, and linear region, followed by a nonlinear increase in stress until the UTS is reached, then by a decrease in stress until failure. The UTS increased with increasing stretch rate. These results are consistent with the model and those observed by Roeder et al [10].

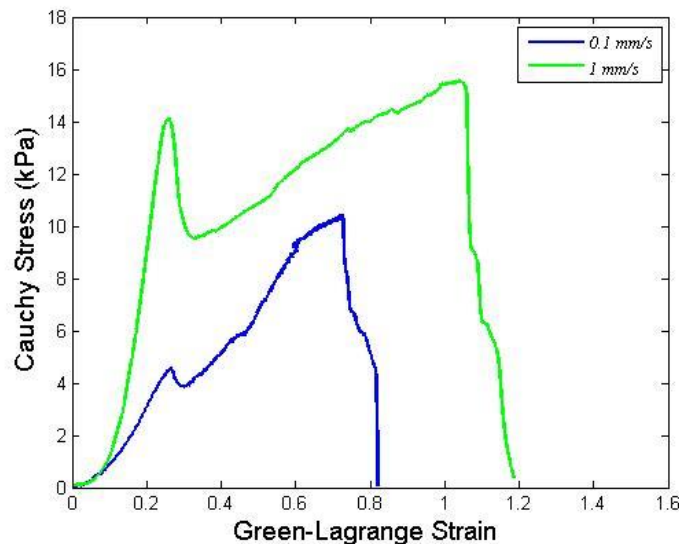


Figure 5-4. Representative Cauchy stress-Green strain curves for monotonic uniaxial tests performed at stretch rates of 0.1 mm/s and 1 mm/s

Since the tissue often tore in between markers (Figure 5-5), the DIC method for tracking strains was chosen for further analysis. Further analysis was only performed on rings stretched at 0.1 and 1 mm/s.

5.3.2 Uniaxial Creep Testing

Uniaxial creep tests were performed to determine the combined effects of stress on the mechanical properties of collagen gel TEBVs. Creep tests were performed at 60% and 80% of the UTS determined by tensile tests performed on the same vessel. Typical strain responses over the time of the test are shown in Figure 5-6. The strain increases gradually at first, then rapidly near the time of failure.

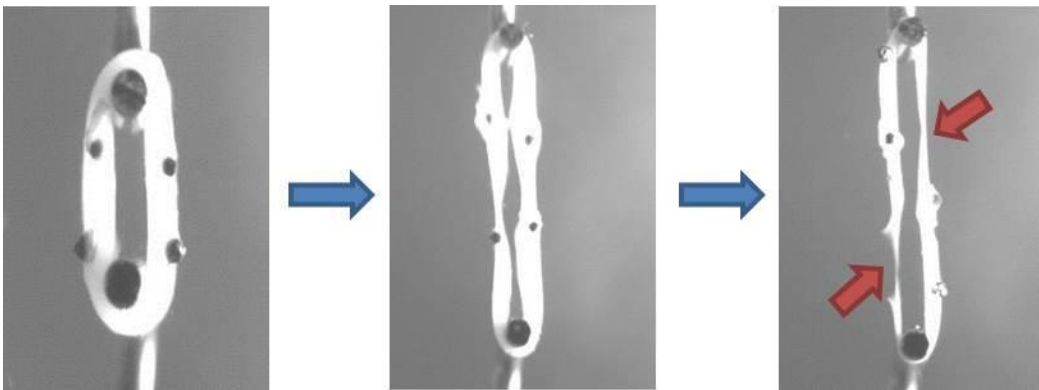


Figure 5-5. Uniaxial test performed from the cross-sectional view. Over the course of the test the markers did not deform equally. Red arrows indicate tearing in between markers.

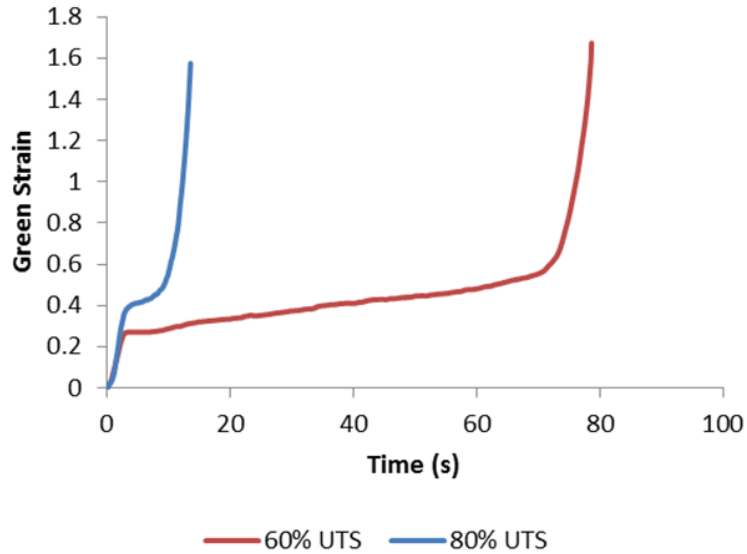


Figure 5-6. Representative change in green strain over time during creep tests performed at different stress magnitudes.

5.3.3 DIC Verification

DIC verification was performed on 20 random uniaxial monotonic tensile and creep tests. Four individual markers in the center of each ring were tracked by hand frame to frame and strain values were obtained. No significant differences were seen between values obtained from DIC or manually tracked markers.

5.3.4 Fatigue Testing

Fatigue tests were performed to determine the effects of both the load and strain rate on the mechanical properties of the TEBV. Due to the plasticity of the TEBV it was impossible to stretch the tissue to the same load every time, instead the tissue had to be strained to a particle stretch every cycle. Since the tissue relaxed with every cycle, fatigue tests could not be performed to failure. Following 30 cycles of repeated stretching to 8 mm, the ring was monotonically stretched at 1mm/s and compared to rings monotonically

tested without cyclic pre-stretching. In addition, the effects of amplitude and frequency were tested.

Figure 5-7 shows the typical response of collagen gel TEBVs during cyclic loading. The force decreases with each cycle as the unloaded length increases. Following 30 cycles of repeated stretching the UTS and modulus decreased significantly as compared to rings of the same vessel that did not undergo cyclic loading (Figure 5-8 and Figure 5-9a-b), while the work to failure and stretch to failure increased significantly (Figure 5-9c-d).

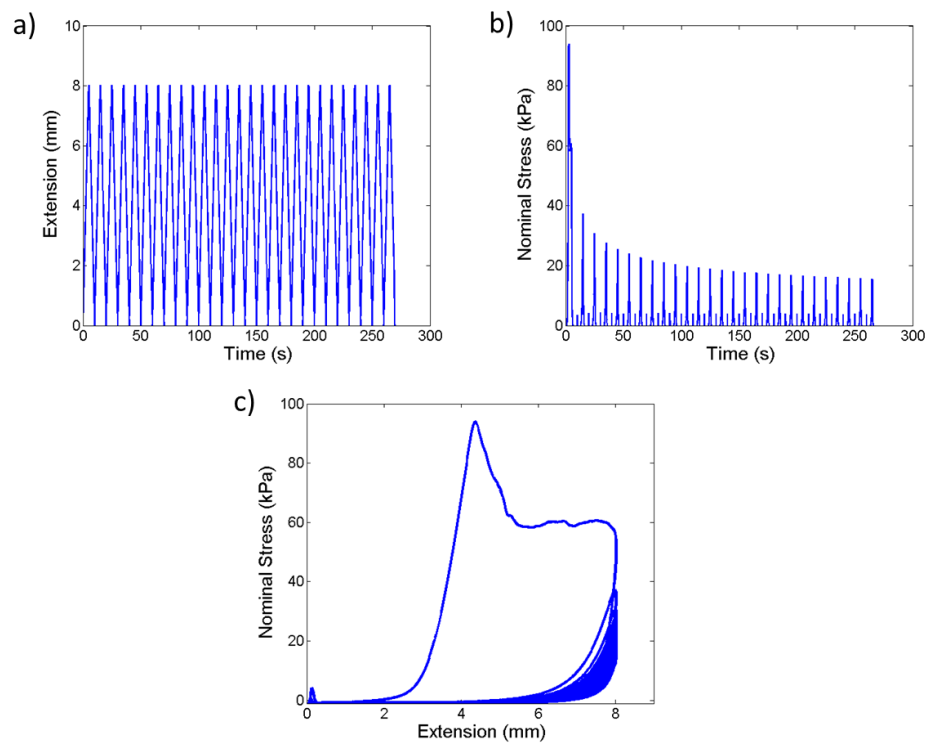


Figure 5-7. Representative typical response during cyclic loading.a) Imposed extension, b) change in nominal stress, and c) nominal stress-extension response.

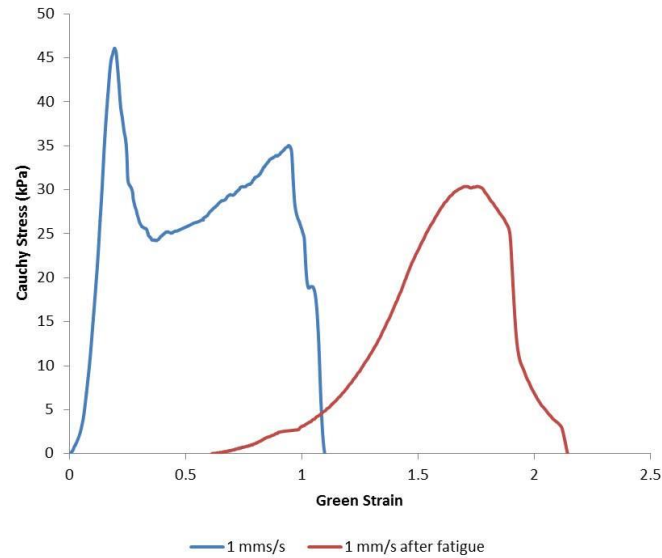


Figure 5-8. Typical monotonic stress-strain response following cyclic loading. Monotonic test prior to cyclic loading is shown in blue and test after cyclic loading is shown in red.

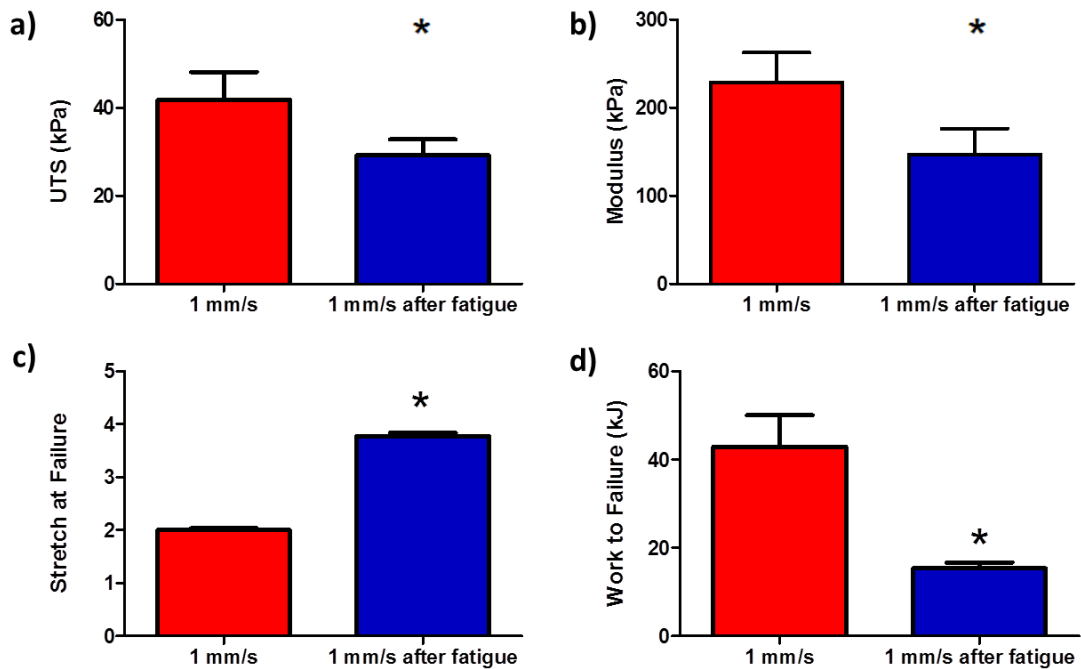


Figure 5-9. Response of TEBVs following cyclic loading. a) UTS, b) modulus, c) stretch at failure, and d) work to failure were all significantly different following cyclic loading ($p < 0.1$).

The effects of increasing load amplitude were tested by performing cyclic loading on separate rings to different extension amplitudes while maintaining the same frequency. As the amplitude of the fatigue test increased, the UTS of the monotonic test decreased (Figure 5-11). In this case the percent UTS is taken as the percent of the stretch of the point at which the maximum stress occurred. The stretch ratio in Figure 5-7c is taken as the ratio of the circumferences: $\lambda = C/C_o$, where C and C_o are defined by

$$C_o = \pi D_i, \quad C = \pi d_h + 2L \quad (5.1)$$

where D_i is the initial inner diameter of vessel, d_h is the hook diameter, and L is the distance between the 2 hooks (Figure 5-10). The Cauchy stress was calculated by $\sigma = f\lambda/A_i$, where f is the measured force and A_i is the initial area ($A_i = H_i L_i$, where H_i is the initial thickness and L_i is the initial length of the ring).

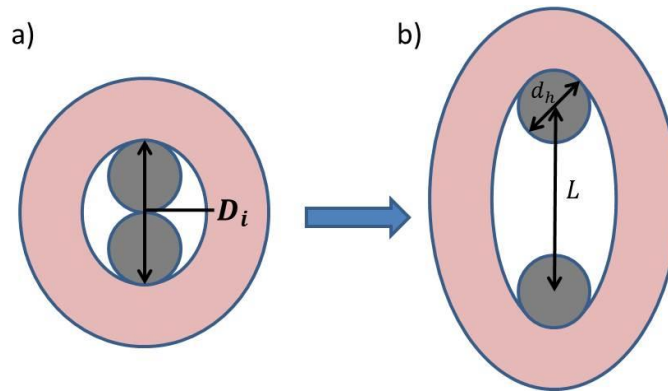


Figure 5-10. Estimation of stretch ratio using hook displacement.

The effects of increasing frequency were tested by performing cyclic loading on separate rings at different frequencies to the same extension (Figure 5-12). No effects in the UTS

or modulus were seen due to frequency, which is consistent with the predictions of the uniaxial model in chapter 3.

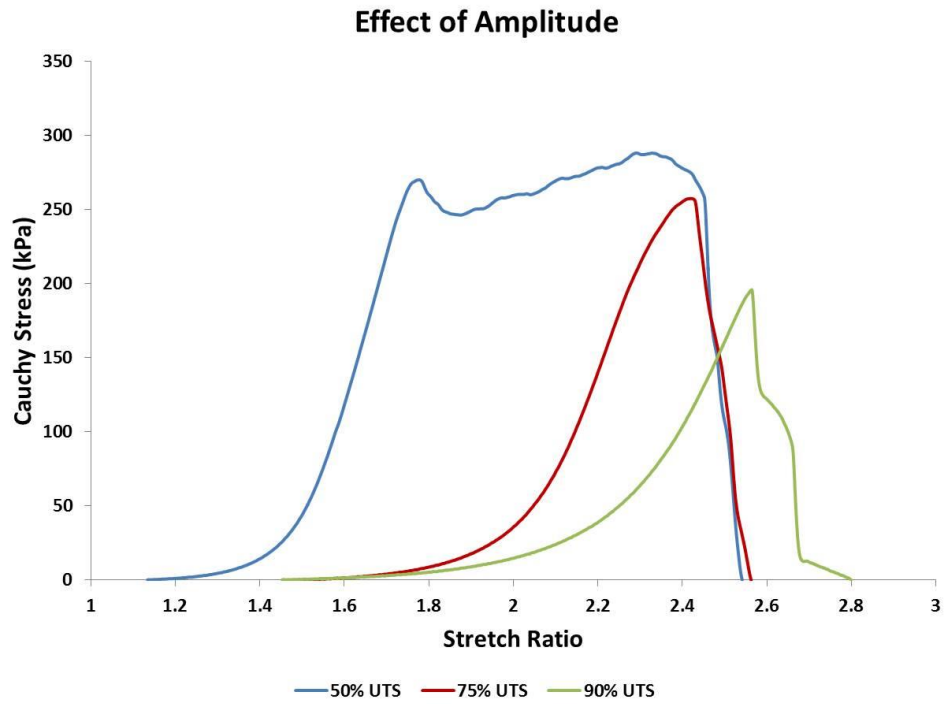


Figure 5-11. Effect of amplitude during cyclic loading.

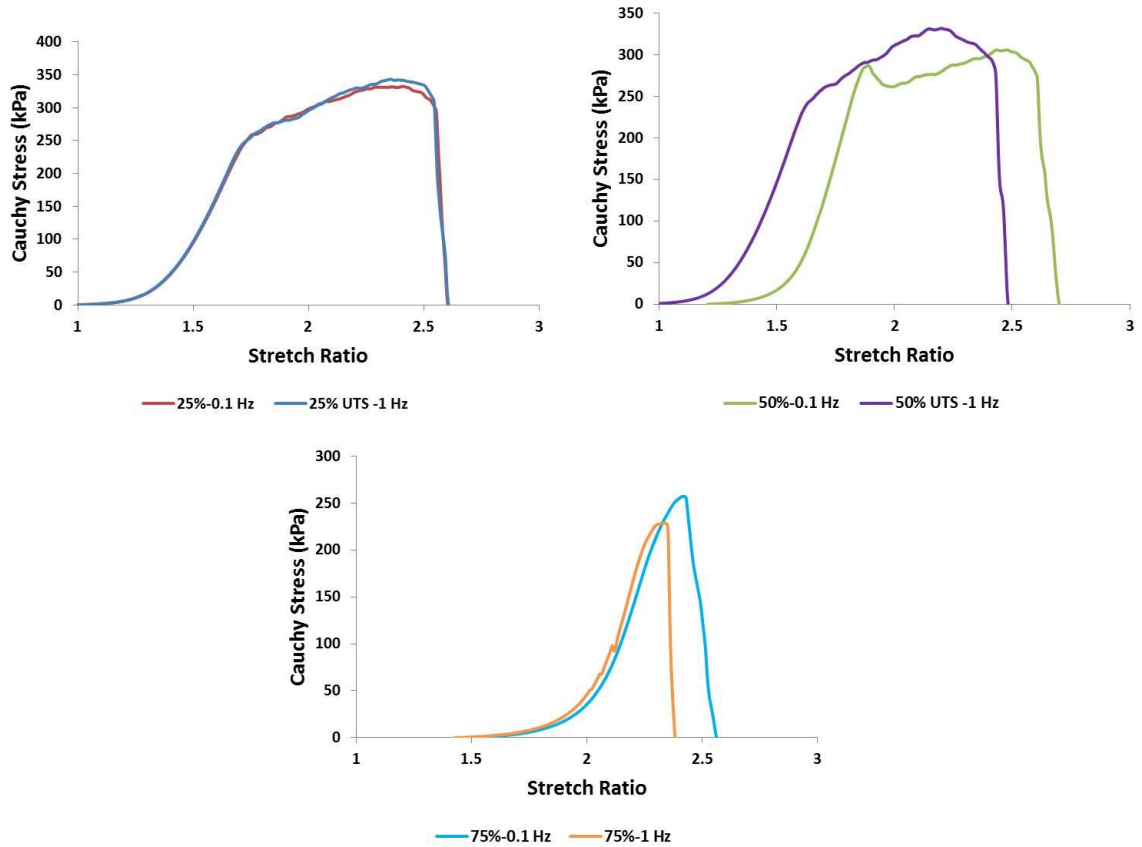


Figure 5-12. Effect of frequency during cyclic loading.

5.3.5 Material and Damage Parameters

The results obtained above were fit to the uniaxial damage model described in chapter 4. The values for α and c in the prescribed strain energy function (equation 4.15) varied greatly from experiment to experiment. This is most likely due to variations in the material properties of the gel due to small differences in preparation such as differences in cell passage number, FBS, or collagen. In addition, there were variations in the material properties along the length of the construct (probably due to differences in compaction). A set of representative experiments were chosen and used to obtain model parameters. The results are shown in Figure 5-13, Figure 5-14, and Figure 5-15. Since the

applied load in the creep tests was controlled by hook extension, the load was frequently over or undershot, which caused the oscillations in the experimental stress in Figure 5-14a. Figure 5-15 is a plot of the stretches at the peak of the loading cycle. The experimental curve was obtained by inputting the applied load into the model and obtaining the theoretical stretches, only the peaks are shown to simplify interpretation of the plots. The theoretical stretch obtained at the end of the cyclic loading was significantly higher than the stretch obtained through experiment. Figure 5-16 shows the experimental and theoretical stress-stretch curves following cyclic stretching. The general trend is the same as that obtained experimentally, however the UTS following fatigue was lower theoretically due to the stretch obtained at the end of cyclic stretching in Figure 5-15 being higher than the experimental one.

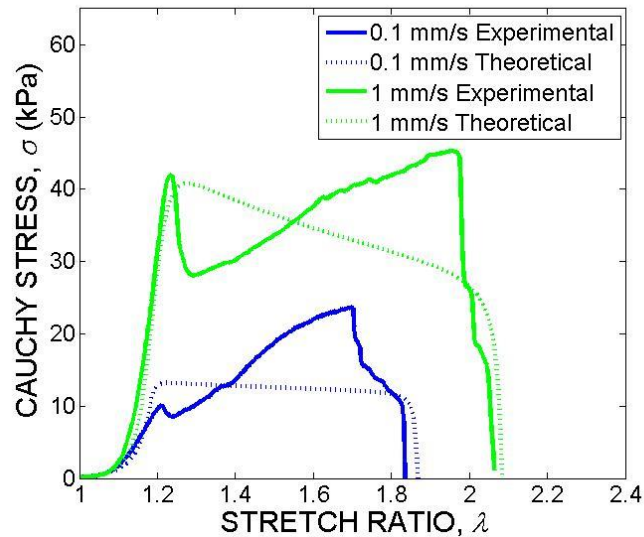


Figure 5-13. Experimentally and theoretically predicted stress-strain response during monotonic loading.

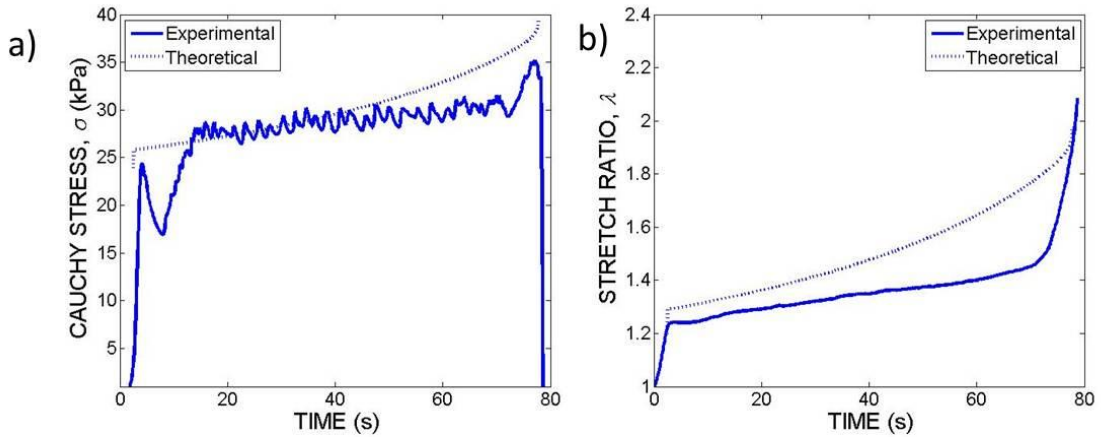


Figure 5-14. Experimental and theoretically predicted creep testing. Change in a) Cauchy stress and b) stretch ratio over the time course of the test.

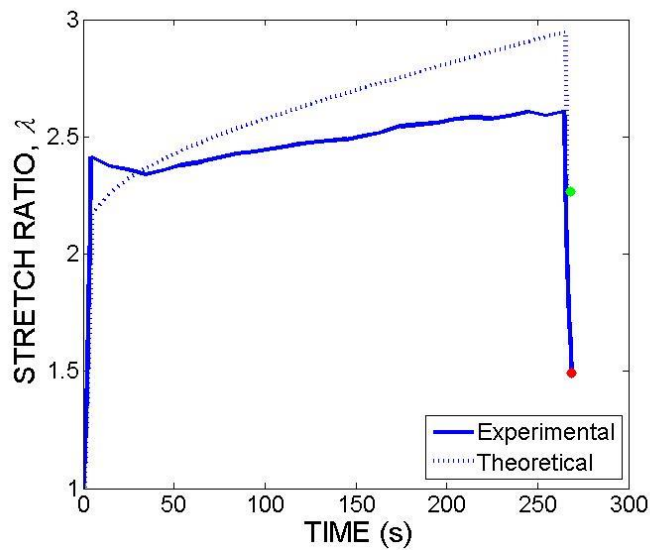


Figure 5-15. Change in stretch ratio over the time course of cyclic loading. The red and green dots indicate experimental and theoretical failure respectively. Note the differences between the predicted and the experimental stretch at failure.

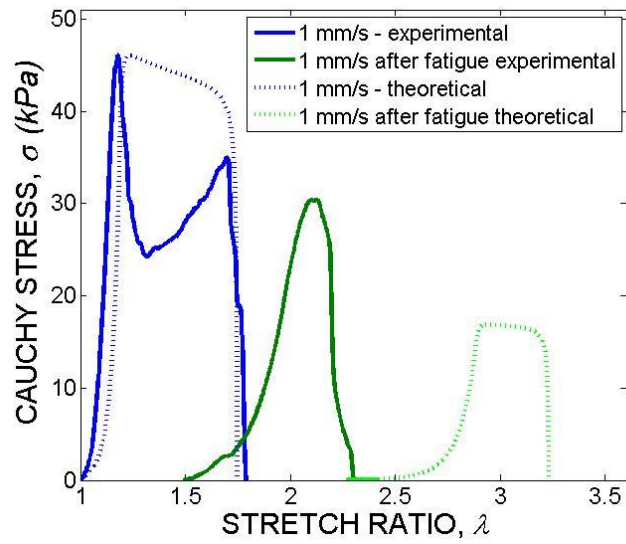


Figure 5-16. Monotonic testing following cyclic loading. Note that the difference between the experimental and theoretical stresses and strains is due to earlier prediction of higher deformation following cyclic loading.

5.4 Conclusions

The aim of this work was to develop experimental methods to study the mechanisms of plasticity and damage of collagen gel TEBVs and to fit the data obtained to the theoretical model proposed in chapter 3. This study confirmed the hypothesis that plasticity and damage are both stress and stress rate-related in collagen gel-based TEBVs.

In this study, a new method for determining the true strain during uniaxial testing of collagen gel rings was also developed. DIC was used to determine local strains during uniaxial mechanical testing. The rings were coated with carbon particles to decrease tissue smoothness and allow tracking of the entire tissue. Using DIC-based analysis proved to be as effective as individual marker tracking, but did not require tracking the particles by hand or gluing large particles onto the tissue. DIC-based strain analysis is limited, however, to lower strain rates or require the use of higher speed cameras.

From this work it is reasonable to assume that collagen gels do exhibit plasticity and damage characteristics even under modest loads. These characteristics should be taken into account during the mechanical stimulation of gel-derived vessels. For example, the commonly used method for mechanical stimulation involves the use of inner elastic sleeve to which the gel is adhered. The gel is then cyclically stretched to a particular strain value. However, the TEBV almost certainly undergoes plastic deformation during this process and is no longer under the initially prescribed strain. This effect can be seen in a study reported by Syedain et al. [11], where the amplitude of cyclically distended

fibrin gels was incrementally increased over time. The mechanical properties were more enhanced than gels cultured under constant amplitude, suggesting that the cells initially responded to the mechanical stimuli (by increasing ECM synthesis, protease secretion, cellular alignment, etc.) followed by a tapering off of the response. Due to the plastic deformation that occurs with every stretch cycle, the stress that the cells experience becomes progressively lower. Therefore, when the stretch was increased the enhanced cellular response occurred again. The actual deformation that the cells experience can be determined by taking into account the plastic deformation that occurs during the cyclic distension, which would significantly reduce the number of experiments that have to be run to determine the optimal incremental loading setup.

There are still large limitations in the current theoretical model, however. The material parameters a and b varied greatly for every test, suggesting that a better understanding of the cause of the material differences is required and possibly a different constitutive relation is required to describe the material fully. In addition, the model developed here only looks at uniaxial ring tests of the collagen-based TEBVs. An extension to include the biaxial behavior of the vessels is ultimately necessary, since it has been shown that collagen gel-based vessels develop transversely isotropic behavior during tissue culture [12-14].

In conclusion, experimental methods to test the effects of strain rate, load amplitude, and load history on the failure mechanisms of collagen-based TEBVs were developed. In addition, a theoretical model to help predict the behavior of the gels under these loads

was proposed. Simulations were compared with experimental results to demonstrate the capabilities of the model. This model can be helpful in determining necessary improvements in TEBV fabrication to minimize TEBV damage and plastic deformation.

5.5 References

1. Yannas, I., et al., *Biologically active collagen-based scaffolds: advances in processing and characterization*. Philosophical Transactions of the Royal Society A: Mathematical, Physical and Engineering Sciences, 2010. **368**(1917): p. 2123-2139.
2. Glowacki, J. and S. Mizuno, *Collagen scaffolds for tissue engineering*. Biopolymers, 2008. **89**(5): p. 338-344.
3. Cleary, M.A., et al., *Vascular tissue engineering: the next generation*. Trends in Molecular Medicine, 2012.
4. Nerem, R.M. and D. Seliktar, *Vascular tissue engineering*. Annu Rev Biomed Eng, 2001. **3**: p. 225-43.
5. Seliktar, D., et al., *Dynamic mechanical conditioning of collagen-gel blood vessel constructs induces remodeling in vitro*. Ann Biomed Eng, 2000. **28**(4): p. 351-62.
6. Isenberg, B.C. and R.T. Tranquillo, *Long-term cyclic distention enhances the mechanical properties of collagen-based media-equivalents*. Ann Biomed Eng, 2003. **31**(8): p. 937-49.
7. Zaucha, M.T., et al., *A novel cylindrical biaxial computer-controlled bioreactor and biomechanical testing device for vascular tissue engineering*. Tissue Eng Part A, 2009. **15**(11): p. 3331-40.
8. Zamir, E.A., et al., *A digital image-based method for computational tissue fate mapping during early avian morphogenesis*. Annals of biomedical engineering, 2005. **33**(6): p. 854-865.
9. Humphrey, J., D. Vawter, and R. Vito, *Quantification of strains in biaxially tested soft tissues*. Journal of biomechanics, 1987. **20**(1): p. 59-65.
10. Roeder, B., et al., *Tensile mechanical properties of three-dimensional type I collagen extracellular matrices with varied microstructure*. Journal of biomechanical engineering, 2002. **124**(2): p. 214.

11. Syedain, Z.H., J.S. Weinberg, and R.T. Tranquillo, *Cyclic distension of fibrin-based tissue constructs: Evidence of adaptation during growth of engineered connective tissue*. Proceedings of the National Academy of Sciences of the United States of America, 2008. **105**(18): p. 6537-6542.
12. Girton, T., T. Oegema, and R. Tranquillo, *Exploiting glycation to stiffen and strengthen tissue equivalents for tissue engineering*. Journal of biomedical materials research, 1999. **46**(1): p. 87-92.
13. Girton, T., et al., *Mechanisms of stiffening and strengthening in media-equivalents fabricated using glycation*. Journal of biomechanical engineering, 2000. **122**(3): p. 216.
14. Wagenseil, J.E., E.L. Elson, and R.J. Okamoto, *Cell orientation influences the biaxial mechanical properties of fibroblast populated collagen vessels*. Annals of biomedical engineering, 2004. **32**(5): p. 720-731.

CHAPTER 6

A MECHANICAL TESTING SYSTEM TO CHARACTERIZE THE PLASTICITY AND DAMAGE OF TEBVS UNDER BIAXIAL LOADING

6.1 Introduction

In chapters 4 and 5, the uniaxial mechanical properties of collagen gel-based TEBVs were examined. It was assumed that the collagen gels were isotropic and homogenous. Due to different cellular and collagen alignment induced by different mechanical constraints during collagen gel maturation, the mechanical properties of collagen gel TEBVs vary along the length and thickness of the vessel. The standard protocol of collagen gel-based TEBV development uses a tubular mold with a central mandrel to maintain the luminal shape. The mandrel imposes a radial constraint, which induces circumferential cell alignment [1]. Imposing longitudinal constraints on the vessel, yields a more isotropic material, with a lower circumferential modulus and UTS [2]. It has also been shown by Wagenseil et al., [3] that cellular orientation influences the biomechanical properties of the gels.

In this chapter, a system to test the biaxial mechanical properties of collagen-based TEBVs was developed. Since the ring is unconstrained axially during uniaxial testing, the tests do not accurately predict the response of the vessel *in vivo*. Though uniaxial (ring) tests provide information on the material response in the circumferential direction, including an effective modulus, yield stress, ultimate tensile stress, a predictive model

requires a constitutive equation, which is valid for multi-axial loading. Given that these TEBVs are anisotropic, multiaxial mechanical testing is required.

An important physiologic feature for TEBVs is the ability to constrict or dilate in response to changes in their environment [4]. Healthy arteries adjust their diameter in response to changes in pressure or flow [5, 6]. SMC-seeded gel-derived TEBVs have been shown to exhibit vasoactivity in response to various vasoagents [7-9]. The development of an experimental graft verification system will require the ability to test the short-term cellular response to perturbations in pressure or flow.

The objectives of this study were to develop methods of characterizing the biaxial mechanical behavior and vasoactivity of collagen-based TEBVs and to extend the theoretical model of damage and plasticity developed in chapter 4 for uniaxial loading to include biaxial loading. This chapter is divided into three components. First, the capabilities of the biaxial mechanical testing system are demonstrated. Then experiments necessary for obtaining the parameters of the proposed theoretical model are described. The final part focuses on fitting the data to the theoretical model.

6.2 Materials and Methods

6.2.1 Experimental Methods

6.2.1.1 Rat Aortic Smooth Muscle Cells

RASMCs were isolated from Sprague-Dawley rats. The cells were expanded and used at passages between 6 and 10. RASMC cell culture medium consisted of Dulbecco's

modified Eagle's medium (DMEM; Mediatech Cellgro) supplemented with 10% FBS (Hyclone), 1% L-glutamine (Mediatech Cellgro), and 1% penicillin-streptomycin (Mediatech Cellgro).

6.2.1.2 Collagen Gel-derived TEBV Fabrication

Collagen constructs were made with type I bovine collagen (MP Biomedicals) at 2 mg/mL collagen. The lyophilized collagen was dissolved in 0.02 N acetic acid and neutralized with 0.1 M NaOH. RASMCs were added to this solution at a concentration of 1×10^6 cells/mL. This solution was then poured into a tubular mold, placed at 37°C to allow the collagen to polymerize and form a tubular gel. Following gel formation, the TEBVS were removed from the mold and placed in a tissue culture dish containing 120 mL of the RASMC cell culture medium. The culture medium was changed weekly, if necessary depending on the time-point tested.

6.2.1.3 Biaxial Mechanical Testing System

A biaxial mechanical testing system was developed in order to obtain biaxial information on the collagen gels for the model. A custom built cylindrical biaxial testing device was modified from Gleason et al. and Zaucha et al. [10, 11] to test the collagen-based TEBVs. The TEBV was mounted onto two glass cannula and the lumen was filled with DMEM, which were submerged in a bath filled with DMEM (Figure 6-2). A flow loop was connected to the cannula and filled with culture medium (Figure 6-1 and Figure 6-2). Two pressure transducers (Honeywell Sensotec FPG, Columbus, OH) were used to measure the pressure the vessel. The pressure was controlled by pressurizing the reservoir using a flow constricting pressure controller (PC-5PSIG-D, Alicat Scientific, Inc., Tucson, AZ). A load cell (Delta Metrics Inc. model XLU68s, Worthington, OH) was

mounted to one of the cannula to record the axial force. The device was placed on top of an inverted microscope (Axiovert 40CFL, Carl Zeiss, Inc.), equipped with a digital camera (Allied Marlin F131B IRF), during testing to record the change in diameter during the course of the mechanical testing (Figure 6-2). All components were controlled using a custom written LabVIEW (National Instruments v7.1, Austin, TX) program.

6.2.1.4 Biaxial Mechanical Tests

6.2.1.4.1 *Cyclic Pressure-Diameter Tests*

Fixed length pressure-diameter tests were performed at an axial stretch of $\lambda_z = 1$, in reference to the original unloaded length. The vessels were cyclically pressurized 0-10 mm Hg for five cycles, then 0-20 mm Hg for five cycles, and so forth until the vessel burst (Figure 6-6a). This protocol allows the analysis of the stress-strain behavior of the collagen gels in response to increasing loading rate and increasing cycle number.

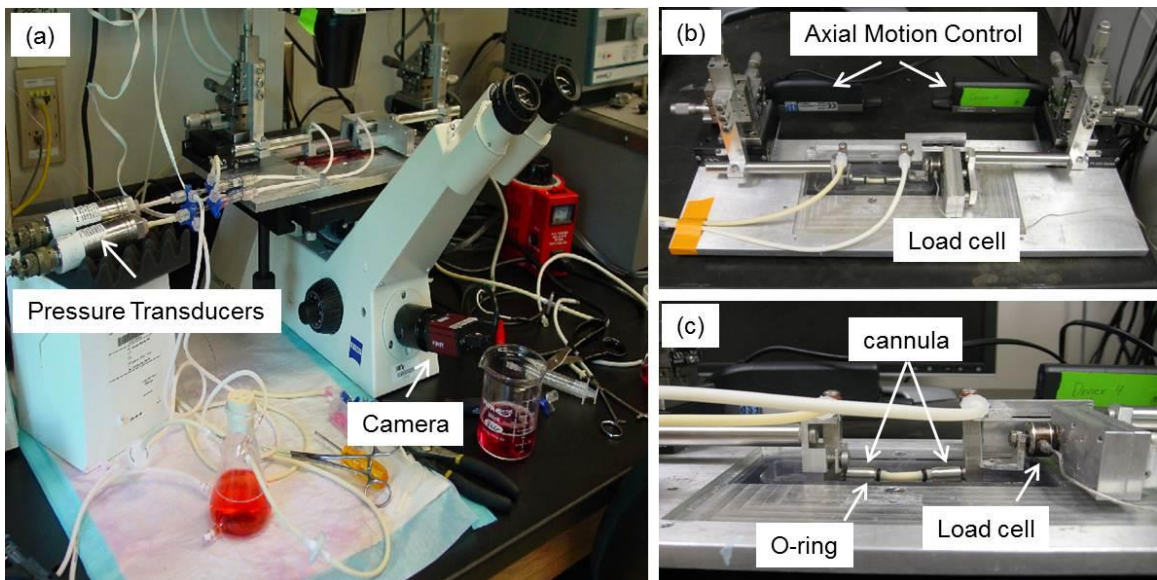


Figure 6-1. Biomechanical Testing System. (a) Computer controlled testing system capable of precise control of flow, pressure, and axial motion while monitoring diameter

and axial load. (b) A close up of the testing device. Included are linear actuators to control axial stretch and a load cell to measure axial load. (c) A close up of a silicone tube showing o-rings used to attach the construct, and how the load cell and cannula are connected.

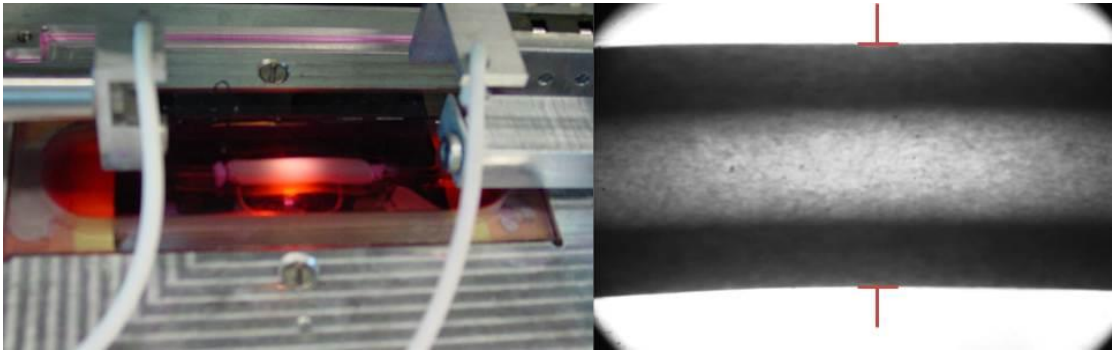


Figure 6-2. Image of a collagen gel TEBV undergoing biaxial mechanical testing. (a) Image of the vessel on the testing device. (b) Image of diameter measurement during mechanical testing.

6.2.1.4.2 Axial Force-Length Tests

Fixed pressure axial force-length tests were performed at a fixed pressure of 10 mm Hg. The vessels were cyclically stretched at $\lambda_z = 1.0 - 1.2$, $\lambda_z = 1.0 - 1.3$, and so forth until $\lambda_z = 1.0 - 1.5$.

6.2.1.4.3 Vasoactivity Testing

Functional tests to determine the vasoactivity of collagen-based TEBVs were performed by mounting the vessel onto the biaxial testing system and pressurizing it to 10 mm Hg.

Increasing concentrations (10^{-9} – 10^{-5} M) of endothelin-1 (ET-1) were added to the bath that the vessel was submerged in and the change in diameter was recorded.

6.2.1.4.4 Burst Pressure Testing

Burst pressure tests were performed under constant loading rates of 0.4 and 1.4 mm Hg/s. The vessels were not preconditioned for burst pressure tests because preconditioning did not produce reproducible curves.

6.2.1.4.5 Isobaric Tests to Failure

Isobaric tests were performed by loading the vessel at 1.4 mm Hg/s to 50%, 60%, and 75% of the burst pressure. The pressure was maintained until vessel failure and the change in diameter was recorded throughout the test.

6.2.1.4.6 Cylindrical Fatigue Testing

Fatigue tests were performed on collagen gel TEBVs to 60% of the burst pressure at 1.4 mm Hg/s. The vessel was cyclically inflated and deflated to the required pressures, while the change in diameter was recorded.

6.2.1.4.7 Statistical Analysis

Comparisons of burst pressures at different rates were performed using a Student's t-test using a 95% confidence interval.

6.2.2 Mathematical Modeling

The model developed in chapter 4 for uniaxial mechanical tests of collagen gel TEBVs was adapted for biaxial mechanical tests. The strain energy function in equation (4.17)

can also be used to predict inflation of a cylindrical tube [12]. Isotropic and anisotropic damage are considered. The vessel is considered as a thin-walled (2D) and a thick-walled tube (3D). Since these tests were performed acutely to failure no biological adaptation could occur and the growth and remodeling components are ignored.

6.2.2.1 Theoretical Framework

6.2.2.1.1 *Kinematics*

In this section, the kinematics described for the uniaxial deformation of a strip (Figure 4.1) in chapter 4 are extended to the general case. Consider a stress free body at time $t = 0$ that is loaded to the configuration $\beta_\ell(t)$; the deformation gradient for the mapping of points from $\beta_o(0)$ to $\beta_\ell(t)$ is denoted \mathbf{F} (Figure 6-3). If the applied loads induce stresses beyond the yield stress, *plasticity* (the irreversible deformation) will ensue. This results in the evolution of the stress-free, natural configuration. Let the plastic deformation map points from the stress-free configuration $\beta_o(0)$ to an intermediate, stress-free configuration $\beta_p(t)$ (which consists of discontinuous (fictitious) elements) have gradient \mathbf{F}_p . The mapping from the unloaded configuration $\beta_p(t)$ to the loaded configuration $\beta_\ell(t)$ has gradient \mathbf{F}_e . Therefore, the deformation gradient from the unloaded state, $\beta_o(0)$, to the loaded state, $\beta_\ell(t)$, is $\mathbf{F} = \mathbf{F}_{ep} = \mathbf{F}_e \mathbf{F}_p$.

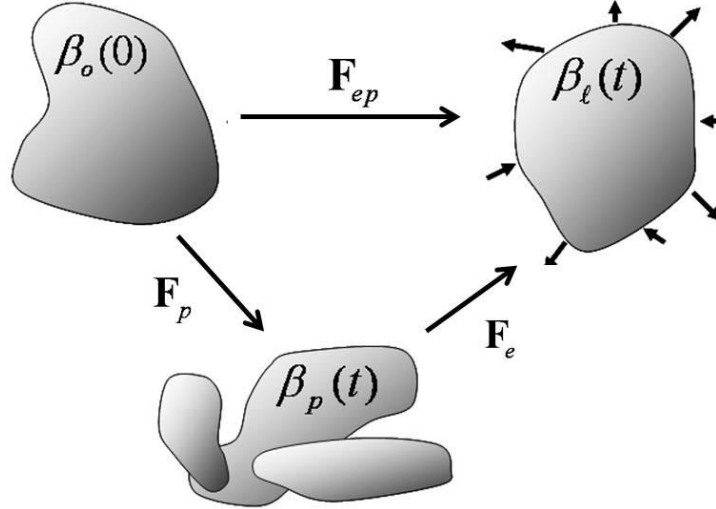


Figure 6-3. General kinematics for plastic deformation.

6.2.2.1.2 Anisotropic Damage

In addition to plastic deformation, the material can undergo changes in the material properties. For the cylindrical case, equation (4.10) becomes

$$\boldsymbol{\sigma} = \mathbf{D}\boldsymbol{\sigma}_o \quad (6.1)$$

where \mathbf{D} is the damage tensor; $\mathbf{D}=\mathbf{I}$ corresponds to no damage and $\mathbf{D}=\mathbf{0}$ corresponding to complete damage and $\boldsymbol{\sigma}_o$ is the effective Cauchy stress. It is assumed

that the original, undamaged material may be modeled as an incompressible material,

$$\boldsymbol{\sigma}_o = -p\mathbf{I} + 2\mathbf{F}_e \frac{\partial W_o}{\partial \mathbf{C}_e} \mathbf{F}_e^T \quad (6.2)$$

where W_o is the strain energy density function for the original, undamaged material and

p is a Lagrange multiplier that enforces the incompressibility constraint. Let

$$[\mathbf{D}] = \text{diag}[D_{rr}, D_{\theta\theta}, D_{zz}] \quad (6.3)$$

where $D_{rr} = D_{\theta\theta} = D_{zz} \in [0,1]$ and $D_{rr} = D_{\theta\theta} = D_{zz} = 1$ corresponds to no damage.

6.2.2.1.3 Constitutive Equation and Equilibrium

For these simulations, at any time $t = 0$ let the strain energy density function be

$$W_o = \frac{a}{c} \exp[c(I_{c_\varepsilon} - 3)] \quad (6.4)$$

where a and c are material parameters and $I_{c_\varepsilon} = \text{tr}(\mathbf{C}_\varepsilon)$ is the first invariant of \mathbf{C}_ε . Note

that equation (6.4) describes an isotropic material, however, as damage progresses anisotropies may develop via equation (6.1).

6.2.2.1.4 Cylindrical Biaxial Loading (2D)

Consider a thin-walled tube with an initial radius $R^*(0)$ (the star denoting that this is one location within the wall; e.g., the mid-wall), initial thickness $H(0)$, and initial axial length $L(0)$ (Figure 6-4). The plastic deformation gradient has components

$$[\mathbf{F}_p] = \text{diag}[1/(\lambda_{p\theta}\lambda_{pz}), \lambda_{p\theta}, \lambda_{pz}] \quad (6.5)$$

where $\lambda_{p\theta} = R_p^*(t)/R^*(0)$, $\lambda_{pz} = L_p(t)/L(0)$, $R_p^*(t)$ is the unloaded radius and $L_p(t)$ is

the unloaded length in β_p at time t ; note that the constraint that the plastic deformation is

isochoric is enforced; thus $\det[\mathbf{F}_p] = 1$, so that

$$\lambda_{pr} = H_p(t)/H(0) = 1/(\lambda_{p\theta}\lambda_{pz}) = R^*(0)L(0)/(R_p^*(t)L_p(t)).$$

The elastic deformation gradient has components

$$[F_e] = \text{diag}[1/(\lambda_{e\theta}\lambda_{ez}), \lambda_{e\theta}, \lambda_{ez}] \quad (6.6)$$

where $\lambda_{e\theta} = r^*(t)/R^*(t)$, $\lambda_{ez} = l(t)/L(t)$, where $r^*(t)$ is the loaded radius, and $l(t)$ is the loaded length at time t ; the elastic deformation, too, is assumed to be isochoric; thus $\det[F_e] = 1$. Thus, the overall deformation, from $\beta_o(0)$ to $\beta_i(t)$, is $[F] = \text{diag}[\lambda_r, \lambda_\theta, \lambda_z]$, where

$$\lambda_r = 1/\lambda_\theta\lambda_z, \quad \lambda_\theta = \lambda_{p\theta}\lambda_{e\theta}, \quad \text{and} \quad \lambda_z = \lambda_{pz}\lambda_{ez}. \quad (6.7)$$

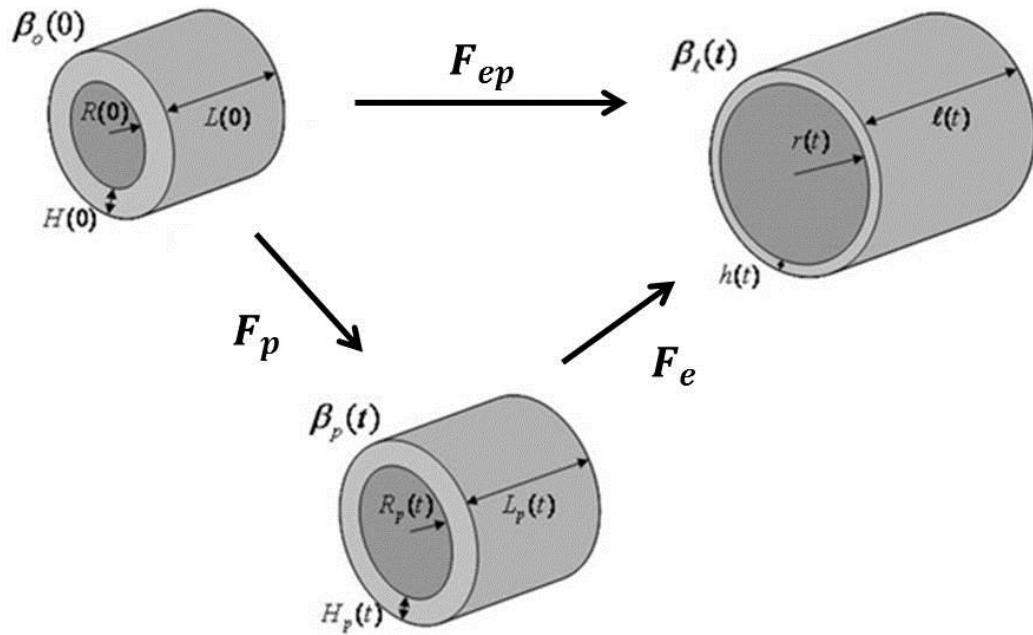


Figure 6-4. Kinematics of the plastic deformation of a thin-walled tube.

For the cylindrical inflation and extension of a thin-walled tube $\sigma_{rr} \ll \sigma_{\theta\theta}$ and $\sigma_{rr} \ll \sigma_{zz}$ Combining equilibrium conditions and equations (6.1) and (6.2) gives

$$\sigma_{\theta\theta} = \frac{Pr_i}{h} = D_{\theta\theta} \left(\lambda_{\theta\theta}^2 - \frac{1}{(\lambda_{\theta\theta}\lambda_{zz})^2} \right) c \exp(a(I_c - 3)) \quad (6.8)$$

$$\sigma_{zz} = \frac{f_v}{\pi h(2r_i + h)} = D_{zz} \left(\lambda_{zz}^2 - \frac{1}{(\lambda_{\theta\theta}\lambda_{zz})^2} \right) c \exp(a(I_c - 3)) \quad (6.9)$$

where P is the transmural pressure, f_v is the axial force applied to the vessel wall, and r_i and h are the inner radius and the wall thickness in the loaded configuration. For ex vivo testing, $f_v = f_m + \pi r_i^2 P$, where f_m is the axial force measured by a force transducer and $\pi r_i^2 P$ accounts for the end-cap pressure acting in the axial direction.

6.2.2.1.5 Cylindrical Biaxial Loading (3D)

Consider a thick-walled tube with initial axial length $L(0)$ and initial radius $R(0) \in [A(0), B(0)]$, where $A(0)$ and $B(0)$ are the inner and outer radii, respectively.

The plastic deformation gradient has components $[\mathbf{F}_p] = \text{diag}[\lambda_{pr}, \lambda_{p\theta}, \lambda_{pz}]$ where

$$\lambda_r = \frac{\partial R_p(t)}{\partial R(0)} = \frac{R(0)L(0)}{R_p(t)L_p(t)}, \quad \lambda_{p\theta} = \frac{R_p(t)}{R(0)}, \quad \lambda_{pz} = \frac{L_p(t)}{L(0)} \quad (6.10)$$

$L_p(t)$ is the unloaded length and $R_p(t)$ is the unloaded radius in β_p of the cylindrical shell that passes through radial location $R(0)$ in $\beta_o(0)$ (Figure 6-5). Note that $L_p(t)$ and

$R_p(t)$ are functions of $R(0)$. Note, too, that the constraint that the plastic deformation is isochoric ($\det[\mathbf{F}_p] = 1$) in equation (6.10)₁ is enforced.

The elastic deformation gradient has components $[\mathbf{F}_e] = \text{diag}[\lambda_{er}, \lambda_{e\theta}, \lambda_{ez}]$, where

$$\lambda_{er} = \frac{\partial r(t)}{\partial R(t)} = \frac{R(t)L(t_0)}{r(t)l(t)}, \quad \lambda_{e\theta} = \frac{r(t)}{R(t)}, \quad \lambda_{ez} = \frac{l(t)}{L(t)} \quad (6.11)$$

where $l(t)$ is the loaded length and $r(t)$ is the loaded radius in β_t of the cylindrical shell that passes through radial location $R(0)$ in $\beta_o(0)$; the constraint that the elastic deformation is isochoric ($\det[\mathbf{F}_e] = 1$) in equation (6.11)₁ is enforced. Thus, the overall deformation, from $\beta_o(0)$ to $\beta_t(t)$, is $[\mathbf{F}] = \text{diag}[\lambda_r, \lambda_\theta, \lambda_z]$, where

$$\lambda_r = 1/\lambda_\theta\lambda_z, \quad \lambda_\theta = \lambda_{p\theta}\lambda_{e\theta}, \quad \text{and} \quad \lambda_z = \lambda_{pz}\lambda_{ez} \quad (6.12)$$

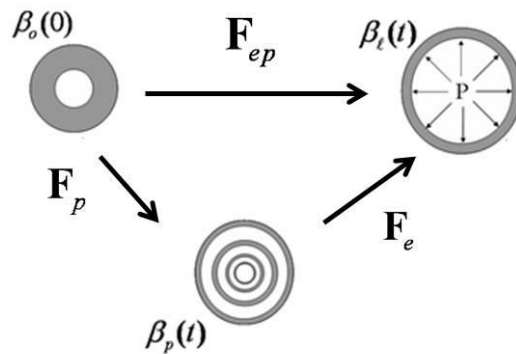


Figure 6-5. Kinematics of growth and plasticity of a thick-walled axisymmetric tube.

The linear momentum balance under quasi-static conditions in the absence of body forces requires that $T_{r\theta} = T_{rz} = 0$ and that $\frac{\partial \sigma_{rr}}{\partial r} + (\sigma_{rr} - \sigma_{\theta\theta}) = 0$. Noting that $\sigma_{rr}(r_o) - \sigma_{rr}(r_i) = P$ is the transmural pressure, the linear momentum balance requires that

$$P = \int_{r_i}^{r_o} \frac{D_{\theta\theta}(-p + \hat{T}_{\theta\theta}^o) - D_{rr}(-p + \hat{T}_{rr}^o)}{2r} dr \quad (6.13)$$

where p is a Lagrange multiplier that enforces incompressibility and $\hat{T}_{ii}^o = F_{\theta i i}^2 \partial W_o / \partial C_{\theta i i}$; recall in this 3D model that values of D_{jj} and $\lambda_{\theta j}$ will vary with radial location. Thus, equation (6.13) cannot be solved for the general case of anisotropic damage. If, however, transversely isotropic damage is considered; i.e., let $D_{rr} = D_{\theta\theta}$, then equation (6.13) reduces to

$$P = \int_{r_i}^{r_o} \frac{D_{\theta\theta}(\hat{T}_{\theta\theta}^o - \hat{T}_{rr}^o)}{2r} dr \quad (6.14)$$

which can be solved. Note, too, for transversely isotropic damage and remodeling the Lagrange multiplier is

$$p(r) = \frac{2}{D_{\theta\theta}} [\hat{T}_{rr}^o + P - \int_{r_i}^{r_o} \frac{D_{\theta\theta}(\hat{T}_{\theta\theta}^o - \hat{T}_{rr}^o)}{2r} dr] \quad (6.15)$$

Axial equilibrium requires that the magnitude of the axial force, f , maintaining the in vivo axial extension in a bioreactor be

$$f = 2\pi \int_{r_i}^{r_o} T_{zz} r dr - \pi r_i^2 P \quad (6.16)$$

where the first term on the right hand side is due to the force applied to the vessel wall and the second term on the right hand side is due to the pressure acting over the end-cap. Equation (6.16) can be written as

$$f = \pi \int_{r_i}^{r_o} \left[\frac{D_{zz}}{2} \hat{T}_{rr}^o - p(r) \right] r dr - \pi r_i^2 P \quad (6.17)$$

where $p(r)$ is given via equation (6.16) for transversely isotropic damage [13].

6.3 Results and Discussion

Figure 6-6 shows a typical mechanical response of collagen gel TEBVs to cyclic loading. The testing protocol consisted of gradually increasing the cyclic testing pressure from 0–10 mmHg to 0–20 mmHg, and so forth (Figure 6-6a). The pressure-diameter curve shifted to the right dramatically with every cycle. Note the large shift in the unloaded diameter from the first cycle to the last (Figure 6-6c). A similar trend was observed in the axial force (Figure 6-7). The axial load increases during the first few cycles and then decreases during the later cycles at higher pressures. The decrease in the axial load coincides with an increase in the unloaded length of the vessel. This suggests that the TEBVs undergo significant plastic deformation in the circumferential and axial directions during each pressurization cycle.

Figure 6-8 shows representative results of cyclic pressure tests performed at different axial stretches. In these tests, the vessel was cyclically inflated to 30 mm Hg for three cycles at fixed axial stretches. Only the last cycle at each stretch is shown. Counter to expectation, the pressure-diameter curve shifts to the right with increasing stretch. This is most likely due to an increase in the unloaded diameter. The plastic deformation in the circumferential direction appears to be much greater than in the axial direction, since the axial load still increases with increasing stretch.

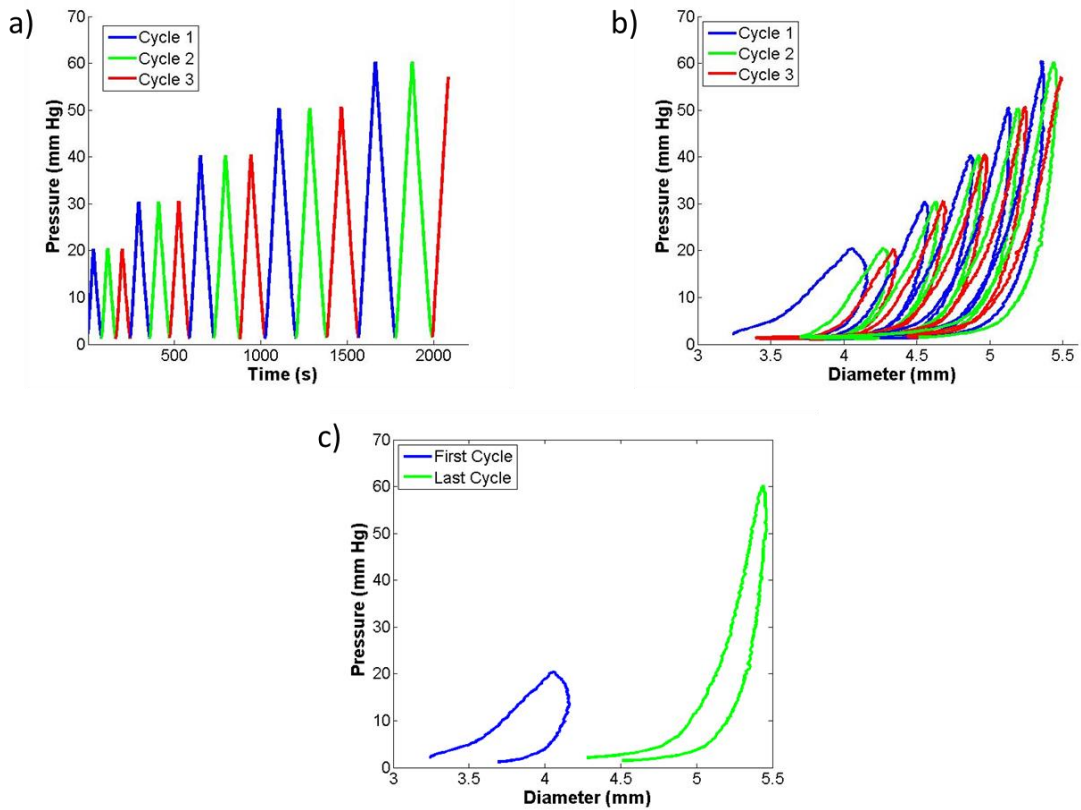


Figure 6-6. Biomechanical tests on collagen-based TEBVs. a) Testing protocol for the vessels. At a fixed length of $\lambda_z = 1.10$, the vessels were cyclically inflated and deflated to the pressures shown. b) Pressure-diameter response for the TEBVs. Note that the same color is used for the respective cycle for each pressure range. c) Change in diameter between the first and last complete cycle.

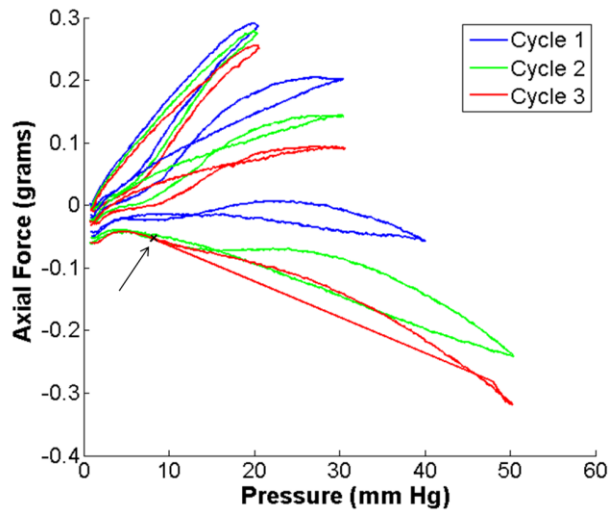


Figure 6-7. Axial force-pressure data with increasing cyclic pressure. The black x indicates the point of vessel failure.

Figure 6-9 is a representative force-length response of collagen gel TEBVs. In these tests, the vessel was inflated to 10 mm Hg and cyclically stretched to $\lambda_z = 1.2$, $\lambda_z = 1.3$, $\lambda_z = 1.4$, and $\lambda_z = 1.5$, for 5 cycles each. Only the last cycle at each stretch is shown. The maximum axial force increased with increasing stretch. The axial force decreased with increasing cycle at each particular extension, demonstrating that some plastic deformation was occurring. However, much less plastic deformation was seen due to axial extension than due to pressurization.

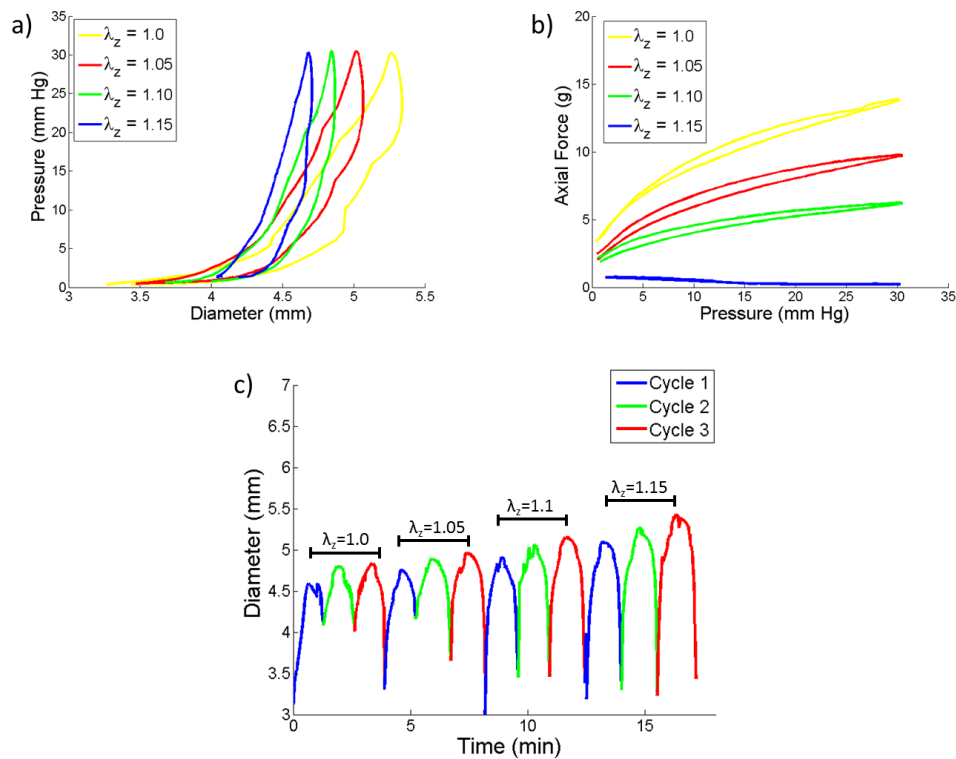


Figure 6-8. Effect of axial extension on pressure and axial load. a) Pressure-diameter and b) axial force-pressure responses of collagen-based TEBVs. Three pressure cycles of 0-30 were performed at $\lambda_z = 1.00$, $\lambda_z = 1.05$, $\lambda_z = 1.10$, and $\lambda_z = 1.15$. Only the last cycle at each extension is shown. c) Change in diameter over each cycle. Note that the diameter at the maximum pressure of the last cycle increases with each extension.

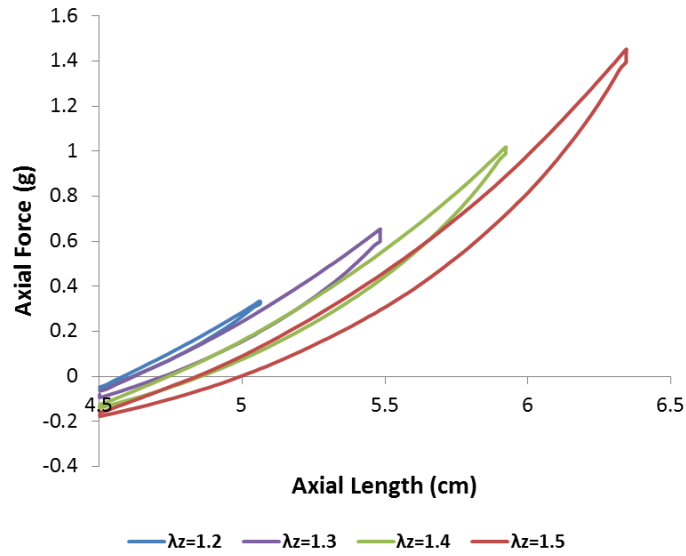


Figure 6-9. Axial force-length response at constant pressure.

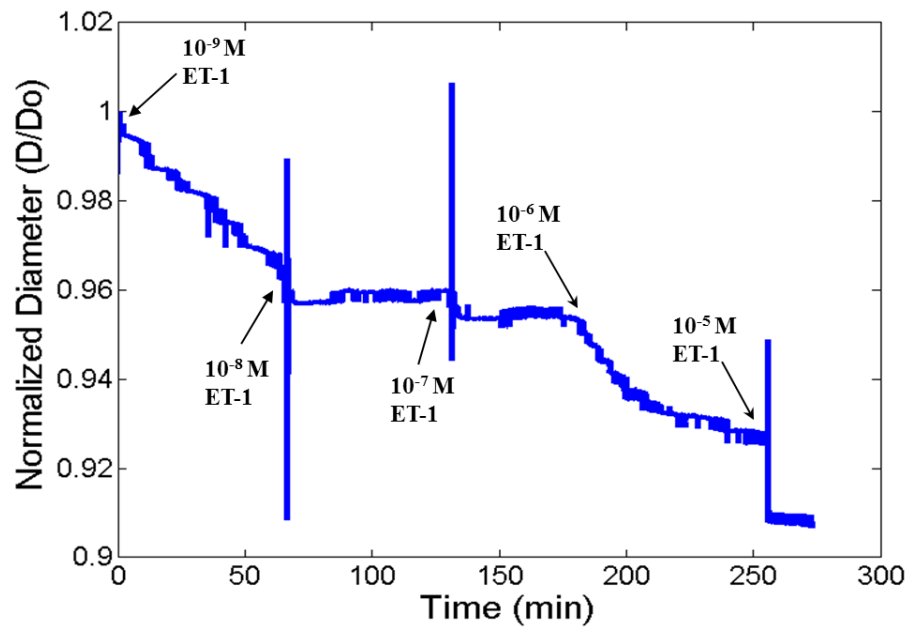


Figure 6-10. Functional testing of a collagen-based TEBV. Endothelin-1 (ET-1) was used as the vasoactive agent.

Figure 6-10 is a representative vasoactivity test performed on our biaxial testing system. The vessel was mounted onto the biaxial testing system. The diameter decreased instantly with each increasing addition of ET-1, suggesting that the SMCs were constricting causing the diameter to decrease.

Burst pressure tests were performed at 0.4 mm Hg/s and 1.4 mm Hg/s on collagen gel TEBVs cultured for 7 days. The pressure-diameter curves were different Figure 6-11, confirming the hypothesis that biaxial behavior is pressurization rate-dependent. There was a significant increase in burst pressures (Figure 6-12) between vessels tested at 0.4 and 1.4 mm Hg/s.

The time to failure under steady pressure (below the burst pressure) for collagen gel TEBVs is pressure dependent (Figure 6-13). Isobaric tests were performed at 20, 30 and 40 mm Hg; the times to failure were 24.1, 4.25, and 1.53 minutes, respectively. The diameter increased gradually at first, followed by rapid dilation near the time of failure. The initial loss of strength appears to be slow, then followed by sudden accelerated softening immediately prior to failure.

Fatigue tests performed on constructs to 50% of the burst pressure, failed after 1-3 hours. Cyclic pressure causes a gradual decrease in the structural stiffness followed by a sudden rupture. A representative pressure-diameter for fatigue testing is shown in Figure 6-14.

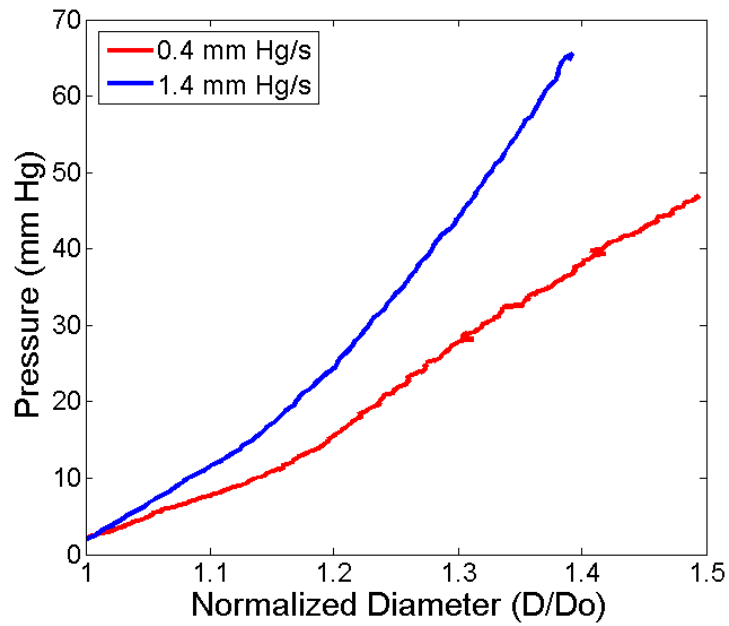


Figure 6-11. Representative burst pressure tests for collagen gel TEBVs. Vessels were inflated to failure at 0.4 mm Hg/s and 1.4 mm Hg/s.

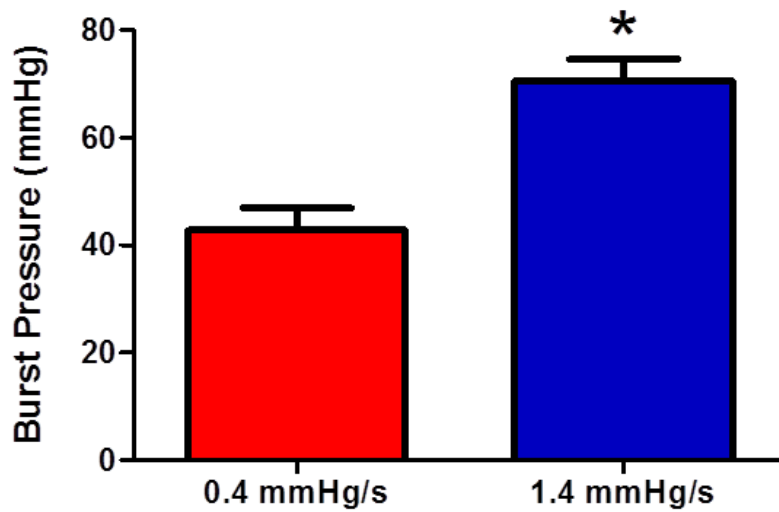


Figure 6-12. Mean burst pressures at 0.4 mm Hg/s and 1.4 mm Hg/s. Results are reported as mean \pm SEM (*p<0.05).

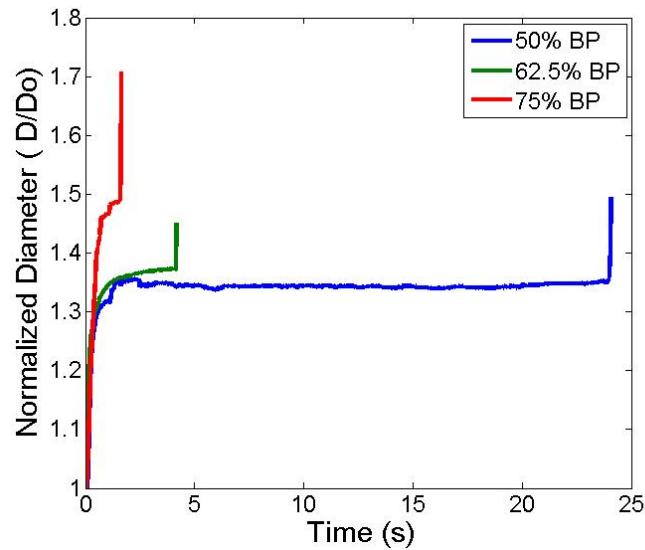


Figure 6-13. Representative isobaric tests of collagen gel TEBVs. Vessels were held at 20, 30, and 40 mm Hg until failure.

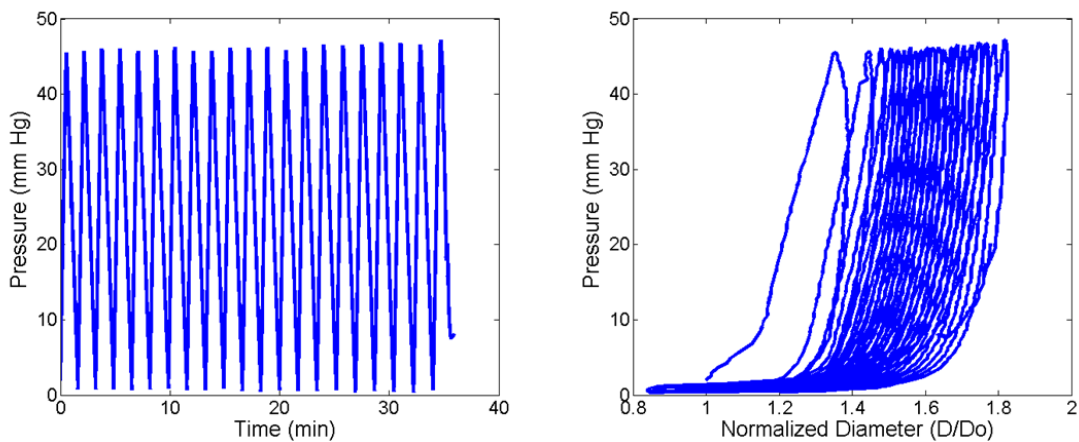


Figure 6-14. Representative fatigue test collagen gel TEBVs. a) Vessels were cyclically inflated and deflated to 45 mm Hg. b) Pressure-diameter response of the fatigue tests.

6.3.1 Simulation Results

6.3.1.1 Material and Damage Parameters

Similar to the uniaxial results, the values for a and c varied greatly from experiment to experiment. A set of representative experiments were chosen and used for these simulation results. In these studies, considered damage in the circumferential direction

was considered. The proposed strain energy function (equation (6.4)) was verified using experimental pressure-diameter response of collagen-based TEBVs. Values of $\alpha = 9$ and $c = 0.4$ demonstrated a reasonably good fit between the experimental and theoretical results (Figure 6-15). Four separate cases were considered: 2D isotropic, 2D anisotropic, 3D isotropic, and 3D anisotropic damage.

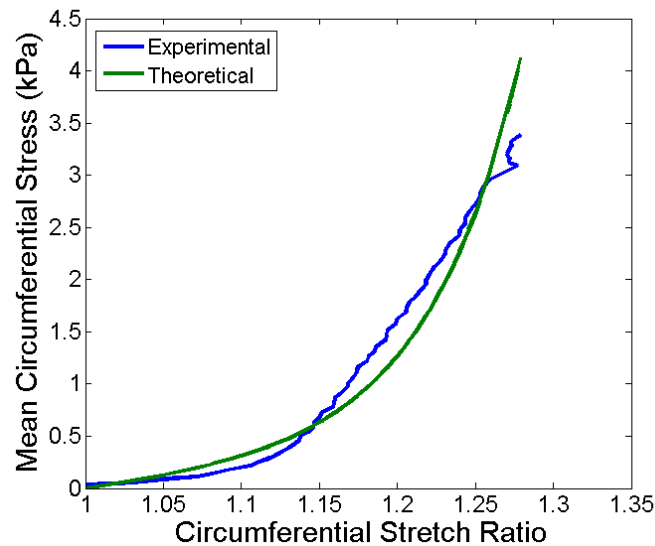


Figure 6-15. Verification of the proposed strain energy function. Comparison of the experimental and theoretical stress-stretch response of a tubular collagen gel.

For simplicity, only simulations where the vessel was modeled as a thin-walled tube kept at a constant length that underwent anisotropic damage are shown. The results were similar for all cases. Since tests in the axial direction were not performed, these responses were guessed. Burst pressure (Figure 6-16), isobaric (Figure 6-17), and fatigue testing (Figure 6-18) are shown. The trends compare well to the experimental results (Figure 6-11, Figure 6-13, and Figure 6-14). Figure 6-17b and Figure 6-18b are parametric

studies of variable pressurization rates and loading pressures, respectively. These studies could provide valuable predictions into experiments that were not performed.

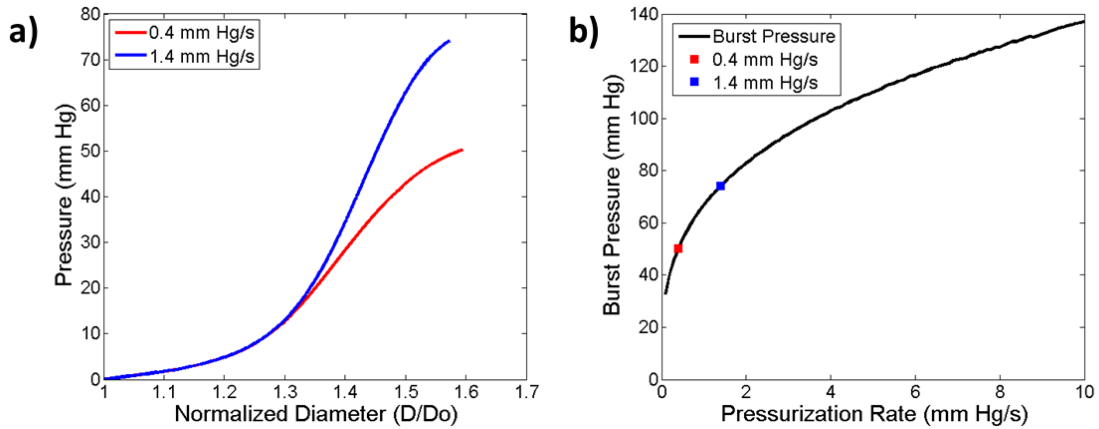


Figure 6-16. Predicted burst pressure test response.a) Pressure-normalized diameter and b) prediction of burst pressure with increasing inflation rate.

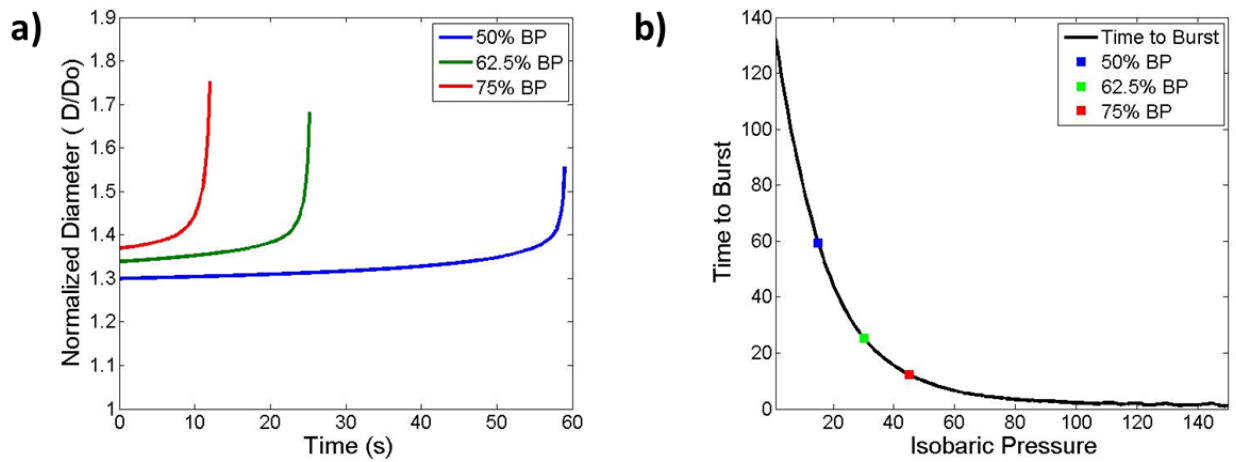


Figure 6-17. Predicted isobaric response of collagen gel TEBVs a) at 25 mm Hg, 30 mm Hg, and 35 mm Hg and b) predicted time to failure versus imposed pressure.

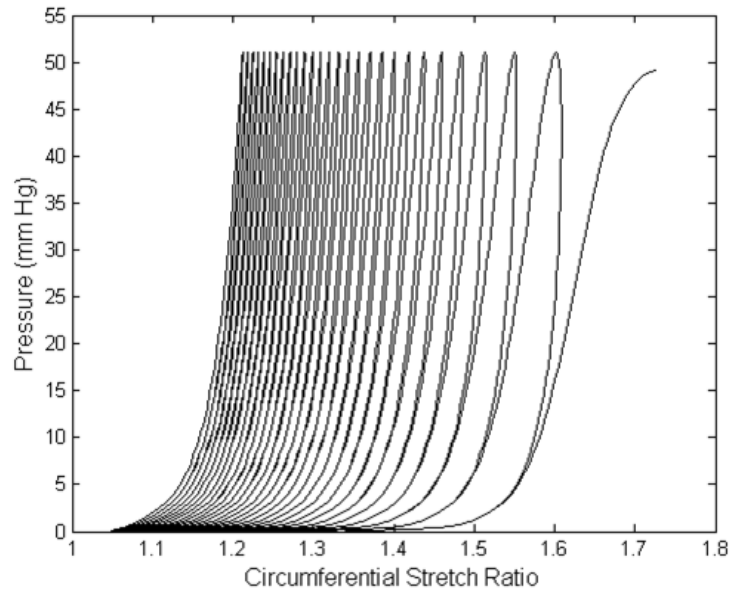


Figure 6-18. Representative predicted fatigue response of a collagen gel TEBV. The vessels were simulated to be cyclically inflated and deflated to 50 mm Hg (60% BP).

6.4 Conclusions

A biaxial testing system for TEBVs that can simultaneously control pressure, luminal flow, and axial extension and record changes in vessel diameter in response to these loads was developed. Cyclic inflation-deflation and force-length tests were performed on collagen-based TEBVs. The tissue demonstrated significant plastic deformation in the circumferential and axial directions during cyclic pressure tests. Plastic deformation exhibited during force-length tests was not as high. Therefore, plastic deformation and damage of collagen-based TEBVs is not isotropic. Development of alternative testing methods was necessary to accurately describe the mechanical behavior of these vessels.

An experimental and modeling framework for the damage and plasticity of gel-derived TEBVs via appropriate evolution equations was proposed. Given that plasticity and damage typically occur over shorter time-scales than growth and remodeling, it is necessary to consider the effects separately. The effect of plasticity and damage can be experimentally quantified independently of those of growth and plasticity by performing acute tests to failure; such tests do not allow enough time for significant growth and remodeling, thereby isolating the non-cell-mediated mechanisms of damage and plasticity. Tests such as cylindrical biaxial isobaric, fatigue, and burst pressure testing can be sufficient to quantify evolution equations for damage and plasticity. Once the evolution equations and kinetic parameters are specified for damage and plasticity, culture experiments can be used to identify growth and remodeling equations and parameters. It was shown that the burst pressure of collagen gel TEBVs is rate-dependent (Figure 6-12) and therefore any comparison of the mechanical properties of TEBVs developed by different methods must be done at the same rate of pressurization. These results also suggest that burst pressure tests are not sufficient to assess a TEBVs' suitability as a coronary substitute, isobaric and/or fatigue tests are also needed. Further experimental data and modeling simulations are still needed to verify and refine the model. This model can be used to identify insightful experiments for predicting TEBV failure and decrease the number of costly in vivo experiments necessary for graft testing.

6.5 References

1. Girton, T., T. Oegema, and R. Tranquillo, *Exploiting glycation to stiffen and strengthen tissue equivalents for tissue engineering*. Journal of biomedical materials research, 1999. **46**(1): p. 87-92.

2. Girton, T., et al., *Mechanisms of stiffening and strengthening in media-equivalents fabricated using glycation*. Journal of biomechanical engineering, 2000. **122**(3): p. 216.
3. Wagenseil, J.E., E.L. Elson, and R.J. Okamoto, *Cell orientation influences the biaxial mechanical properties of fibroblast populated collagen vessels*. Annals of biomedical engineering, 2004. **32**(5): p. 720-731.
4. Ku, D.N. and H.-C. Han, *Assessment of function in tissue-engineered vascular grafts*, in *Functional tissue engineering*. 2003, Springer. p. 258-267.
5. Matsumoto, T. and K. Hayashi, *Mechanical and dimensional adaptation of rat aorta to hypertension*. Journal of biomechanical engineering, 1994. **116**(3): p. 278.
6. Kamiya, A. and T. Togawa, *Adaptive regulation of wall shear stress to flow change in the canine carotid artery*. Am J Physiol 1980. **239**.
7. Yao, L., et al., *Fibrin-based tissue-engineered blood vessels: differential effects of biomaterial and culture parameters on mechanical strength and vascular reactivity*. Tissue engineering, 2005. **11**(7-8): p. 991-1003.
8. Swartz, D.D., J.A. Russell, and S.T. Andreadis, *Engineering of fibrin-based functional and implantable small-diameter blood vessels*. American Journal of Physiology-Heart and Circulatory Physiology, 2005. **288**(3): p. H1451-H1460.
9. Schutte, S.C., et al., *Tissue engineering of a collagen-based vascular media: Demonstration of functionality*. Organogenesis, 2010. **6**(4): p. 204-211.
10. Gleason, R.L., E. Wilson, and J.D. Humphrey, *Biaxial biomechanical adaptations of mouse carotid arteries cultured at altered axial extension*. J Biomech, 2007. **40**(4): p. 766-76.
11. Zaucha, M.T., et al., *A novel cylindrical biaxial computer-controlled bioreactor and biomechanical testing device for vascular tissue engineering*. Tissue Eng Part A, 2009. **15**(11): p. 3331-40.
12. Rachev, A., T. ElShazly, and D.N. Ku. *Constitutive formulation of the mechanical properties of synthetic hydrogels*. 2004. ASME.
13. Humphrey, J.D., *Cardiovascular solid mechanics: cells, tissues, and organs*. 2002: Springer.

CHAPTER 7

EFFECT OF CULTURE TIME AND CROSSLINKING ON TEBV DAMAGE

7.1 Introduction

In chapter 6, an experimental-theoretical framework was developed for quantifying the plasticity and damage of collagen gel-derived TEBVs. This chapter focuses on identifying the role of tissue transglutaminase (Tg) induced crosslinking and the effects of time in static culture in reducing the plasticity and damage of the TEBVs.

It has been shown previously that the strength of cell-seeded collagen gel-based TEBVs significantly increases over time in static culture [1]. During culture, the cells compact and reorient the matrix, leading to circumferential cellular and collagen fiber alignment [2]. The compaction of the gel against a central rigid mandrel induces mechanical constraints that lead to a stronger vessel [3].

Tissue Tg is an enzyme that has been demonstrated to be involved in many different physiological processes. In collagen gels, tissue Tg acts as a calcium-dependent enzyme that catalyzes the formation of an amide bond between glutamine and lysine residues of the collagen polypeptide chains [4]. Enzymatic crosslinking with tissue Tg has been demonstrated to significantly increase the burst pressure of collagen gels [5].

In chapter 3, a mathematical model was developed to predict the changes in material parameters due to mechanical stimulation and time in culture. In this chapter, the effects

of static culture time on the growth and remodeling of TEBVs are examined. The mechanical tests described in chapters 5 and 6 were performed to quantify differences in the failure properties of these gels. In addition, the role of tissue Tg crosslinking in reducing the plasticity and damage of collagen-based TEBVs was quantified.

7.2 Materials and Methods

7.2.1 Experimental Methods

7.2.1.1 Collagen gel-derived TEBV Fabrication

Control collagen constructs were made as described in chapters 5 and 6. Tg-crosslinked vessels were made by adding a 5000:1 weight ratio of porcine Tg (Sigma, St. Louis, MO), 2.5 mM CaCl₂, and 1 mM DL-dithiothreitol (DTT) to the solution.

7.2.1.2 Uniaxial and Biaxial Testing

The mechanical testing systems described in chapters 5 and 6 were used to test the TEBVs in this study. Uniaxial tensile tests were performed at 0.1 and 1 mm/s. The Cauchy stress-Green strain relationship was obtained using the DIC method described in chapter 5. The UTS was determined as the maximum stress during the test. The modulus was calculated as the slope of the linear region of the stress-strain curve. The work to failure was calculated as the area under the stress-strain curve. Creep tests were performed at 60% and 80% of the UTF of the monotonic tensile tests at 1 mm/s from the same batch of vessels. For comparison between Tg-crosslinked and control, the UTF of the control was used. Burst pressure tests were performed at an inflation rate of 1.4 mm Hg/s, while the outer diameter was monitored throughout the test. The mean circumferential stress was calculated as follows:

$$\sigma_{\theta} = \frac{Pr_i}{h} \quad (7.1)$$

where P is the luminal pressure, r_i is the inner radius, and h is the thickness of the vessel.

The inner radius was calculated by assuming incompressibility:

$$r_i^2 = r_o^2 - (R_o^2 - R_i^2)L_o/\ell \quad (7.2)$$

where r_o is the current outer radius, ℓ is the current length of the vessel. R_o , R_i , and L_o are the unloaded, initial, outer radius, inner radius, and axial length, respectively. The circumferential stretch ratio was calculated by r_i/R_i . The modulus was determined as the slope of the stress-strain curve at 10 mm Hg increments. The diameters and lengths of each construct were measured prior to testing to determine initial volumes.

7.2.1.3 Statistical Analysis

Statistical significance was established using a one way ANOVA with a post hoc tukey's t-test. $p < 0.05$ was considered significant.

7.3 Results and Discussion

7.3.1 Change in Material Properties due to Time in Culture

To show the effects of compaction and collagen synthesis on the mechanical testing parameters, TEBVs were tested at 3, 7, and 14 days of culture. The results of monotonic tensile tests are shown in Figure 7-1. Significant differences were seen in the UTS between 3 day, 7 day, and 14 day statically cultured constructs (Figure 7-1a). The modulus and work to failure were significantly greater at 14 days, but not at 7 days

(Figure 7-1b and Figure 7-1d). The stretch at failure significantly decreased at 14 days but not at 7 days (Figure 7-1c). Most of the cell-mediated remodeling appears to occur within the last week of static culture. This is in agreement with findings in the literature [6].

Creep tests were performed at 2 and 7 days of culture. Average times to failure and strains at failure for creep tests performed at 60% and 80% of the UTF (obtained from monotonic tensile tests performed at 1 mm/s) are shown in Figure 7-2. No significant differences were seen in the UTS between different time-points, but the UTS was significantly higher after 7 days of culture (Figure 7-2a). In agreement with the proposed model, higher imposed loads lead to faster damage (Figure 7-2b). The stretch at failure increased with increasing loads and but decreased with culture time (Figure 7-2c). The work to failure did not seem to be affected by the time in culture (Figure 7-2d).

In addition, burst pressure testing was performed on collagen gel-based TEBVs cultured for 2, 7, and 14 days (Figure 7-3). Significant differences were seen between all time-points tested ($BP = 464 \pm 4.5$, $BP = 70.5 \pm 4.1$, and $BP = 107.8 \pm 2.8$, for 2, 7, and 14 days, respectively, $p < 0.05$). The mean circumferential stresses and circumferential stress ratios (normalized diameter) were significantly higher with decreasing time in culture at each measured pressure (Figure 7-4). No significant differences were seen between the moduli of different time-points in culture (Figure 7-5).

The volume of each construct was measured prior to testing. As predicted by the theoretical model in chapter 3 (Figure 3-3) and in agreement with the literature [1, 3, 7], a

decrease in volume corresponds with an increase in the strength of the gel and a decrease in the induced plastic deformation (Figure 7-1c and Figure 7-2c).

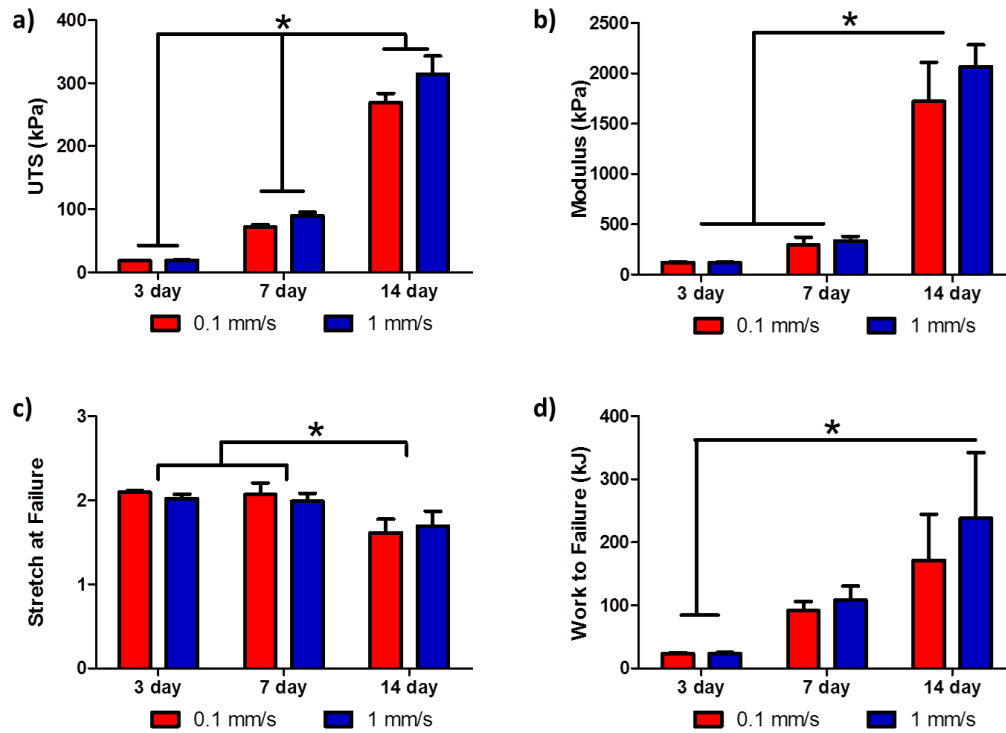


Figure 7-1. Uniaxial tensile tests performed at different times of static culture. a) UTS, b) modulus, c) stretch at failure, and d) work to failure are shown. Results are reported as mean \pm SEM ($*p < 0.05$).

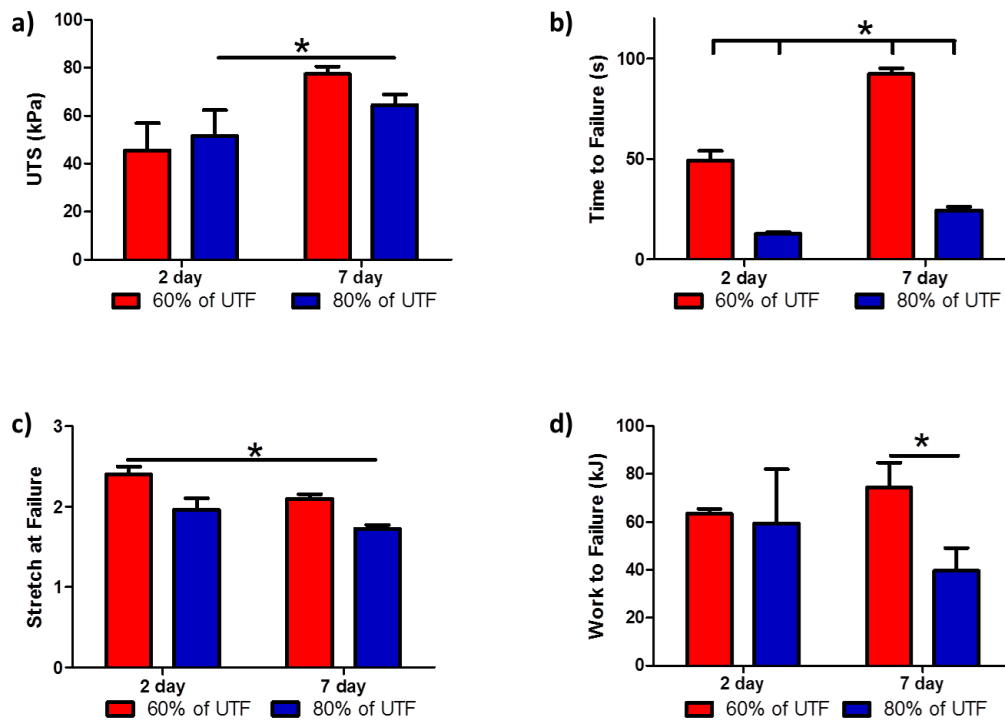


Figure 7-2. Uniaxial creep tests performed at 2 and 7 days of static culture. a) UTS, b) time to failure, c) stretch at failure, and d) work to failure are shown. Results are reported as mean \pm SEM (* p <0.05).

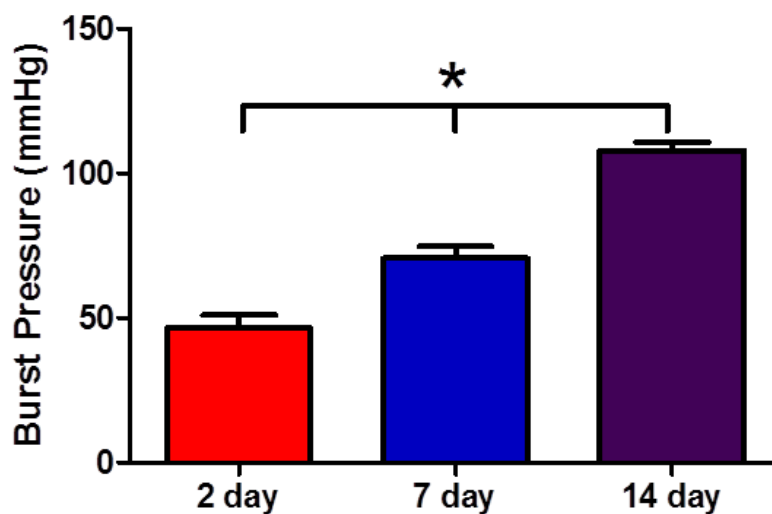


Figure 7-3. Burst pressure tests performed at 2, 7, and 14 days of static culture. Results are reported as mean \pm SEM (* p <0.05).

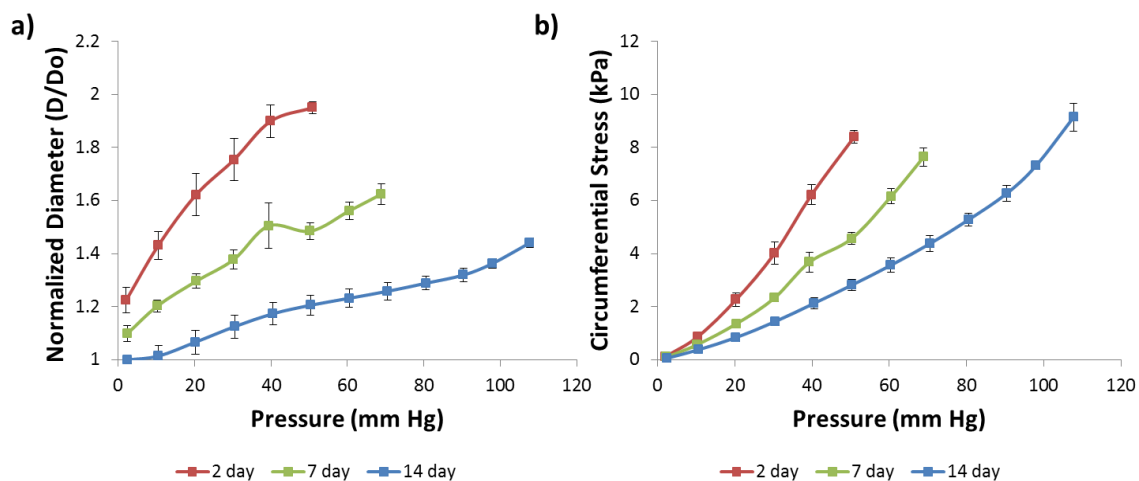


Figure 7-4. Mechanical responses of TEBVs cultured statically for 2, 7, and 14 days. a) Pressure-diameter relationship and b) mean circumferential stress and pressure relationship at different time-points of static culture. The diameters are normalized to their initial values. Results are reported as mean \pm SEM. Significant differences at all pressures above 40 between all time-points and between 2 day and 14 day at all pressures ($p < 0.05$).

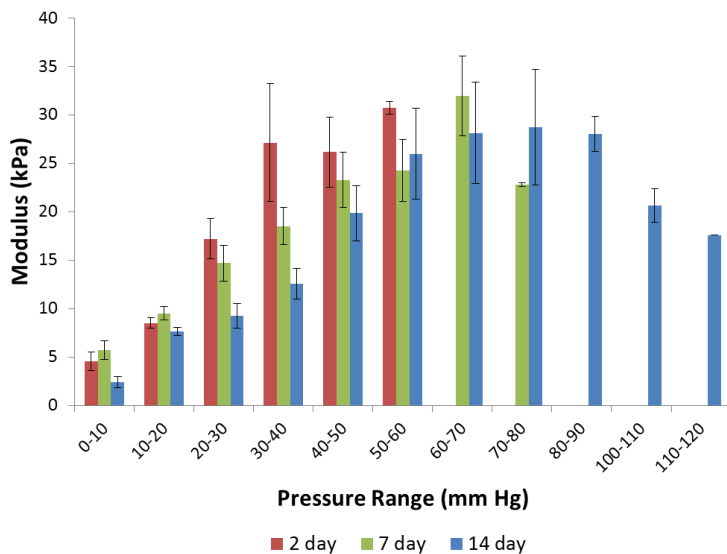


Figure 7-5. Differences in moduli between different time-points in culture. Moduli were assessed at increments of 10 mm Hg. Results are reported as mean \pm SEM. No significant differences were seen between different time-points.

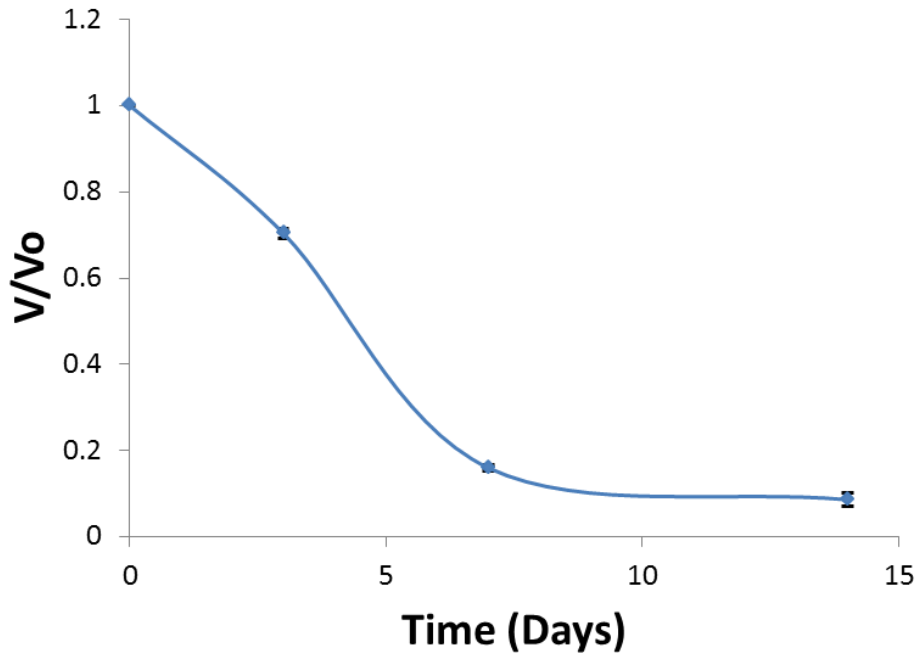


Figure 7-6. Change in the volume of collagen-based TEBVs over time in culture. The volume was normalized to the initial volume of the gel. Results are reported as mean \pm SEM.

7.3.2 Change in Material Properties with Tg Crosslinking

Mechanical tests were performed on Tg-crosslinked constructs and compared to control at day 7 of static culture, to determine the effects of crosslinking in the reduction of plasticity and damage of collagen gel TEBVs.

To determine the effects of Tg crosslinking on the plasticity and damage of collagen gel TEBVs, monotonic tests were performed at extension rates of 0.1 mm/s and 1 mm/s. The UTS of the Tg vessels was significantly higher than the control (Figure 7-7a). The modulus of the Tg-crosslinked constructs was significantly higher only at 1 mm/s than

the control (Figure 7-7b). No differences in stretch at failure were observed (Figure 7-7c-d).

Creep tests were performed at 7 days of culture and compared between Tg and control constructs. Average times to failure and strains at failure for creep tests performed at 60% and 80% of the UTF of the control (obtained from monotonic tensile tests performed at 1 mm/s) are shown in Figure 7-8. Due to the large variation in the data obtained, no significant results were obtained from these tests.

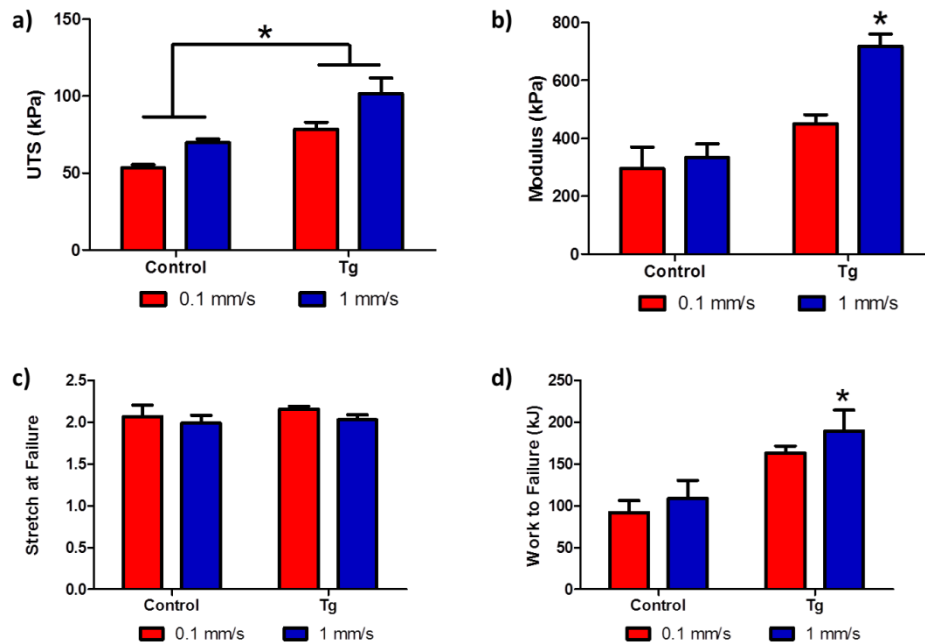


Figure 7-7. Uniaxial monotonic tensile tests performed on control and Tg-crosslinked TEBVs. a) UTS, b) modulus, c) stretch at failure, and d) work to failure are shown. Results are reported as mean \pm SEM (* $p < 0.05$).

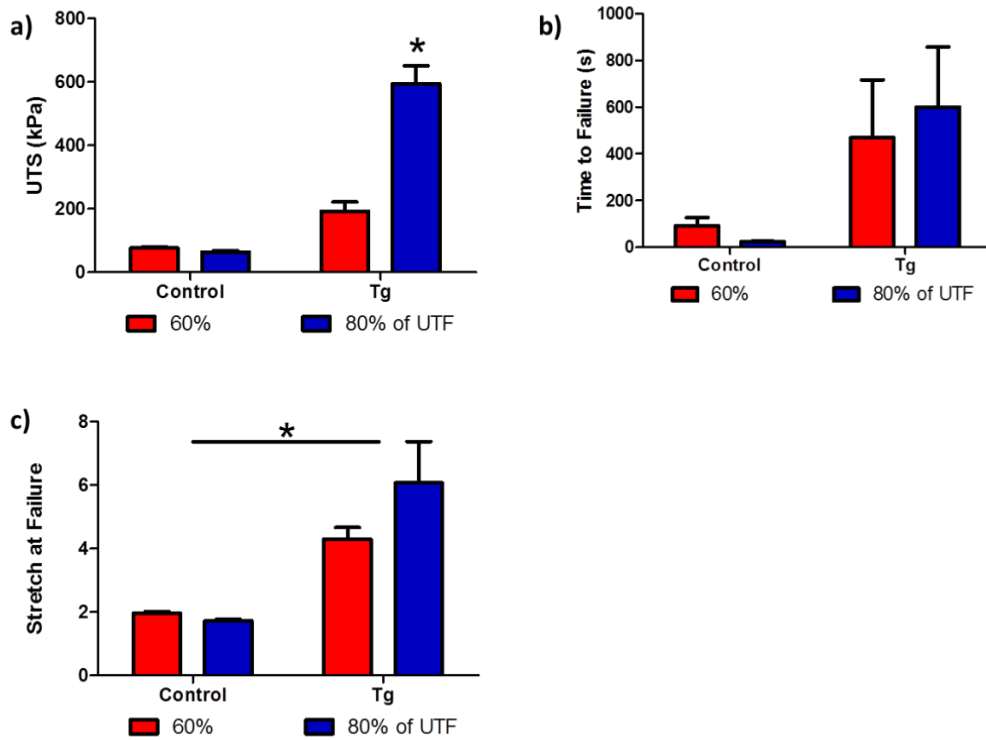


Figure 7-8. Uniaxial creep tests performed on control and Tg-crosslinked TEBVs. a) UTS, b) time to failure, and c) stretch at failure. Results are reported as mean \pm SEM (* $p < 0.05$).

The average burst pressure of Tg-treated constructs was significantly higher than that of controls (BP=205 \pm 10 mm Hg for Tg-treated and BP=137 \pm 7.6 for controls, $p < 0.05$). The trends of the mean circumferential stresses and circumferential stress ratios (normalized diameter) appear to be higher for the controls (Figure 7-10). The moduli were not significantly different between the Tg and control groups (data not shown).

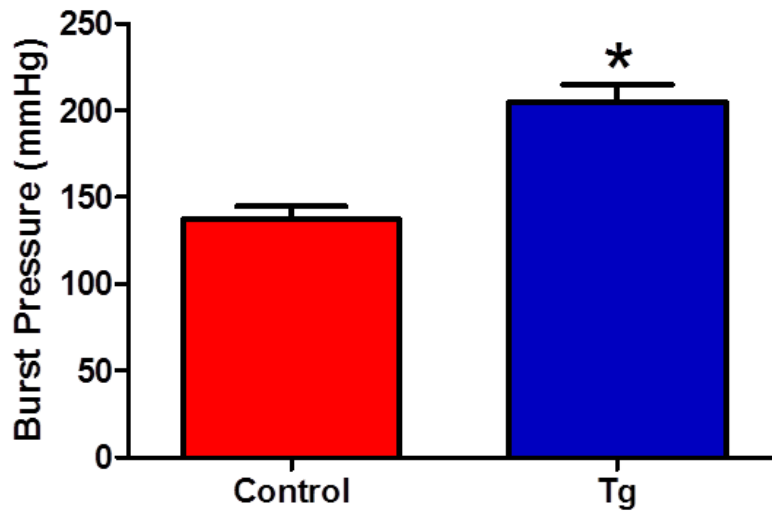


Figure 7-9. Burst pressure tests of control and Tg-treated collagen gel TEBVs. Results are reported as mean \pm SEM (* $p < 0.05$).

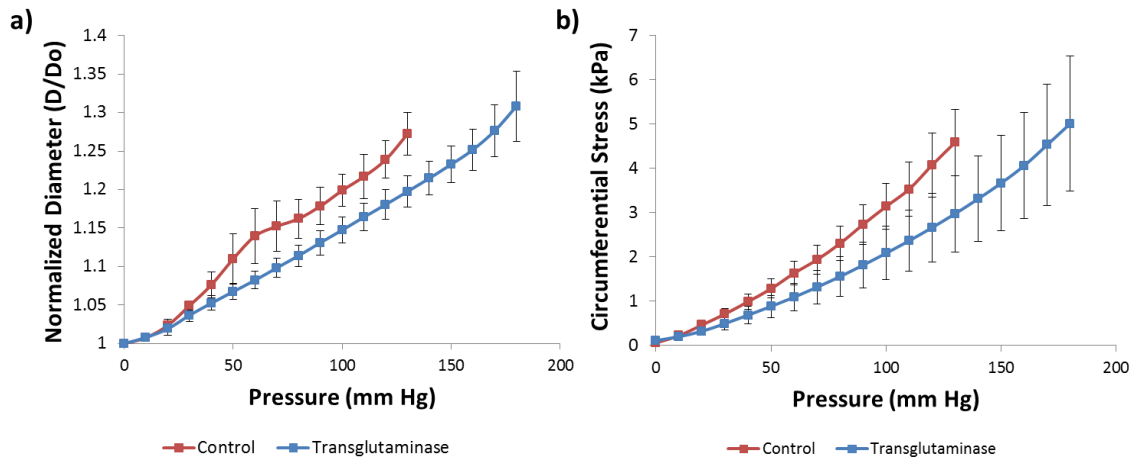


Figure 7-10. Mechanical responses of control and Tg-treated TEBVs. a) Pressure-diameter relationship and b) mean circumferential stress and pressure relationship at different time-points of static culture. The diameters are normalized to their initial values. Results are reported as mean \pm SEM.

No significant differences in compaction were seen between the control and Tg crosslinked groups after 14 days of static culture (Figure 7-11), suggesting that the increase in strength is due to the internal structure of the construct and not due to any cell-mediated compaction.

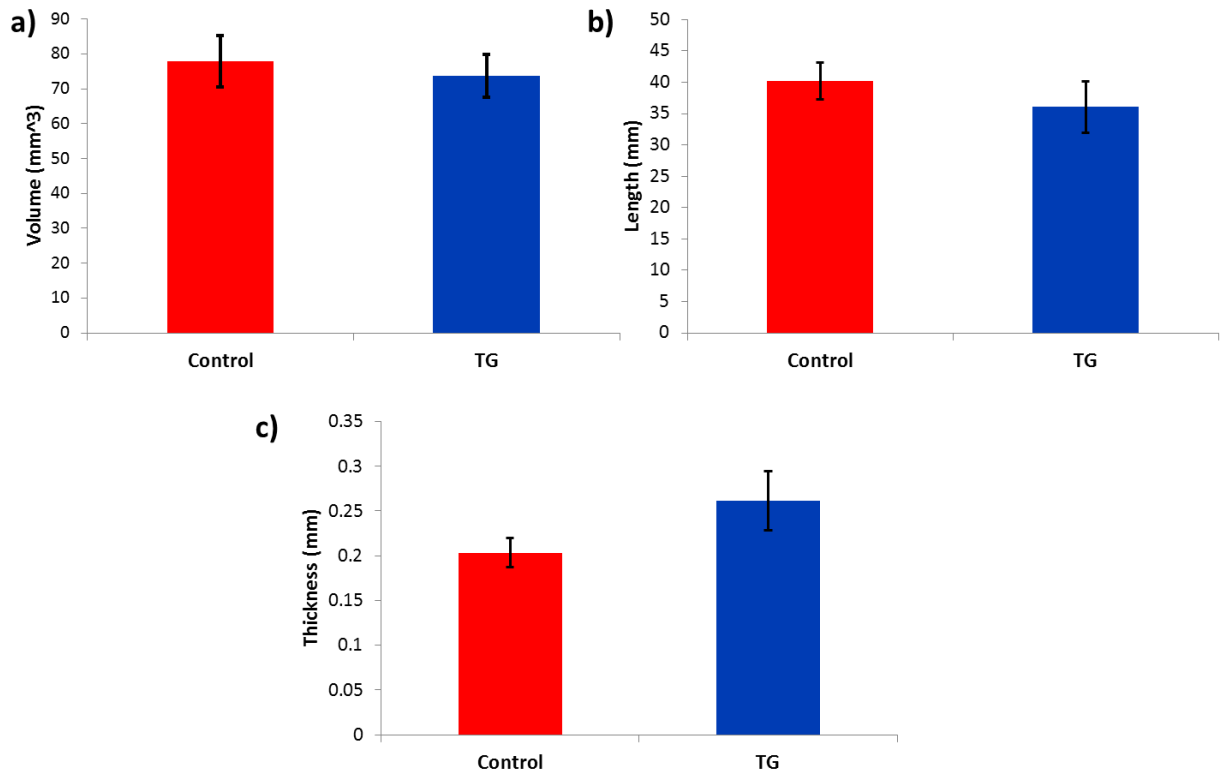


Figure 7-11. Changes in the geometric properties of control and Tg-treated collagen gel-based TEBVs. a) Volume, b) length, and c) thickness of control and Tg-treated vessels. Results are reported as mean \pm SEM. No significant differences were seen in any dimension.

7.4 Conclusions

The goal of this work was to study the effects of culture time and Tg-crosslinking on the changes in the mechanical properties of collagen-based TEBVs. The results of this study suggest that both time in culture and crosslinking with tissue Tg increase the strength of the TEBVs. During creep testing, the times to failure increased with time in culture and

were generally higher for the Tg-crosslinked TEBVs, suggesting that the process of damage accumulation is slower in these vessels. However, the percent differences in the UTS between monotonic tensile tests run at stretching rates of 0.1 mm/s and 1 mm/s were approximately the same between the Tg-crosslinked and control groups. This suggests that crosslinking may affect only the stress-dependent component but not the stress rate-dependent component of the plastic deformation and damage of collagen gel TEBVs. The differences between varying strain rates, however, seemed to be affected by time in static culture. Therefore, the reduction in damage in plasticity during culture is both stress and stress rate-dependent.

The results presented here were limited due to significant variations in the uniaxial testing. This is probably due to non-homogenous compaction, which yields differences in the material properties of the gels. In addition, collagen gels are very fragile and slight differences in handling could affect the results. Due to the variations in results, modeling parameters could not be fit to the experimental data. To demonstrate the capabilities of the theoretical model, a hypothetical change in the monotonic tensile stress-strain response between Tg-crosslinked vessels and controls is presented in (Figure 7-12). The stress-rate dependent component of damage was kept the same, while the stress-dependent component was varied. More biaxial experiments need to be performed to quantify the functional forms and parameter for the model.

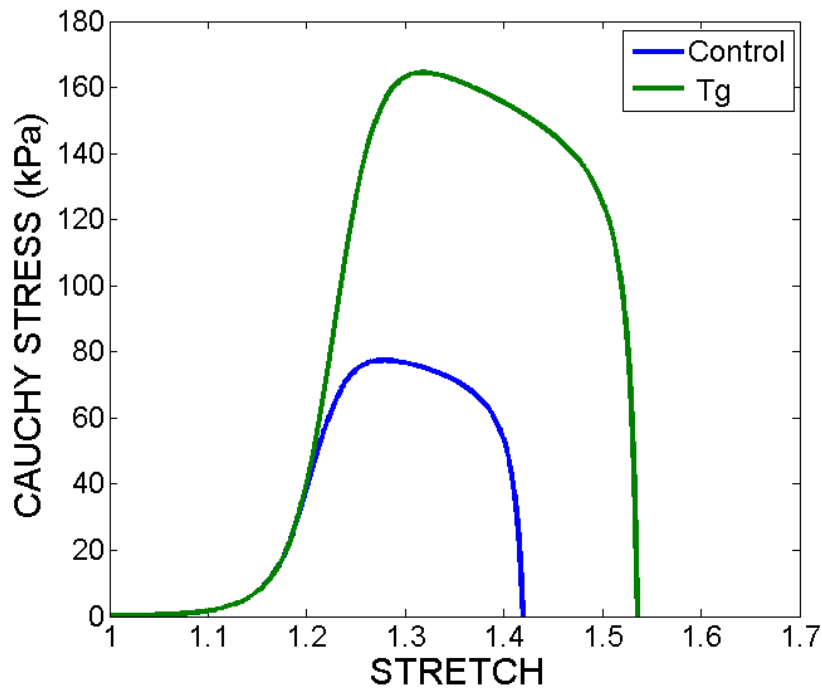


Figure 7-12. Theoretical change in the uniaxial tensile response between the control and Tg-crosslinked TEBVs.

The model can be used to quantify the effects that mechanically-induced changes in the material properties and various types of crosslinking agents have on the damage and plastic deformation of the TEBVs. Variations in the parameters of the evolution equations of damage described in chapters 4 and 5 could be quantified. Then parametric studies could be performed on the effects of various factors, such as changes in the concentration of the crosslinking agent, changes in cellular concentration, and changes in the mechanical constraints imposed on the vessel during tissue culture. These predictions could then be used to determine the optimal conditions for TEBV development without performing costly experiments for each condition.

7.5 References

1. Seliktar, D., et al., Dynamic mechanical conditioning of collagen-gel blood vessel constructs induces remodeling in vitro. *Ann Biomed Eng*, 2000. 28(4): p. 351-62.
2. L'Heureux, N., et al., In vitro construction of a human blood vessel from cultured vascular cells: a morphologic study. *Journal of vascular surgery*, 1993. 17(3): p. 499-509.
3. Barocas, V., T. Girton, and R. Tranquillo, *Engineered alignment in media equivalents: magnetic prealignment and mandrel compaction*. *Journal of biomechanical engineering*, 1998. 120(5): p. 660-666.
4. Chen, J.S. and K. Mehta, *Tissue transglutaminase: an enzyme with a split personality*. *The international journal of biochemistry & cell biology*, 1999. 31(8): p. 817-836.
5. Orban, J.M., et al., *Crosslinking of collagen gels by transglutaminase*. *Journal of Biomedical Materials Research Part A*, 2004. 68(4): p. 756-762.
6. Girton, T., et al., Mechanisms of stiffening and strengthening in media-equivalents fabricated using glycation. *Journal of biomechanical engineering*, 2000. 122(3): p. 216.

CHAPTER 8

CONCLUSIONS AND FUTURE DIRECTIONS

In summary, a model that combines the concepts of growth, remodeling, damage, and plasticity was developed. The model predictions are in agreement with typical experiments presented in the literature and experiments performed in our lab. However, more experiments are still needed to quantify functional forms and parameters for the model. These modeling simulations can be used to design insightful experiments and ultimately reduce the number of experiments required to identify the failure mechanisms of a vessel.

The development of a TEBV with sufficient mechanical properties and fast enough development times still remains a challenge. The theoretical-experimental framework developed in this study provides several directions for future research. These include using the collagen gel-based TEBV as a model system to study various processes, extending the theoretical model to include microstructural parameters, measuring the effects of different culture conditions on the damage and plasticity parameters, and extending the theoretical model to other forms of TEBVs.

The collagen-based TEBV could serve as an *in vitro* model for various cardiovascular events. A system that can mimic the physiological environment of blood vessels has already been setup in our lab. Shear and pressure can be independently controlled and the responses of the vessels can be monitored. One of the first steps of atherosclerosis is

monocyte binding. It has been shown that monocyte binding increases when ECs are exposed to oscillatory shear as compared to non-reversing shear. In addition, areas of the vasculature that are more prone to atherosclerosis are in areas that experience reversal of flow. A model vessel that can be made out of human cells that can be exposed to a similar mechanical environment as native vessels will provide a 3D platform for testing the effects of various factors on the initiation and progression of atherosclerosis. Once the parameters in this model are refined, the model could be used to approximate the stresses on the cells during in vitro experiments and better compare the cellular response to physiologic processes.

The mathematical model can be refined by redefining the constitutive equation to include microstructural constituents. The main components of collagen-based TEBV that contribute to its mechanical properties are collagen, SMCs, and water. Microstructural constitutive models that have been developed for native arteries [1] or for hydrogels [2-4], can be modified and used to improve the predictive capabilities of this model.

A microstructural model that predicts changes in the microstructural organization during growth, damage, and remodeling of collagen TEBVs would greatly increase the predictive capabilities of this model. Obtaining microstructural metrics such as volume fractions and the distribution of fiber orientations and stretches is required for microstructurally-motivated models of growth, remodeling, damage, and plasticity. Multiphoton microscopy can be used to obtain microstructural information during tissue development and mechanical testing [5-7]. Collagen gel microstructure has been shown

to correlate with the mechanical properties of the gel [8-10]. Feng et al. showed that uniaxial mechanical testing induced collagen fibril realignment in the direction of loading [11]. The collagen fiber distribution obtained through microstructural imaging can also be incorporated into the constitutive equations [12]. In addition, this model considers only a passive response from the SMCs. However, vasoactivity has been demonstrated in collagen-based and fibrin-based TEBVs in chapter 6 and the literature [13-16]. Constitutive equations accounting for SMC contraction [17-19] also might need to be incorporated into the model.

Multiple factors affect the mechanical properties of TEBVs. It has been demonstrated that TEBVs developed under different conditions exhibit different mechanical properties. For example, different environmental effects such as pH, temperature, mechanical constraints under static culture, and different cyclic strain parameters have all been shown to influence the mechanical behavior of the collagen gels [20, 21]. Many different methods are currently utilized in different labs and the experimental data is difficult to compare between labs. The theoretical model presented here can help elucidate the causes of failure in these seemingly diverse sets of experiments.

In addition, the remodeling process is very complex and involves many different factors. For example, MMP activity was shown to dramatically increase following cyclic mechanical stimulation, which also coincided with increased mechanical strength of the TEBVs. Refinement of the model should take into account the activity of these proteases

and perhaps other biochemical factors that could significantly impact the properties of the material.

Different cell or collagen concentrations have also been shown to have profound effects on the mechanical properties of the TEBVs. Accounting for these factors in the model would help improve the versatility of this model. If these factors are taken into account for comparison between results it could help explain the discrepancies in the data.

Finally, the model can be extended to other platforms of TEBV design. Because collagen gel-based TEBVs lack strength and undergo considerable plastic deformation, their use as a replacement graft is highly unlikely. However, the theoretical framework for damage and plasticity developed in this dissertation can apply to any type of vessel. The mechanisms of damage and failure of various tissue engineering platforms could be studied *in vitro*, which could significantly reduce the number of costly *in vivo* animal experiments. The forms of the evolution equations and parameters can then be determined by performing the uniaxial or biaxial mechanical tests described in chapters 4 and 5. The vessel behavior *in vivo*, following implantation, can then be predicted by performing model simulations using physiological conditions.

8.1 References

1. Holzapfel, G.A., T.C. Gasser, and R.W. Ogden, *A new constitutive framework for arterial wall mechanics and a comparative study of material models*. Journal of elasticity, 2000. **61**(1): p. 1-48.
2. Barocas, V.H. and R.T. Tranquillo, *An anisotropic biphasic theory of tissue-equivalent mechanics: the interplay among cell traction, fibrillar network*

- deformation, fibril alignment, and cell contact guidance.* Journal of biomechanical engineering, 1997. **119**(2): p. 137-145.
3. Zahalak, G.I., et al., *A cell-based constitutive relation for bio-artificial tissues.* Biophysical journal, 2000. **79**(5): p. 2369-2381.
 4. Wagenseil, J.E. and R.J. Okamoto, *Modeling cell and matrix anisotropy in fibroblast populated collagen vessels.* Biomechanics and modeling in mechanobiology, 2007. **6**(3): p. 151-162.
 5. Robertson, A.M., M.R. Hill, and D. Li, *Structurally motivated damage models for arterial walls. Theory and application,* in *Modeling of Physiological Flows.* 2012, Springer. p. 143-185.
 6. Wan, W., H. Yanagisawa, and R.L. Gleason, Jr., *Biomechanical and microstructural properties of common carotid arteries from fibulin-5 null mice.* Ann Biomed Eng, 2010. **38**(12): p. 3605-17.
 7. Zaucha, M.T., et al., *A novel cylindrical biaxial computer-controlled bioreactor and biomechanical testing device for vascular tissue engineering.* Tissue Eng Part A, 2009. **15**(11): p. 3331-40.
 8. Raub, C.B., et al., *Noninvasive assessment of collagen gel microstructure and mechanics using multiphoton microscopy.* Biophysical journal, 2007. **92**(6): p. 2212-2222.
 9. Raub, C.B., et al., *Image correlation spectroscopy of multiphoton images correlates with collagen mechanical properties.* Biophysical journal, 2008. **94**(6): p. 2361-2373.
 10. Raub, C., et al., *Predicting bulk mechanical properties of cellularized collagen gels using multiphoton microscopy.* Acta biomaterialia, 2010. **6**(12): p. 4657-4665.
 11. Feng, Z., et al., *Investigation on the mechanical properties of contracted collagen gels as a scaffold for tissue engineering.* Artificial organs, 2003. **27**(1): p. 84-91.
 12. Wan, W., J.B. Dixon, and R.L. Gleason, *Constitutive modeling of mouse carotid arteries using experimentally measured microstructural parameters.* Biophysical journal, 2012. **102**(12): p. 2916-2925.
 13. L'Heureux, N., et al., *A human tissue-engineered vascular media: a new model for pharmacological studies of contractile responses.* The FASEB journal: official publication of the Federation of American Societies for Experimental Biology, 2001. **15**(2): p. 515.

14. Schutte, S.C., et al., *Tissue engineering of a collagen-based vascular media: Demonstration of functionality*. Organogenesis, 2010. **6**(4): p. 204-211.
15. Swartz, D.D., J.A. Russell, and S.T. Andreadis, *Engineering of fibrin-based functional and implantable small-diameter blood vessels*. American Journal of Physiology-Heart and Circulatory Physiology, 2005. **288**(3): p. H1451-H1460.
16. Yao, L., et al., *Fibrin-based tissue-engineered blood vessels: differential effects of biomaterial and culture parameters on mechanical strength and vascular reactivity*. Tissue engineering, 2005. **11**(7-8): p. 991-1003.
17. Rachev, A. and K. Hayashi, *Theoretical study of the effects of vascular smooth muscle contraction on strain and stress distributions in arteries*. Annals of biomedical engineering, 1999. **27**(4): p. 459-468.
18. Zulliger, M.A., A. Rachev, and N. Stergiopoulos, *A constitutive formulation of arterial mechanics including vascular smooth muscle tone*. American Journal of Physiology-Heart and Circulatory Physiology, 2004. **287**(3): p. H1335-H1343.
19. Fridez, P., et al., *Model of geometrical and smooth muscle tone adaptation of carotid artery subject to step change in pressure*. American Journal of Physiology-Heart and Circulatory Physiology, 2001. **280**(6): p. H2752-H2760.
20. Kokini, K., et al., *Tensile mechanical properties of three-dimensional type I collagen extracellular matrices with varied microstructure*. 2002.
21. Joshi, S.D. and K. Webb, *Variation of cyclic strain parameters regulates development of elastic modulus in fibroblast/substrate constructs*. Journal of orthopaedic research, 2008. **26**(8): p. 1105-1113.